



Advanced Flow Cytometry for Stem Cells

ARTICLE COLLECTION

Sponsored by:



Get to Your Destination Faster With the New iQue® 3

When time is of the essence, the iQue® 3 platform offers a complete platform solution of instrument, software, and reagents. This user friendly walk away system provides the fastest plate sampling combined with built in data analysis and novel data reduction tools that take you from samples to actionable answers in minutes.

www.sartorius.com/iQue-products

Simplifying Progress

SARTORIUS

Contents

4

Introduction

5

Role of flow cytometry in evaluation of the cellular therapy products used in haematopoietic stem cell transplantation

BY VLADIMIRA RIMAC, INES BOJANIĆ

International Journal of Laboratory Hematology

13

Novel strategy to improve hepatocyte differentiation stability through synchronized behavior-driven mechanical memory of iPSCs

BY MEE-HAE KIM, NARUCHIT THANUTHANAKHUN, MASAHIRO KINO-OKA

Biotechnology Bioengineering

28

Generation of universal natural killer cells from a cryopreserved cord blood mononuclear cell-derived induced pluripotent stem cell library

BY WEI DU, LIJUAN CUI, JINMEI ZHANG, HUA ZHANG, RONGZHI LIU, WENLING YANG, YU ZHANG

FEBS Open Bio

39

Production of homogenous size-controlled human induced pluripotent stem cell aggregates using ring-shaped culture vessel

BY FUAD GANDHI TORIZAL, SEONG MIN KIM, IKKI HORIGUCHI, KOUSUKE INAMURA, IKUMI SUZUKI, TAKASHI MORIMURA, MASAKI NISHIKAWA, YASUYUKI SAKAI

Tissue Engineering and Regenerative Medicine

52

Characterization and Optimization of Induced Pluripotent Stem Cell Culture Using Advanced Flow Cytometry and Live-Cell Analysis

BY DARYL COLE, KIRSTY MCBAIN, NINA SENUTOVITCH, NICOLA BEVAN

Sartorius

FURTHER READING AND RESOURCES

Utilizing Advanced Flow Cytometry and Live-Cell Imaging to Evaluate iPSC Pluripotency During Cell Line Selection and Differentiation Procedures

COVER IMAGE © SARTORIUS

Introduction

Induced pluripotent stem cells (iPSCs), derived from numerous sources such as primary fibroblasts or hematopoietic stem cells (HSCs), are rapidly becoming the gold standard model system for drug development, as well as a scalable source for cell-based therapies. Characterization of iPSCs to ensure quality and cell fate are key to their use. Advanced flow cytometry methods are an instrumental part of the characterization process, able to accurately and efficiently phenotype cells during different stages of derivation and expansion.

In this article collection, we highlight four recent publications that illustrate not only the use of pluripotent stem cells for cell-based therapies but how flow cytometry can be utilized to measure cell parameters. First, Vladimira and Bojanić (2021) discuss the current state of advanced flow cytometry for the evaluation of cellular therapies based on (HSCs) from several sources. The authors provide a review of the use of flow cytometry, validation methods, and the principles of evaluating the quality and viability of HSC. Next, Du et al (2022) details the derivation of natural killer (NK) cells from a source of HSCs, in this case cryopreserved human cord blood. Flow cytometry for markers such as CD34, CD45 and NKp46 was used to examine phenotypic changes during the derivation process to characterize the differentiated cells. Correct evaluation of the state of the iPSC-derived cells by advanced flow cytometry is a crucial step in creation of cellular therapies for quality control and cell line establishment.

Generation of large-scale iPSC culture requires careful maintenance and regulation of processes such as cell division and metabolism to confirm pluripotency and to eventually ensure the culture differentiates towards the target cell type. Kim et al (2022) introduces a novel method for synchronizing iPSC cultures by application of botulinum hemagglutinin (HA) to block the activity of E-cadherin, which impacts both cytoskeletal activity and stem cell pluripotency. The authors employed flow cytometry to evaluate the degree of cellular synchronicity induced by the HA treatment. Finally, in the production of iPSC cultures, a key parameter in promoting high quality, on-target cell fate derivation is the size of the cell aggregates. This is even more critical in the use of large-scale cultures required for cell-based therapies.

Torizal et al (2021) explores the use of a ring-shaped culture vessel for iPSC culture expansion as an alternate to large scale suspension cultures. They found that cell aggregates formed and expanded in a manner that produced multiple dermal lineages based on aggregate size and produced improved metabolic and pluripotency states, using flow cytometry assays to measure stage-specific markers.

We hope that readers of this article collection will gain a deeper appreciation for the utility and role of advanced flow cytometry in the production, characterization and expansion of induced pluripotent stem cells for clinically relevant applications.

References

- Rimac, V, Bojanić, I. Role of flow cytometry in evaluation of the cellular therapy products used in haematopoietic stem cell transplantation. *International Journal of Laboratory Hematology*. 2022; 44(3): 446- 453. doi:10.1111/[ijlh.13849](https://doi.org/10.1111/ijlh.13849)
- Du, W., Cui, L., Zhang, J., Zhang, H., Liu, R., Yang, W. and Zhang, Y. (2022), Generation of universal natural killer cells from a cryopreserved cord blood mononuclear cell-derived induced pluripotent stem cell library. *FEBS Open Bio*, 12: 1771-1781. <https://doi.org/10.1002/2211-5463.13460>
- Kim, M.-H., Thanuthanakhun, N., & Kino-oka, M. (2023). Novel strategy to improve hepatocyte differentiation stability through synchronized behavior-driven mechanical memory of iPSCs. *Biotechnology and Bioengineering*, 120, 593– 607. <https://doi.org/10.1002/bit.28285>
- Torizal, F. G., Kim, S. M., Horiguchi, I., Inamura, K., Suzuki, I., Morimura, T., Nishikawa, M., & Sakai, Y. (2022). Production of homogenous size-controlled human induced pluripotent stem cell aggregates using ring-shaped culture vessel. *Journal of Tissue Engineering and Regenerative Medicine*, 16(3), 254– 266. <https://doi.org/10.1002/term.3278>

REVIEW

Role of flow cytometry in evaluation of the cellular therapy products used in haematopoietic stem cell transplantation

Vladimira Rimac  | Ines Bojanić

Clinical Department of Transfusion Medicine and Transplantation Biology, University Hospital Centre Zagreb, Zagreb, Croatia

Correspondence

Vladimira Rimac, Clinical Department of Transfusion Medicine and Transplantation Biology, University Hospital Centre Zagreb, Zagreb, Croatia.

Email: vrimal@kbc-zagreb.hr and kutnjakvl@gmail.com

[Correction added on 29 April 2022, after first online publication: Both the authors' first and last names were previously wrongly swapped and were corrected in this version.]

Abstract

Cellular therapy nowadays includes various products from haematopoietic stem cells (HSC) collected from bone marrow, peripheral blood, and umbilical cord blood to more complex adoptive immune therapy for the treatment of malignant diseases, and gene therapy for inherited immune deficiencies. Broader utilization of cellular therapy requires extensive quality testing of these products that should fulfil the same requirements regarding composition, purity, and potency nevertheless they are manufactured in various centres. Technical improvements of the flow cytometers accompanied by the increased number of available reagents and fluorochromes used to conjugate monoclonal antibodies, enable detailed and precise insight into the function of the immune system and other areas of cell biology, and allows cell evaluation based on size, shape, and morphology or assessment of cell surface markers, as well as cell purity and viability, which greatly contributes to the development and progress of the cell therapy. The aim of this paper is to give an overview of the current use and challenges of flow cytometry analysis in quality assessment of cellular therapy products, with regard to basic principles of determining HSC and leukocyte subpopulation, assessment of cells viability and quality of thawed cryopreserved HSC as well as the importance of validation and quality control of flow cytometry methods according to good laboratory practice.

KEYWORDS

cellular therapy, flow cytometry, haematopoietic stem cell transplantation

1 | INTRODUCTION

The field of cellular therapy has been constantly evolving since the first bone marrow (BM) transplantation in the 1950s, and currently has been successfully implemented as a treatment for patients with malignant, congenital, or acquired diseases of the haematopoietic system.¹ Cellular therapies that initiated with haematopoietic stem cell (HSC) transplantation, now are becoming more complex including adoptive immune therapy for malignant diseases and gene therapy for the treatment of inherited immune deficiencies.² The novel promising cellular therapies are immune effector cells (IECs), such as gene-modified T cells and natural killer (NK) cells.³ Broader utilization of cellular therapy requires extensive quality testing of these products that

should fulfil the same requirements regarding composition, purity, and potency nevertheless they are manufactured in various centres.⁴ In order for cellular therapy products to be exported from one centre to another for further clinical use, it is critical to have mechanisms in place to ensure that the cell collection and processing procedures yield safe, effective, and comparable products at all centres.

Initially, the evaluation of the quality of BM graft was limited to enumeration of total nucleated cells and colony forming unit (CFU) testing, while nowadays various assays have been used for assessing the quality of cellular therapy products. The assessment of the cell type may involve evaluations based on cell size, shape, and morphology, or the evaluation of cell surface markers by flow cytometry. The purity of the cells is also often evaluated by flow cytometry, as well as

cell viability measured by dye exclusion assays. Flow cytometry has applications in various fields such as immunology, cellular biology, bacteriology, virology, cancer biology and infectious disease monitoring. It has seen dramatic advances over the last 30 years, allowing detailed and precise insight into the function of the immune system and other areas of cell biology.⁵ This paper aims to give an overview of the current use and challenges of flow cytometry analysis in the quality assessment of cellular therapy products used in HSC transplantation setting.

2 | FLOW CYTOMETRY: PRINCIPLES, INSTRUMENTS, REAGENTS

Flow cytometry is a technique utilized in many different settings, both in the routine laboratory and in research facilities. With the advancement of technology, the field of flow cytometry is also evolving, so today special types of instruments have been designed for specific purposes, for example, system that combines microscopy and flow cytometry or flow cytometry with mass spectrometry. This technique allows simultaneous analysis of cell characteristics of mixed cell population from peripheral blood (PB) and BM as well as solid tissues that can be dissociated into single cells, with cell sorting for further analysis, which is one of the main application of flow cytometry.⁵

Technical improvements of the flow cytometer are accompanied by an increase in the number of available reagents and fluorochromes used to conjugate monoclonal antibodies which results in the complexity of the analysis and requires the use of newer cluster data analysis algorithms. All that improves methods of data mining allow useful information to be extracted from the high-dimensional data now available from flow cytometry.⁵

In addition to immunophenotyping, which is the most used application in flow cytometry, apoptosis analysis, cell cycle analysis and cell sorting are also used in the quality assessment of cellular therapy products.⁵⁻⁸

3 | ENUMERATION OF HAEMATOPOIETIC STEM CELL

HSC sources currently used for transplantation are BM, mobilized PB and umbilical cord blood (UCB).⁹ Each type of HSC graft requires a different method of collection and processing, and has its advantages and disadvantages. BM has been almost completely replaced as a source of HSC with peripheral blood stem cells (PBSC), due to easier collection with leukapheresis procedure without the need for general anaesthesia and more rapid haematopoietic reconstitution after transplantation.^{10,11} HSCs from UCB have a high clonogenic potential and because they are immunologically naive and immature, can be transplanted with only partial histocompatibility. But due to their limited volume, UCB is mainly applicable in transplantation of paediatric patients.⁹

Regardless of the source of HSCs, haematopoietic stem and progenitor cells appear morphologically as either small lymphocytes in the case of the earliest stem cells or in the case of maturing progenitors, as blast forms. Therefore, they can be identified only by functional assays or by immunophenotypic surface marker analysis. Phenotype of HSC is CD34⁺/CD45^{dim}/SSC^{low}/FSC^{low and intermediate}.¹²

Later progenitors may be functionally assayed in soft agar culture systems. When supported by the proper growth factors, they form colonies of their progeny that can be enumerated and expressed as a particular number of CFUs per total number of cells plated. Functional assays for enumerating different species of HSCs require several weeks of sterile culture incubation. Therefore, these assays have some disadvantages, and the most significant being poor intra- and inter-laboratory reproducibility, non-standardization, and long turnaround time.^{13,14} Hence, functional haematopoietic cell assays in transplantation clinical practice are generally limited to quality-control procedures of cryopreserved cells and are rarely used in routine laboratory testing.

The measurement of CD34⁺ cells by flow cytometry has, however, become the universal assay for measuring the potency of HSC products. The evaluation of absolute CD34⁺ cell count in patient PB is also important for the decision of optimal timing to start the leukapheresis procedure. According to the Joint Accreditation Committee of International Society of Cellular Therapy (JACIE) standards, enumeration of viable CD34⁺ cells must be performed in fresh PBSC products to access the graft quality.¹⁵ Minimal CD34⁺ cell count for one transplantation is $\geq 2 \times 10^6$ CD34⁺ cells/kg of recipient's body weight, while the optimal is 5×10^6 CD34⁺ cells/kg of body weight, which is associated with faster recovery of neutrophil and platelet count after transplantation.^{16,17}

Although laboratories for quality control in transplant centres use different protocols for determining CD34⁺ cells, the protocol of International Society of Hemotherapy and Graft Engineering (ISHAGE) is the most commonly used (Figure 1).¹⁸ This protocol has been continuously updated, by introducing counting beads and including viability dyes.¹² However, there are still differences between laboratories using the ISHAGE protocol: some use single platform method, while others dual platform.¹⁹ The benefit of the single platform is the simultaneous determination of the percentage and absolute count of CD34⁺ cells using fluorescent microspheres (beads), which can be in liquid phase or in lyophilized form. The main advantage of lyophilized beads is that the tube contains an exact number of beads which allows the calculation of the absolute cell count. Furthermore, there is a difference in the cell labelling protocol which depends on whether the single or dual platform method is used. Some laboratories use lyse-wash method (dual platform), while others use lyse-no wash method (single platform) which lasts shorter and potential cell loss is prevented. Although the ISHAGE protocol for CD34⁺ cell determination is used in many laboratories, the mentioned differences indicate that standardization is necessary.

Although according to EBMT guidelines, CD34⁺ evaluation is not mandatory for the assessment of BM many centres include it in quality testing.²⁰ If the laboratory performs determination of viable

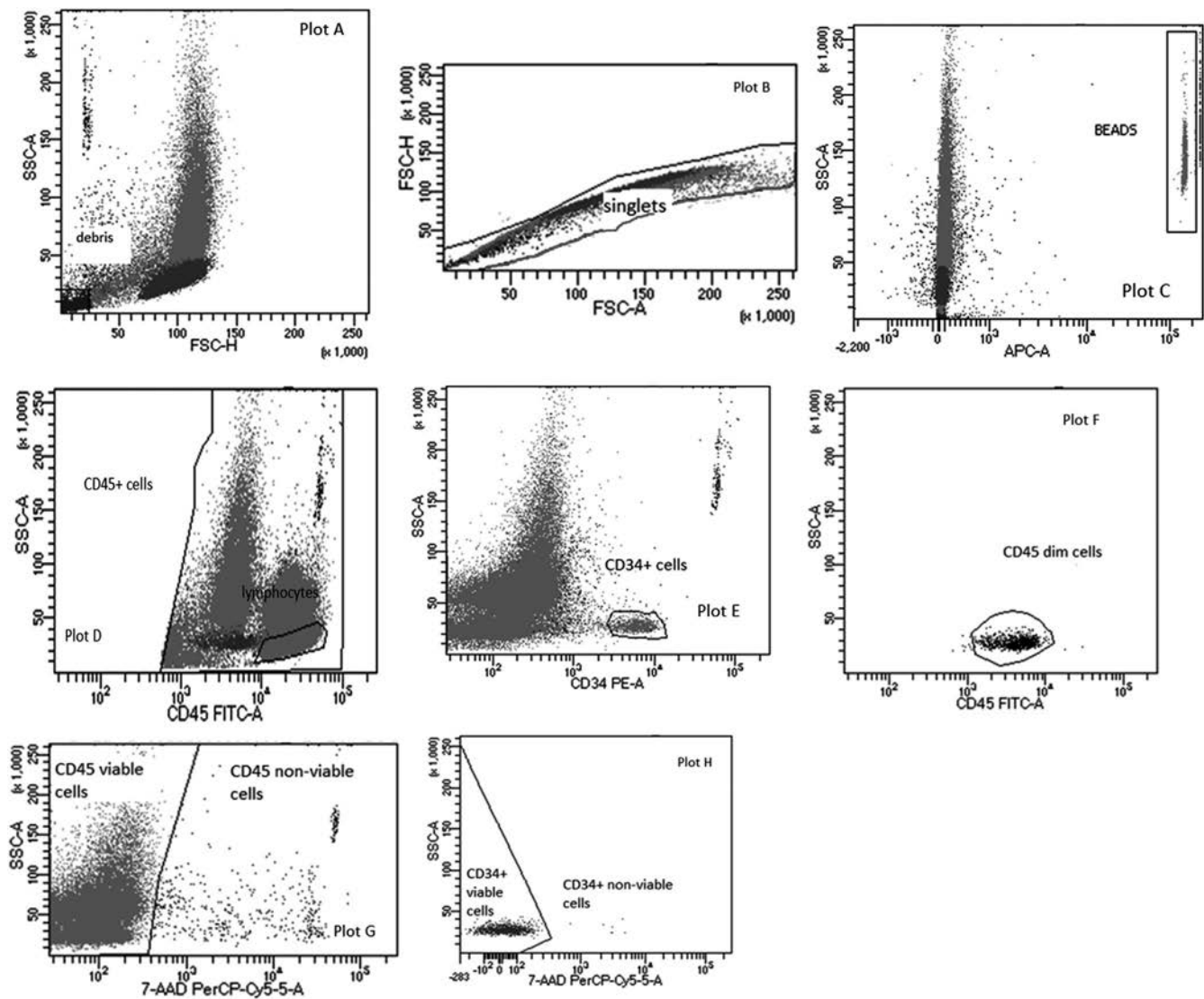


FIGURE 1 Gating strategy for analysis of CD34+ cells haematopoietic stem cells for single platform using modified ISHAGE protocol. ISHAGE, International Society of Hemotherapy and Graft Engineering

CD34+ cells in BM samples, it is necessary to carefully set up protocols and templates for cells analysis on flow cytometer. Compared to CD34+ cells enumeration in PB or in PBSC graft, the analysis of BM samples is challenging because they contain high red blood cell count and may contain fat, cell clumps which all complicate the analysis. Therefore, the settings on the flow cytometer must be adjusted to reduce debris and allow a more accurate determination of the population of CD34+ cells.

4 | ASSESSMENT OF CELLS VIABILITY

The viability of cells was firstly evaluated using the dye exclusion tests, based on the principle that live cells possess intact cell membranes that exclude certain dyes, whereas dead cells do not. The cell suspension is mixed with dye and then visually examined to determine

whether cells take up or exclude dye. The most common dyes used for performing dye exclusion tests are trypan blue, eosin Y, acridine orange, or propidium iodide. Dye exclusion is a simple and rapid technique, but the limitation of the method is that viability is determined indirectly from the assessment of cell membrane integrity. It is important that the test be performed accurately because a small amount of dye uptake indicative of cell injury may go unnoticed.^{21,22}

As already mentioned, in addition to the number of CD34+ cells, according to the JACIE standards it is necessary to determine the viability of collected and processed/cryopreserved cells. In the assessment of CD34+ cells viability, the most commonly used dye is 7-aminoactinomycin D (7-AAD), which binds to GC region of the cell DNA, and allows the determination of necrotic cells and those in late apoptosis (7-AAD positive) using flow cytometer.²² Besides 7-AAD, some laboratories still used dye excluding tests in routine work, but because 7-AAD has become a standard part of the ISHAGE protocol,

most laboratories use it to determine the viability of CD34⁺ cells.²¹ The main disadvantage of the method with 7-AAD, as well as the previously mentioned dye exclusion tests, is a failure to detect cells in early apoptosis, which may lead to overestimation of graft cell viability.²³ Several studies have shown that the method using Annexin V (Ann V) is suitable for detection of cells in early apoptosis.^{14,24} Annexin V is a protein that has a high affinity for negatively charged phospholipids, such as phosphatidylserine, which are characteristic of the cytoplasmic side of the viable cell membrane. But in early apoptosis phosphatidylserine becomes exposed on the cell surface due to cell membrane asymmetry and can be detected using a reagents containing Ann V protein and Ann V binding buffer with calcium, which allows binding Ann V to negatively charged phospholipids. It may be useful to evaluate the apoptotic status of progenitor cells before beginning ex vivo manipulation procedures such as stem cell expansion or gene therapy.²⁵ Other assays for the determination of apoptotic cells that are used in research settings are method with DNA binding dye Syto 16, method for detecting activation of caspases, TUNEL (TdT dUTP Nick End Labeling) assay for detection of endonuclease digestion of DNA, and method for detection of mitochondrial apoptosis using dyes that determine mitochondrial membrane potential and chromatin condensation in the nucleus using method with specific dye.^{5,26}

5 | ASSESSMENT OF QUALITY OF THAWED CRYOPRESERVED HSC

Fresh HSCs, once harvested, are only viable for several hours to a few days, limiting their use and geographical reach. Currently, HSCs and other cell therapies are cryopreserved using the same techniques with cryoprotectant dimethyl sulfoxide (DMSO) at a slow cooling rate.²⁷ Cryopreservation of HSCs allows their transportation from the site of processing to the site of clinical use, creates a larger window of time in which cells can be administered to patients, and enables sufficient time for quality control and regulatory testing. Despite these benefits, during processing, cells are exposed to some factors (e.g., centrifugation, condition of storage, and thawing process) that can lead to the reduction of the cell count in graft, but also to a decline in cell viability after thawing.²⁷

The gold standard for cryopreservation for HSCs is still DMSO. The timing of cell exposure to DMSO is very important because DMSO can directly impact cellular function by affecting metabolism, enzyme activity, apoptosis, and cell cycle. In addition, the effect of DMSO depends on the type of cells, the stage of cell differentiation, the duration of exposure, and DMSO concentration.²⁸ Since DMSO has the toxic effect on the cells in thawed graft and could also cause adverse reactions during the infusion, in some transplant centres it is removed from thawed HSCs before transplantation.²⁷ However, the question is how many cells are lost and damaged by this process, because it is known that the number of viable CD34⁺ cells in a thawed product is actually a real number transplanted to the patient.^{11,29} In addition to the DMSO, some other factors affect the

recovery of the cells after cryopreservation, such as cell concentration, pre-freeze storage conditions, freezing rate, and storage temperature, which also affect cell viability.²⁷

It is well known that 'single platform' method in combination with 7-AAD represents the reference method for determining the count of viable CD34⁺ cells in fresh samples. However, for analysing thawed cryopreserved samples modification of the method is necessary. It is recommended to adjust the gates Side scatter versus Forward scatter and CD45 versus SSC in order to allow the acquisition of a higher number of dead and live cells. Therefore, analysis of thawed samples requires the adaption of gating strategy and acquisition settings for the purpose of more precise and accurate analysis of HSC.^{11,30}

According to NetCord – Foundation for the Accreditation of Cellular therapy (FACT) standards for Cord Blood Banks the post-thaw CD34⁺ cell viability should be $\geq 70\%$.³¹ There are no such recommendations for minimal CD34⁺ cell post-thaw viability of PBSCs, and it is only required that the viability of nucleated cells should be $>50\%$ after freezing and thawing of apheresis product.³² It is therefore questionable how to perform the quality control of the PBSC graft after thawing and which assays and methods should be used. Although some studies evaluated the methods for post-thaw viability of PBSC and CB, as well as attempted to standardize process from sample preparation to acquisition on flow cytometer, still there are no guidelines defining each step in the process after thawing of cryopreserved samples, for example, exact conditions of sample thawing, is it necessary to wash cells, dilute the samples and remove cryoprotectant before labelling, and acquisition on flow cytometer.^{33,34}

In quality specifications for UCB, post-thaw CFU is still one of the requirements, but due to the before mentioned disadvantages of CFU assay, in routine work it would be desirable to use assay with higher reproducibility and a shorter turnaround time for faster assessment of graft quality.^{35,36} Although 7-AAD is the most commonly used dye for the determination of cell viability on flow cytometer in HSC transplants, the lack of a test is that it cannot determine cells in early apoptosis. Since it is known that in early apoptosis the functioning of the cell is impaired, the question is whether such damaged cells have the possibility of proliferation. Thus, it would be useful to determine the viability of cells, in addition to the method with 7-AAD use the method for determining cells in early apoptosis, such as the method with annexin V. Few studies showed that for UCB samples, assay using 7-AAD and Ann V was a feasible method for prediction of CFU results.^{14,24} Duggleby and coworkers²⁴ showed that significant numbers of CD34⁺ AnnV⁺ events were found within the 7AAD-gated population on their custom protocol for determining viable CD34⁺ cells. In their study, the measured results indicated a good correlation between nonapoptotic cells (CD34⁺ AnnV⁻) and CFU results, so they confirmed the fact that the current standard enumeration of CD34⁺ viable cells does not fully reflect potency after thawing because standard enumeration with 7-AAD does not measure the early apoptotic cell. Radke and coworkers¹⁴ in their study presented that in comparison to the standard ISHAGE protocol, the method with AnnV resulted in similar good correlations between CFU and CD34⁺ cells seeded, which leads to an improved conformability

with the theoretically expected colony formation. The results of these studies were especially important because the Ann V method can be used in the case the number of viable cells needs to be determined as soon as possible before transplantation.

6 | ASSESSMENT OF LEUKOCYTE SUBPOPULATION

In addition to CD34+ cell determination, the quality assessment of allogeneic HSC graft must include enumeration of other leukocyte subpopulation, especially CD3+ T cells. Besides T cells, for different types of cell therapy it is necessary to determine leukocytes subpopulation in the graft. Nowadays, flow cytometers used in laboratory work enable the detection of several cell markers at once, depending on the laser and detector configuration of flow cytometer (e.g., 10-colour flow cytometer with three lasers [violet 405 nm, blue 488 nm, and red 638 nm]). Therefore, it is possible to determine leukocytes subpopulations using monoclonal antibodies (mAb) in one test tube, reducing the price and time to test results. Leukocyte subpopulations are usually detected using anti-CD 19 mAb for B-cells, anti-CD 16 and anti-CD 56 for NK cells, anti-CD3, anti-CD 4 and anti-CD8 mAb for subpopulation of T-cells and anti-CD 14 and anti-CD16 for monocytes (Table 1).

When the laboratory defines the protocol for detecting cells of interest, it is necessary to choose the antibodies (Abs) and fluorochromes which will allow accurate cell identification. This is especially important when performing multiple analysis in one step (e.g., enumeration of lymphocytes subpopulation). In addition to individual Ab, there are commercial kits that contain predefined Abs labelled with fluorochromes and reagents for determining cells of interest, for example, for determining HSC or lymphocyte subpopulations.^{16,37,38} The advantage of these kits is that they contain pre-assembled Ab panels, which facilitates the creation and implementation of protocols in laboratories that have no experience with setting up in-house methods. Furthermore, some manufacturers offer software for acquisition and analysis which have an auto-gating algorithm for isolation of the cells of interest, which also contributes to more user-friendly cell analysis, for example, BD FACSCanto Clinical software (BD Bioscience, San Jose, CA).³⁹

TABLE 1 The antibodies most commonly used in the evaluation of the cellular therapy products intended for haematopoietic stem cell transplantation

Antibody	Cell line	References
Anti-CD34	Haematopoietic stem cells	[14,17,18,23,24,33,34,37,39,43,45,47,48,54–56]
Anti-CD3	T cells	[38,40,45,47,48,50,52]
Anti-CD19 Anti-CD20	B cells	[38,40,43,45,47,48,50,52]
Anti-CD14	Monocytes	[50]
Anti-CD56/CD16	NK cells	[38,40,48,50]

Transplantation of allogeneic HSC is sometimes followed with additional administration of donor lymphocytes, for example, donor lymphocyte infusion (DLI). Lymphocytes for DLI could be collected during allo-HSC collection procedure or from unstimulated PB, and cryopreserved as a simple and effective therapeutic option for patients in case of disease relapse.^{40,41} The purpose of DLI is to enhance donor T-cells potency against leukaemic cells (graft-vs.-tumour effect), that is, to treat disease relapse and improve immune recovery.⁴²

In the fresh apheresis products which will be cryopreserved for DLI, CD3+ cells are determined on flow cytometer. Since there are only a few reports on how this cell population tolerates the cryopreservation and thaw process, and because of difference among laboratories in cryopreservation protocols, each centre should determine the viability of CD3+ cells in the thawed sample before infusion.³⁸

In the case of partial HLA matching, the HSC graft could be manipulated before administration in order to remove unwanted cells. The transplantation of HSC graft obtained from haploidentical donors carries an increased risk of developing graft-versus host disease (GvHD). In order to avoid that potential complication after transplantation, immunomagnetic techniques can be used prior to the infusion of the graft: indirect T cell depletion by the enrichment of CD34+ cells or the depletion of unwanted CD3+ T cells and CD19+ B cells.^{43–45} The method of enrichment of target CD34+ cells is based on magnetic isolation technique using anti-CD 34 mAb conjugated to superparamagnetic iron dextran particles and magnetic cell separator.⁴⁵ After selection, the number of viable CD34+ and CD3+ cells is determined using flow cytometer. The challenge in the analysis is to determine the count of CD3+ cells in the positive fraction after selection. The residual number of CD3+ cells is usually less than 1% and for analysis is needed special protocol for the rare number of T cells. In addition, multigating strategy protocol should be implemented.⁴⁶ Nowadays, two different T-cell depletions are used in haploidentical HSC transplantation: in vitro T-cell depletion of PBSC and post-transplantation cyclophosphamide for in vivo T-cell depletion.⁴⁷ Immunological techniques for depletion of T-cell receptor alpha/beta and CD19+ cells is even more demanding than enrichment techniques. After the depletion process, very few residual TCR $\alpha\beta^+$ and CD19+ cells must be determined using flow cytometry.⁴⁸ For the analysis of the products obtained using immunological techniques, it is very important to devise gating strategies, set up a protocol on flow cytometer and then accurately analyse the cells of interest, because regardless of their very small number in the product, the effect of the procedure is assessed according to result from flow cytometer.

7 | IMMUNE EFFECTOR CELLS

Adoptive cellular therapy with IECs is an exciting and rapidly developing field that is evolving from a clinical manufacturing model, generally occurring in academic institutions, to an industry model with centralized manufacturing. Immune effector cells currently comprise cells that express broad cytotoxicity against tumours or targeted

cytotoxicity against tumour-associated antigens, as well as the cells that induce tolerance by suppressing inflammatory responses or enhancing immune recognition. Their identity, enumeration, and viability are critical information for initiating manipulation and releasing the products for infusion.^{49,50}

Despite rapid development, IECs therapy still faces several challenges such as manufacturing processes, logistic and coordination aspects and toxicity profiles. Therefore, the Immune Effector Cell Task Force was created the standards and accreditation program for IEC.⁵¹ The standards clearly state that relevant and validated assay should be employed to evaluate cellular therapy products undergoing manipulation that alters the function of the target cell population, where multi-colour flow cytometry is the technology of choice for cell surface marker detection, viability and enumeration. Accurate quantification of viable absolute numbers of cells is a prerequisite for several activities: standardization of input cellular material for CAR-transduced T or NK cell manufacturing, cell selection, in-process quality controls and dosing of IEC.^{50,51}

CAR-T cell therapy is increasingly applied in clinical practice, in which genetic modification optimizes the T cells to actively proliferate and recognize cancer cells.⁴⁹ As with CD34+ cells collection for HSC transplantation, obtaining a sufficient concentration of T-cells is a critical part of the collection process. It is therefore important to perform quality control of leukapheresis products using anti-CD3 mAb, because quality of the final product depends on the quality of the starting material used in CAR-T cells manufacturing.^{42,52} After the manufacturing process, a sample of the CAR-T cell product is taken for quality control, which includes, among other things, phenotyping, viability and purity of effector cell population.⁴²

In addition to the determination of the quality of the leukapheresis product, flow cytometry is used in the monitoring of expansion and persistence of the therapeutic cells after the infusion and in the evaluation of treatment response in patients who received graft with CAR-T cells.⁵³

8 | QUALITY CONTROL AND VALIDATION OF FLOW CYTOMETRY METHODS

Before the introduction of new methods in routine work, it is necessary to perform validation that usually includes assessment of precision and accuracy, linearity, limit of quantification, method comparison between two or more flow cytometers and carryover, and sometimes a sample stability study.^{37,39,50}

8.1 | Stability of the cellular therapy product samples

Sample stability study is an important part of validation of the protocol used for quality assessment, especially when implementing a new type of cell therapy product. Several studies have examined the stability of fresh leukapheresis samples and thawed cryopreserved UCB

samples.^{37,39,54,55} The results showed that fresh leukapheresis samples were stable up to 24 h stored at 4°C.^{37,39} The results of stability studies of thawed UCB samples were conflicting. Lee et al.⁵⁴ in their study showed that thawed UCB samples were stable up to 6 h after thawing, regardless of whether samples were stored at room temperature or at 4°C. On the other hand, Huang and colleagues reported that CD34+ cell viability decreased significantly after only 20 min when thawed UCB samples were stored at RT.⁵⁵ Krasna et al.⁵⁶ evaluated the stability of the HSC products after immunoselection and reported that CD34+ cells after selection were less stable than CD34+ cells in leukapheresis product during refrigerated storage up to 6 days. Since the results of the studies conducted so far have varied depending on the type of cellular therapy products and storage conditions, each laboratory should perform a sample stability study as part of the validation protocol.

Before performing validation, it is necessary to optimize the settings of clones combined with the best possible fluorochromes and also antibody concentration to minimize nonspecific background fluorescence.

In routine work, after initialization and start up procedure, lasers on flow cytometer need to be adjusted and commercial reagents (fluorescent beads) are most commonly used for this purpose. If necessary, spectar overlap compensation can be performed.⁵⁷

8.2 | Internal and external quality control

According to good laboratory practice, it is necessary to provide quality control for the methods used in routine laboratory work. Internal quality control should be performed every day before routine work, for which commercial controls are used, usually from the same manufacturer as the reagents. Beside internal control, it is also important to participate in external quality assessment (EQA). Samples for EQA are usually analysed several times per year, and laboratories decide in which scheme will participate (e.g., for CD34 count, or for lymphocyte immunofenotyping). Laboratories that are part of HSC transplantation program usually participate in the UK NEQAS quality scheme and/or in national schemes.^{58,59} It is very important that samples from EQA are processed in the same way as routine samples, because the external control allows periodic verification of the method, and at the same time checks the technical performance of the test. Validation and verification of the methods, internal and EQA are part of the accreditation procedure.⁶⁰ If the laboratory wants to meet the requirements for accreditation, it is necessary to implement the mentioned procedures.

9 | CONCLUSION

Flow cytometry methods nowadays open new views and insights into the quality of various cellular products used in the field of HSC transplantation which greatly contributes to the development and progress of cell therapy. They are now in routine use in clinical as well as in research laboratory work, and application of good laboratory practice,

constant education and training are needed for the implementation and maintenance of the methods in this fast-growing field of laboratory testing.

CONFLICT OF INTEREST

The authors declare no potential conflict of interest.

DATA AVAILABILITY STATEMENT

All data from this study are available from the corresponding author upon reasonable request.

ORCID

Vladimira Rimac  <https://orcid.org/0000-0002-4598-4870>

REFERENCES

- Chabannon C, Kuball J, Bondanza A, et al. Hematopoietic stem cell transplantation in its 60s: a platform for cellular therapies. *Sci Transl Med*. 2018;10:1-10.
- Kohn DB. Historical perspective on the current renaissance for hematopoietic stem cell gene therapy. *Hematol Oncol Clin North Am*. 2017;31:721-735.
- Maus MV, Nikiforow S. The why, what, and how of the new FACT standards for immune effector cells. *J Immunother Cancer*. 2017;5:36.
- Stroncek DF, Jin P, Ren J, et al. Quality assessment of cellular therapies: the emerging role of molecular assays. *Korean J Hematol*. 2010;45:14-22.
- McKinnon KM. Flow cytometry: an overview. *Curr Protoc Immunol*. 2018;120:5.1.1-5.1.11.
- Murray C, Pao E, Jann A, Park DE, Di Carlo D. Continuous and quantitative purification of T-cell subsets for cell therapy manufacturing using magnetic ratcheting cytometry. *SLAS Technol*. 2018;23:326-337.
- Desoutter J, Ossart C, Lacassagne MN, Regnier A, Marolleau JP, Harrivel V. Cryopreservation and thawing of hematopoietic stem cell CD34-induced apoptosis through caspase pathway activation: key role of granulocytes. *Cytotherapy*. 2019;21:612-618.
- Passegué E, Wagers AJ, Giuriato S, Anderson WC, Weissman IL. Global analysis of proliferation and cell cycle gene expression in the regulation of hematopoietic stem and progenitor cell fates. *J Exp Med*. 2005;202:1599-1611.
- Panch SR, Szymanski J, Savani BN, Stroncek DF. Sources of hematopoietic stem and progenitor cells and methods to optimize yields for clinical cell therapy. *Biol Blood Marrow Transplant*. 2017;23:1241-1249.
- Kong JH, Hu Y, Kong SY, et al. Analysis of laboratory parameters for optimal autologous peripheral blood stem cell collection from lymphoma and myeloma patients. *J Clin Apher*. 2021;36:135-142.
- Lanza F, Saccardi R, Seghatchian J. New horizons on stem cell cryopreservation through the artificial eyes of CD34+, using modern flow cytometry tools. *Transfus Apher Sci*. 2020;59:102785.
- Whitby A, Whitby L, Fletcher M, et al. ISHAGE protocol: are we doing it correctly? *Cytometry B Clin Cytom*. 2012;82:9-17.
- European Committee (Partial Agreement) on Organ Transplantation. *Haematopoietic Progenitor Cells from Bone Marrow and Peripheral Blood. Guide to the Quality and Safety of Tissues and Cells from Human Application*. European Directorate for the Quality of Medicine and Health Care (EDQM), Council of Europe; 2019:267-288.
- Radke TF, Barbosa D, Duggleby RC, Saccardi R, Querol S, Kögler G. The assessment of parameters affecting the quality of cord blood by the appliance of the Annexin V staining method and correlation with CFU assays. *Stem Cells Int*. 2013;2013:823912.
- FACT-JACIE. *International Standards for Hematopoietic Cellular Therapy. Product Collection, Processing, and Administration*. 7th ed. FACT-JACIE; 2021. Accessed April 20, 2021. www.ebmt.org/jacie-standards
- Mohammed RN, Ahmad D, Khoshnaw N, et al. Leukapheresis cell concentration adjustment required for a successful recovery of HSC after cryopreservation. *Cryobiology*. 2020;92:21-25.
- Jansen EM, Hanks SG, Terry C, et al. Prediction of engraftment after autologous peripheral blood progenitor cell transplantation: CD34, colony-forming unit-granulocyte-macrophage, or both? *Transfusion*. 2007;47:817-823.
- Gratama JW, Kraan J, Keeney M, Sutherland DR, Granger V, Barnett D. Validation of the single-platform ISHAGE method for CD34(+) hematopoietic stem and progenitor cell enumeration in an international multicenter study. *Cytotherapy*. 2003;5:55-65.
- Murugesan M, Nair CK, Nayanar SK, Pentapati KC. Flow cytometric enumeration of CD34+ hematopoietic stem cells: a comparison between single- versus dual-platform methodology using the International Society of Hematotherapy and Graft Engineering protocol. *Asian J Transfus Sci*. 2019;13:43-46.
- Gorin NC. Bone marrow harvesting for HSCT. In: Carreras E, Dufour C, Mohty M, Kröger N, eds. *The EBMT Handbook Hematopoietic Stem Cell Transplantation and Cellular Therapies*. European society for blood and marrow transplantation; 2019:109-115.
- Takanashi M, Selogie E, Reems JA, et al. Current practices for viability testing of cryopreserved cord blood products: an international survey by the cellular therapy team of the biomedical excellence for safer transfusion (BEST). *Collaborative Transfusion*. 2018;58:2184-2191.
- Varan HD, Bay M, Ozturk A, Dalva K, İlhan O. Comparison of the methods evaluating post thawing viability of peripheral blood stem cell graft. *Transfus Apher Sci*. 2019;58:192-195.
- Watz E, Remberger M, Ringden O, et al. Quality of the hematopoietic stem cell graft affects the clinical outcome of allogeneic stem cell transplantation. *Transfusion*. 2015;55:2339-2350.
- Duggleby RC, Querol S, Davy RC, et al. Flow cytometry assessment of apoptotic CD34+ cells by annexin V labeling may improve prediction of cord blood potency for engraftment. *Transfusion*. 2012;52:549-559.
- Anthony RS, McKelvie ND, Cunningham AJ, Craig JI, Rogers SY, Parker AC. Flow cytometry using annexin V can detect early apoptosis in peripheral blood stem cell harvests from patients with leukaemia and lymphoma. *Bone Marrow Transplant*. 1998;21:441-446.
- Sparrow RL, Komodromou H, Tippett E, Georgakopoulos T, Xu W. Apoptotic lymphocytes and CD34+ cells in cryopreserved cord blood detected by the fluorescent vital dye SYTO 16 and correlation with loss of L-selectin (CD62L) expression. *Bone Marrow Transplant*. 2006;38:61-67.
- Hornberger K, Yu G, McKenna D, Hubel A. Cryopreservation of hematopoietic stem cells: emerging assays, Cryoprotectant agents, and technology to improve outcomes. *Transfus Med Hemother*. 2019;46:188-196.
- Shu Z, Heimfeld S, Gao D. Hematopoietic SCT with cryopreserved grafts: adverse reactions after transplantation and cryoprotectant removal before infusion. *Bone Marrow Transplant*. 2014;49:469-476.
- Lee S, Kim S, Kim H, Beak EJ, Jin H, Kim HS. Post-thaw viable CD34 (+) cell count is a valuable predictor of haematopoietic stem cell engraftment in autologous peripheral blood stem cell transplantation. *Vox Sang*. 2008;94:146-152.
- Lanza F, Mangianti S, Accorsi P, et al. Manipulation, and cryopreservation of autologous peripheral blood stem cell products in Italy: a survey by GITMO, SIDem and GIIMA societies. *Transfus Apher Sci*. 2020;59:102753.
- Foundation for the Accreditation of Cellular Therapy, ed. *NerCord-FACT International Standards for Cord Blood Collection, Banking, and*

- Release for Administration*. 7th ed. Foundation for the Accreditation of Cellular Therapy; 2019.
32. Wuchte P. Processing, cryopreserving and controlling the quality of HSCs. In: Carreras E, Dufour C, Mohty M, Kröger N, eds. *The EBMT Handbook Hematopoietic Stem Cell Transplantation and Cellular Therapies*. European society for blood and marrow transplantation; 2019: 127-130.
 33. Fournier D, Lewin A, Simard C, et al. Multi-laboratory assay for harmonization of enumeration of viable CD34⁺ and CD45⁺ cells in frozen cord blood units. *Cytotherapy*. 2020;22:44-51.
 34. Castelhana MV, Reis-Alves SC, Vigorito AC, et al. Quantifying loss of CD34⁺ cells collected by apheresis after processing for freezing and post-thaw. *Transfus Apher Sci*. 2013;48:241-246.
 35. European Committee (Partial Agreement) on Organ Transplantation. *Umbilical Cord Blood Progenitors. Guide to the Quality and Safety of Issues and Cells from Human Application*. European Directorate for the Quality of Medicine and Health Care (EDQM), Council of Europe; 2019:289-298.
 36. Quarol S, Rocha V. Procurement and management of cord blood. In: Carreras E, Dufour C, Mohty M, Kröger N, eds. *The EBMT Handbook Hematopoietic Stem Cell Transplantation and Cellular Therapies*. European society for blood and marrow transplantation; 2019:131-136.
 37. Omana-Zapata I, Oreizy F, Mosqueda F, et al. Performance of a novel BD stem cell enumeration kit on two flow cytometry systems. *Int J Lab Hematol*. 2013;35:393-399.
 38. Berens C, Heine A, Müller J, et al. Variable resistance to freezing and thawing of CD34-positive stem cells and lymphocyte subpopulations in leukapheresis products. *Cytotherapy*. 2016;18:1325-1331.
 39. Rimac V, Bojanić I, Gojčeta K, Golubić ČB. Evaluation of the BD stem cell enumeration kit on the BD FACSCanto II flow cytometer using bd facscanto clinical and bd facsdiva software. *Int J Lab Hematol*. 2021; 43:61-67.
 40. Worsham DN, Reems JA, Szczepiorkowski ZM, et al. Clinical methods of cryopreservation for donor lymphocyte infusions vary in their ability to preserve functional T-cell subpopulations. *Transfusion*. 2017;57: 1555-1565.
 41. Castagna L, Sarina B, Bramanti S, Perseghin P, Mariotti J, Morabito L. Donor lymphocyte infusion after allogeneic stem cell transplantation. *Transfus Apher Sci*. 2016;54:345-355.
 42. Mukherjee S, Reddy O, Panch S, Stroncek D. Establishment of a cell processing laboratory to support hematopoietic stem cell transplantation and chimeric antigen receptor (CAR)-T cell therapy. *Transfus Apher Sci*. 2021;60:103066.
 43. Haastrup E, Ifversen MRS, Heilmann C, Fischer-Nielsen A. Depletion of $\alpha\beta$ + T and B cells using the CliniMACS prodigy: results of 10 graft-processing procedures from haploidentical donors. *Transfus Med Hemother*. 2019;46:446-449.
 44. Li Pira G, Biagini S, Cicchetti E, et al. Immunoselection techniques in hematopoietic stem cell transplantation. *Transfus Apher Sci*. 2016;54: 356-363.
 45. Stroncek DF, Tran M, Frodigh SE, et al. Preliminary evaluation of a highly automated instrument for the selection of CD34⁺ cells from mobilized peripheral blood stem cell concentrates. *Transfusion*. 2016; 56:511-517.
 46. Schuum M, Lang P, Handgretinger R. Graft manipulation. In: Carreras E, Dufour C, Mohty M, Kröger N, eds. *The EBMT Handbook Hematopoietic Stem Cell Transplantation and Cellular Therapies*. European society for blood and marrow transplantation; 2019:137-142.
 47. Foell J, Kleinschmidt K, Jakob M, Troeger A, Corbacioglu S. Alternative donor: $\alpha\beta$ /CD19 T-cell-depleted haploidentical hematopoietic stem cell transplantation for sickle cell disease. *Hematol Oncol Stem Cell Ther*. 2020;13:98-105.
 48. Schumm M, Lang P, Bethge W, et al. Depletion of T-cell receptor alpha/beta and CD19 positive cells from apheresis products with the CliniMACS device. *Cytotherapy*. 2013;15:1253-1258.
 49. Karanu F, Ott L, Webster DA, Stehno-Bittel L. Improved harmonization of critical characterization assays across cell therapies. *Regen Med*. 2020;15:1661-1678.
 50. Mfarrej B, Gaude J, Couquiaud J, Calmels B, Chabannon C, Lemarie C. Validation of a flow cytometry-based method to quantify viable lymphocyte subtypes in fresh and cryopreserved hematopoietic cellular products. *Cytotherapy*. 2021;23:77-87.
 51. Foundation for the Accreditation of Cellular Therapy (FACT). Standards for Immune Effector Cells, First Edition, Version 1.1, March 2018.
 52. Demaret J, Varlet P, Trauet J, et al. Monitoring CAR T-cells using flow cytometry. *Cytometry B Clin Cytom*. 2021;100:218-224.
 53. Maryamchik E, Gallagher KME, Preffer FI, Kadauke S, Maus MV. New directions in chimeric antigen receptor T cell [CAR-T] therapy and related flow cytometry. *Cytometry B Clin Cytom*. 2020;98:299-327.
 54. Lee YH, Koh H, Nam E, Kim YJ. Cryopreserved cord blood mononuclear cells in DMSO are healthy for at least 6 hours after thawing. *Transfus Apher Sci*. 2020;59:102603.
 55. Huang L, Song GQ, Wu Y, Wang J, Sun ZM. Optimal length of time of cryopreserved umbilical cord blood infusion after thawing. *Hematology*. 2014;19:73-79.
 56. Krasna M, Malicev E, Rozman JZ, Vrtovec B. Assessment of stability of CD34⁺ cell products enriched by immunoselection from peripheral blood mononuclear cells during refrigerated storage. *Transfus Apher Sci*. 2017;56:566-570.
 57. Matos DM. Standardization of a compensation matrix for the use in an ISHAGE-based single-platform for CD34⁺ stem cell quantitation on the FACS Via™ flow cytometer. *Int J Lab Hematol*. 2020;42:198-205.
 58. Bainbridge J, Rountree W, Louzao R, et al. Laboratory accuracy improvement in the UKNEQAS leucocyte Immunophenotyping immune monitoring program: an eleven-year review via longitudinal mixed effects modeling. *Cytometry B Clin Cytom*. 2018;94:250-256.
 59. Levering WH, Preijers FW, van Wieringen WN, et al. Flow cytometric CD34⁺ stem cell enumeration: lessons from nine years' external quality assessment within the Benelux countries. *Cytometry B Clin Cytom*. 2007;72:178-188.
 60. International Organization for Standardization (ISO). *EN ISO 15189-Medical Laboratories_Requirements for Quality and Competence*. 3rd ed. ISO; 2012.

Novel strategy to improve hepatocyte differentiation stability through synchronized behavior-driven mechanical memory of iPSCs

Mee-Hae Kim¹  | Naruchit Thanuthanakhun¹ | Masahiro Kino-oka^{1,2} 

¹Department of Biotechnology, Graduate School of Engineering, Osaka University, Suita, Osaka, Japan

²Research Base for Cell Manufacturability, Osaka University, Suita, Osaka, Japan

Correspondence

Mee-Hae Kim, Department of Biotechnology, Graduate School of Engineering, Osaka University, 2-1 Yamadaoka, Suita, Osaka, 565-0871, Japan.

Email: mh-kim@bio.eng.osaka-u.ac.jp

Funding information

Japan Agency for Medical Research and Development, Grant/Award Number: JP19be064001

Abstract

Cellular homeostasis is assumed to be regulated by the coordination of dynamic behaviors. Lack of efficient methods for synchronizing large quantities of cells makes studying cell culture strategies for bioprocess development challenging. Here, we demonstrate a novel application of botulinum hemagglutinin (HA), an E-cadherin function-blocking agent, to synchronize behavior-driven mechanical memory in human induced pluripotent stem cell (hiPSC) cultures. Application of HA to hiPSCs resulted in a decrease in actin bundling and disruption of colony formation in a concentration- and time-dependent manner. Interestingly, cytoskeleton rearrangement in cells with prolonged exposure to HA resulted in mechanical memory synchronization with Yes-associated protein, which increased pluripotent cell homogeneity. Synchronized hiPSCs have higher capability to differentiate into functional hepatocytes than unsynchronized hiPSCs, resulting in improved efficiency and robustness of hepatocyte differentiation. Thus, our strategy for cell behavior synchronization before differentiation induction provides an approach against the instability of differentiation of pluripotent cells.

KEYWORDS

botulinum hemagglutinin, cell behavior, hepatocyte differentiation, human induced pluripotent stem cells, mechanical memory, synchronization

1 | INTRODUCTION

Human pluripotent stem cells (hPSCs), including embryonic stem cells (hESCs) and induced pluripotent stem cells (hiPSCs), have promising clinical and industrial applications, including disease modeling, drug discovery, and the development of cell therapies, due to their capacity to self-renew and differentiate into specialized cell types (Takahashi & Yamanaka, 2006; Thomson et al., 1998). However, the development of cell culture strategies for bioprocessing remains challenging owing to the lack of efficient methods for synchronizing cell behavior in large numbers of cultured cells. The behavioral

alteration of cells in growing colonies and their interaction with other colonies lead to a spontaneous emergence of mechanical heterogeneity during hPSC expansion (Adewumi et al., 2007; Rosowski et al., 2015; Shuzui, Kim, & Kino-oka, et al., 2019; Wang, Qin, et al., 2016). It has recently been demonstrated that cell mechanical properties and the associated forces in the intracellular cytoskeleton are critical elements in mechanochemical signaling pathways, which play a major role in regulating stem cell self-renewal as well as lineage specification (Lian et al., 2010; Smith et al., 2018). In hPSC cultures, cells adhere to their neighbors through intercellular adhesion complexes, and the intercellular adhesion is accompanied with the

Mee-Hae Kim and Naruchit Thanuthanakhun contributed equally to this work as the first authors.

activity of actomyosin cytoskeleton (M.-H. Kim et al., 2021; Li et al., 2010; Thanuthanakhun et al., 2021). Mechanical forces generated by the actomyosin cytoskeleton are transmitted to the nucleus through specialized proteins that comprise the linker between the nucleus and the cytoskeleton complex (Hoffman et al., 2020; Ingber, 2006; Li et al., 2010). Mechanical signals can be transferred directly to chromatin through this direct connection (Uhler & Shivashankar, 2017). The chromatin undergoes epigenetic modifications and physical deformation of the nuclear envelope due to contractile forces, resulting in alterations in gene expression (Alisafaei et al., 2019; Bar-Nur et al., 2011; Price et al., 2021). Recent evidence suggests that mechanical and biochemical signals originated from cell–cell adhesion are critical for stem cell fate determination within cultures (Y. Kim et al., 2022; Yang et al., 2014; Zhang et al., 2021). Mechanical transduction may lead to the activation of key signaling pathways and trigger cell behavioral changes, potentially affecting cultured cell properties. Yes-associated protein (YAP), an important transcription factor downstream of the cytoskeletal signaling pathway, is known to play a vital role in cell mechanotransduction (Driscoll et al., 2015; Dupont et al., 2011; Halder et al., 2012). There is compelling evidence for the role of activated YAP mechano-regulated proteins as a mediator in the effect of environmental mechanical cues on the fate of human mesenchymal stem cells (hMSCs) toward adipogenic and osteogenic differentiation (Yang et al., 2014; Zhang et al., 2021). This phenomenon is often termed “mechanical memory” in hMSCs via nuclear YAP localization. The mechanical memory is erased by the HAVDI adhesive motif of N-cadherin (Zhang et al., 2021). Furthermore, this suggests that in cell–cell interactions, N-cadherin induces a mechanical erasing effect in hMSCs by restoring YAP to the cytoplasm. The mechanisms driving such complex spatiotemporal mechano-responses clearly affect YAP localization, but have not been studied in the context of “behavior-driven mechanical memory” following culture.

E-cadherin-mediated cell–cell adhesion has been shown to play an important role in collective cell migration because cell–cell junctions allow close coupling of physical forces and mechanical signaling between cells (Li et al., 2010; Rosowski et al., 2015; Soncin & Ward, 2011). Regulating E-cadherin-mediated adhesion at cell–cell junctions has attracted attention in several studies, with potential implications for improving paracellular delivery across biological barriers (intestinal mucosa and blood–brain barrier) and understanding the mechanisms of cadherin-mediated interactions at intercellular junctions (Lee et al., 2014; Sugawara et al., 2014). E-cadherin has also been shown to play an important role in regulating stem cell pluripotency and the processes of early differentiation (Soncin & Ward, 2011; Sun et al., 2012). Botulinum hemagglutinin (HA) is a component of the large botulinum neurotoxin complex, and its significance in disrupting E-cadherin-mediated adhesion junctions has become clear (Lee et al., 2014; Sugawara et al., 2014). HA is functionally and structurally separable into two parts: HA1, which recognizes cell-surface carbohydrates; and HA2–HA3, which disrupts the paracellular barrier through E-cadherin binding. It has been established that HA binds to E-cadherin with high specificity, involving

extensive intermolecular interactions, as well as cell-surface carbohydrates, and that these interactions disrupt E-cadherin-mediated cell–cell adhesion (Lee et al., 2014; Sugawara et al., 2014). Based on previous studies, we developed a culture strategy for expanding hiPSCs using HA-mediated regulation of cell behavior (M.-H. Kim et al., 2017, 2018; Shuzui, Kim, Azuma, et al., 2019). Although it has long been postulated that cell behaviors influence a variety of cellular functions (M.-H. Kim & Kino-oka, 2015; M.-H. Kim et al., 2014), designing efficient synchronization tools could be a useful culture strategy for improving robust and reproducible cell production. In this study, we established a simple method for achieving the synchronization of cell behavior-driven mechanical memory derived from hiPSC culture, which in turn promotes trilineage differentiation potential as well as functional differentiation. We also demonstrated how the synchronization strategy provides more uniform differentiation and improved efficacy than differentiation medium alone. To the best of our knowledge, this is the first report of the synchronization of behavior-driven mechanical memory with targeted differentiation. We anticipate that this method can greatly improve the mechanical homogeneity of many cell culture systems to better regulate stem cell self-renewal as well as lineage specification.

2 | MATERIALS AND METHODS

2.1 | Culture of hiPSCs

The hiPSC line, 1383D2, was provided by the Center for iPS Cell Research and Application, Kyoto University. Cells were routinely cultured in chemically defined and animal component-free medium (StemFit AK02N; Ajinomoto Co, Inc) on laminin 511-E8-coated dishes (iMatrix-511; Nippi, Inc) according to previously published protocols for hiPSC culture (Nakagawa et al., 2015). Cells were cultured at 37°C in a humidified atmosphere containing 5% CO₂. Cells were passaged as single cells every 4 days using TrypLE™ Select. Cells were seeded at a density of 7.5×10^3 cells/cm² in the presence of a Rho-associated coiled-coil containing protein kinase (ROCK) inhibitor (Y-27632; Fujifilm Wako Chemical Corporation) at 10 μM. The medium was replaced every 24 h post-seeding with fresh medium without ROCK inhibitor.

2.2 | Reconstitution of the functional HA complex

The production and characterization of the functional HA complex have previously been described (Sugawara et al., 2014). Briefly, each HA subcomponent (HA1, HA2, and HA3) was expressed separately in *Escherichia coli* and purified. For reconstitution of the HA complex, purified recombinant HA1, HA2, and HA3 of serotype B were mixed and incubated at 37°C. Consequently, a large molecular HA complex was formed spontaneously. Purified proteins were dialyzed against phosphate-buffered saline (PBS) at pH 7.4. Protein concentration was determined using the bicinchoninic acid (BCA) protein assay reagent (Thermo Fisher Scientific).

2.3 | Synchronization of cells using HA and hepatocyte differentiation

For cell synchronization, hiPSCs were seeded at a cell density of 2.5×10^3 cells/cm² in plates coated with iMatrix-511 (0.25 µg/cm²) in StemFit AK02N medium supplemented with 10 µM ROCK inhibitor, and the cells were exposed to different concentrations of HA (0, 1, 5, and 10 nM) once a day for 3 consecutive days before the end of the 5-day culture period.

Hepatocyte differentiation was performed as previously described (Kajiwara et al., 2012), with minor modifications. On the first day of differentiation, synchronized hiPSCs were induced to differentiate without passaging by directly replacing the StemFit AK02N medium with RPMI1640 medium (Nacalai Tesque) containing $1 \times$ B27 supplement (Thermo Fisher Scientific), 100 ng/ml activin A, and 50 ng/ml Wnt3a (R&D Systems), and maintained for 3 days. The culture medium was supplemented with 0.5 mM NaB (Sigma) on Days 2 and 3 of differentiation. In stage 2, hepatic specification was stimulated by switching the medium to knock-out DMEM containing 20% knockout serum replacement, 1 mM L-glutamine, 1% nonessential amino acids, 0.1 mM 2-mercaptoethanol (Invitrogen), and 1% DMSO (Sigma) for 7 days. In stage 3, the cells were cultured in hepatocyte culture medium (Lonza) supplemented with 20 ng/ml hepatocyte growth factor and 20 ng/ml oncostatin M (PeproTech) for another 7 days. The medium was changed daily during differentiation.

2.4 | Time-lapse observation

To monitor the expansion and differentiation of hiPSCs in the monolayer culture, we used a phase-contrast time-lapse observation incubator (BioStudio T, Nikon) equipped with a camera for video imaging.

2.5 | Immunofluorescence staining

The immunofluorescence staining procedure was similar to that previously described (M.-H. Kim et al., 2017; Thanuthanakhun et al., 2021). The cells were rinsed with PBS and fixed for 10 min at room temperature with 4% paraformaldehyde (Fujifilm Wako Chemical Corporation). After washing with PBS, cells were permeabilized for 5 min at room temperature with 0.25% Triton X-100. The specimens were then blocked with Block Ace (Dainippon Sumitomo Pharma Co, Ltd) for 1 h at room temperature, followed by overnight incubation with primary antibodies at 4°C. The primary and secondary antibodies used in this study are listed in Supporting Information: Table S1. The cells were washed with Tris-buffered saline (TBS) and probed with Alexa Fluor 488-conjugated goat anti-rabbit or Alexa Fluor 594-conjugated goat anti-mouse IgG secondary antibodies (Life Technologies) for 1 h at room temperature. Nuclei were stained with 4,6-diamidino-2-phenylindole (DAPI; Life Technologies). Images were obtained using an IN Cell Analyzer (6000; GE Healthcare Life Sciences) and confocal laser scanning microscope (FV-1000; Olympus).

2.6 | YAP nuclear-to-cytoplasmic ratio quantification

The ratio of nuclear-to-cytoplasmic YAP intensity was computed using image analysis software (CellProfiler) to measure the levels of nuclear-to-cytoplasmic YAP localization, as previously described (Wang, Sinnott-Smith, et al., 2016). Single slices of confocal images of YAP and DAPI were used for the analysis. DAPI was used to determine the nuclear area. The cytoplasmic area was defined as the perinuclear region of a 5-pixel-wide ring, adjacent to the nuclear border. The mean fluorescence intensity of YAP inside the nuclear and cytoplasmic areas was assessed individually in each cell to estimate the nuclear to cytoplasmic YAP ratio.

2.7 | Western blot analysis

The procedure used for western blot analysis was similar to that previously described (M.-H. Kim et al., 2021). Whole-cell proteins were isolated using RIPA lysis buffer (Sigma-Aldrich) supplemented with a protease and phosphatase inhibitor cocktail (Thermo Fisher Scientific). Nuclear and cytoplasmic proteins were isolated according to the manufacturer's instructions using a nuclear extraction kit (Abcam). Total protein concentration was measured using the BCA protein assay reagent (Thermo Fisher Scientific, USA). Protein lysates were separated by sodium dodecyl sulfate-polyacrylamide gel electrophoresis and transferred onto a polyvinylidene difluoride membrane. The membranes were blocked using TBS containing 5% milk powder for 1 h at room temperature and then incubated with primary antibodies overnight at 4°C. The primary and secondary antibodies used in this study are listed in Supporting Information: Table S1. After washing with TBS containing 0.1% Tween-20 (TBS-T), the blots were incubated with the secondary antibodies DyLight 800 and StarBright 700 (BioRad) for 1 h at room temperature and then washed with TBS-T. Protein bands were detected and quantified using ChemiDoc Touch MP (Bio-Rad). β-actin was used as the internal loading control.

2.8 | Quantitative reverse transcription-polymerase chain reaction (qRT-PCR)

The expression levels of stem cell-specific and lineage-specific transcripts were analyzed using qRT-PCR. Total RNA was extracted from cells using an RNeasy Mini Kit (Qiagen) according to the manufacturer's instructions. Reverse transcription was conducted using a PrimeScript RT reagent kit (Takara Bio Inc), and real-time PCR was performed using TB Green Premix Ex Taq (Takara Bio Inc) on a 7300 real-time PCR system (Applied Biosystems). Primer sequences are listed in Supporting Information: Table S2. Data were analyzed according to the comparative C_t method and normalized to β-actin expression level within each sample. The relative expression levels of

the target genes, following normalization to an endogenous sequence, were calculated using $2^{-\Delta\Delta Ct}$.

2.9 | Albumin and urea secretion assays

The cell culture supernatants were collected at the Days 17 and 21 of the differentiation and stored at -80°C until used for assaying. The albumin (ALB) level was measured using a human albumin enzyme-linked immunosorbent assay (ELISA) quantitation kit (R&D Systems) according to the manufacturer's instructions. The urea concentration was measured using the QuantiChrom Urea Assay Kit (Bioassay Systems) according to the manufacturer's instructions. Wells without cells were used as blank controls. Flow cytometry was used to assess albumin secretion, which was standardized to the amount of albumin-positive cells in the respective wells.

2.10 | Flow cytometry

The cells were harvested and dissociated using trypsin for 10–15 min at 37°C . Dissociated single cells were fixed and permeabilized with BD Cytotfix/Cytoperm solution (BD Biosciences) for 30 min at 4°C . The cell suspension was then incubated with fluorescence-conjugated antibodies for 30 min at 4°C in the dark. The antibodies used in this study were PE anti-ALB and Alexa Fluor 488 anti-alpha-fetoprotein (AFP) (R&D Systems). The stained cells were washed and resuspended in PBS containing 2% fetal bovine serum (FBS). Flow cytometry was performed using the Partec Cyflow Cube 6 (Sysmex). The data was analyzed using FlowLogic version 7.3.

2.11 | Analysis of intra-run and inter-run variability

The intra- and inter-run variations were evaluated using the coefficient of variation (CV%; standard deviation divided by the mean). The intra-run variation was determined from 10 culture wells in a single experimental run by calculating the mean, standard deviation (SD), and CV%. The inter-run variation, on the other hand, was calculated from three experimental runs by calculating the mean, SD, and CV%.

2.12 | Statistical analysis

All experimental data is expressed as mean \pm SD. For comparisons between multiple groups, significant differences were determined using one-way analysis of variance (one-way analysis of variance [ANOVA]) followed by post-hoc testing with Tukey's test. Student's *t*-test was used for comparisons between groups. The significance thresholds were $**p < 0.01$ and $*p < 0.05$.

3 | RESULTS

3.1 | HA can be used to improve homogeneity of pluripotent stem cells

To understand how HA affects the cell morphology and colony behavior of hiPSCs, we cultured hiPSCs in maintenance media for 2 days before adding 10 nM HA (Figure 1a). Time-lapse observation revealed that the cell and colony morphologies were drastically changed with the addition of HA compared to the control (Supporting Information: Movie S1 and Figure 1b). In the unexposed (control) culture, most cells started to adhere to the surface and formed colonies within a minimum of 2 days after cell seeding. As the culture proceeded, the colonies grew larger, more densely packed and expanded. As the culture became denser, some colonies merged into a monolayer. These observations revealed significant spatial heterogeneity in the culture vessel at the end of 5-day culture.

For single HA exposure, the 2-day cultured cells were exposed to HA once for 24 h and changed with fresh medium that did not contain HA to remove them from the medium. HA treatment induced random cell migration; cells could move individually, establish transient contacts with other cells, or migrate as a group (Supporting Information: Movie S1 and Figure 1b). They exhibited scattering morphology in individual cells and were dispersed through migration, forming loosely populated colonies. Following routine medium change after 24 h, the intercellular spaces within the culture vessel were filled with dividing neighboring cells and subsequently formed a tight monolayer after prolonged incubation, suggesting that the cells' adhesive activity could be recovered over time. For repeated HA exposure, the cells were exposed to HA every day from 2 to 5 days of culture. As a result of HA exposure, the colonies were scattered in a confluent monolayer, and behavioral changes occurred repeatedly (Supporting Information: Movie S1 and Figure 1b,c). Cells reformed adhesions with neighboring cells, continually grew as the culture progressed, and reached confluency faster within 5 days of culture.

Next, we assessed the pluripotency and differentiation potential of cultured hiPSCs under both culture conditions using RT-PCR analysis. We found that the expression of pluripotency-specific genes as well as endoderm-, mesoderm-, and ectoderm-specific genes was maintained or upregulated in HA-exposed cells compared to the control. These cells were also positively stained with PAX6, Brachyury, and SOX17, which represent the expression of ectoderm, mesoderm, and endoderm markers, respectively (Supporting Information: Figure S1). Additionally, flow cytometry analysis was performed to determine the percentage of cells that expressed pluripotency-associated markers OCT3/4 and SSEA4 (Figure 1c,d). Given the similar yields of total cells (Figure 1f), the percentage of OCT3/4/SSEA4-double positive cells in culture after repeated HA exposure appeared to be of high purity ($>98\%$) and was found slightly higher than that in the control culture (Figure 1e). Taken together, these data suggest that modifying behavioral patterns during hiPSC expansion using HA can improve the production of homogeneous cells without losing pluripotency.

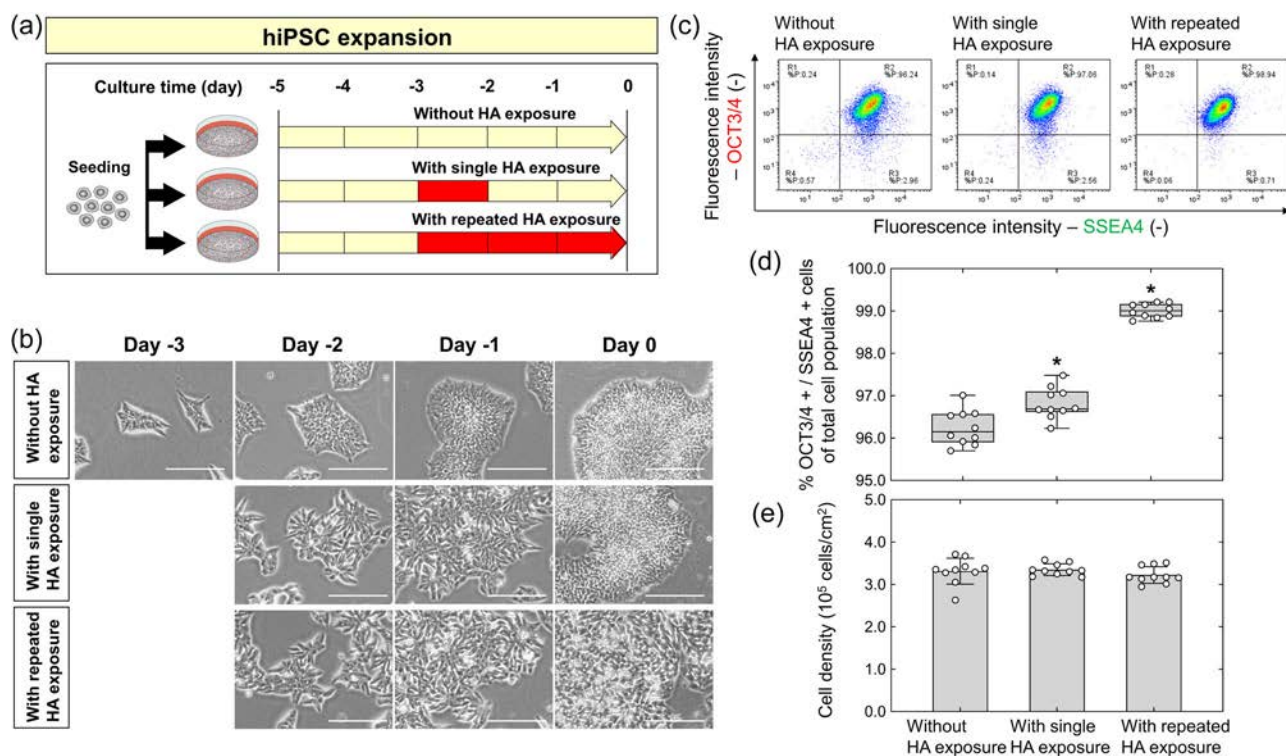


FIGURE 1 HA-mediated regulation of cell behaviors improves the homogeneity in hiPSC pluripotency. (a) Experimental scheme to examine the impact of single and repeated HA exposure in hiPSC culture. Cells were seeded and cultured for 5 days in stem cell maintenance medium, without HA exposure, with 10 nM HA exposure once on Day -3 (single exposure), or with HA exposure once a day for 3 consecutive days from Day -3 to Day 0 (repeated exposure). (b) Morphological characteristics of hiPSCs following single and repeated HA exposure. Scale bar, 200 μ m. (c) Flow cytometry analysis of pluripotency markers (OCT3/4 and SSEA4) of hiPSCs measured at Day 0 following single and repeated HA exposure. (d) Percentage of OCT3/4/SSEA4 double-positive cells measured at Day 0 following single and repeated HA exposure. (e) Cell density measured at Day 0 following single and repeated exposure to HA. Data in (c) and (e) is presented as the mean \pm SD ($n = 10$). Significance was determined using one-way analysis of variance with Tukey's test ($*p < 0.01$, compared to control). HA, hemagglutinin; n.s., non-significant.

3.2 | Temporal disruption of E-cadherin adhesion induces actin cytoskeleton rearrangement

To verify whether HA exposure alters E-cadherin-mediated cell-cell adhesion and cytoskeletal formation in hiPSCs, we performed immunofluorescence staining of cells grown under the same conditions as shown in Figure 1a. Time-course observation of F-actin and E-cadherin revealed E-cadherin localization with F-actin at cell-cell contacts at 3 days of culture (at Day -2) as cells grew as small clusters, and E-cadherin was strongly enriched at cell-cell contact sites at the end of culture (at Day 0) when the cells reached confluence. The actin belt was disrupted locally by HA treatment, but the majority of the belt remained intact at cell-cell boundaries (Figure 2a). Intriguingly, E-cadherin displayed reduced expression at cell-cell contacts, and actin rings formed and colocalized with weakening E-cadherin in hiPSCs. For a single exposure to HA, only a transient effect was observed which allows the rescue of E-cadherin at cell-cell junctions, and the actin-formed ring-like structures visibly recovered. Repeated HA exposure maintained structural changes in E-cadherin and actin filaments at cell-cell contact sites by the end of culture (at Day 0).

Representative immunostaining images from the control culture, labeled with elapsed time, indicated that the distribution and deformation of nuclei in the horizontal images increased, and tightly packed nuclei were observed in cross-sectional images during hiPSC culture (Figure 2b). Cell nuclei in the confluent monolayer partially overlapped at the end of the culture period (at Day 0). In comparison to the control, cells treated with HA had flatter nuclear morphologies and a more uniform distribution of cells.

Subsequently, we used western blot analysis to investigate the changes in the mechanical behavioral properties of cell-cell and cell-substrate adhesion molecules, E-cadherin and integrin $\beta 1$. E-cadherin protein levels remained constant over time, whereas integrin $\beta 1$ levels increased over time (Figure 2c). Changes in E-cadherin and integrin $\beta 1$ were found at similar levels in hiPSC cultures regardless of HA exposure. These results suggest that HA regulates the actin cytoskeleton and E-cadherin-based adhesion junctions of hiPSCs but has no effect on protein abundance. Together with the effects of HA on the actin cytoskeleton, we conclude that HA modulates the disruption of cadherin-dependent cell-cell adhesions and cell spatial distribution through cytoskeletal rearrangement.

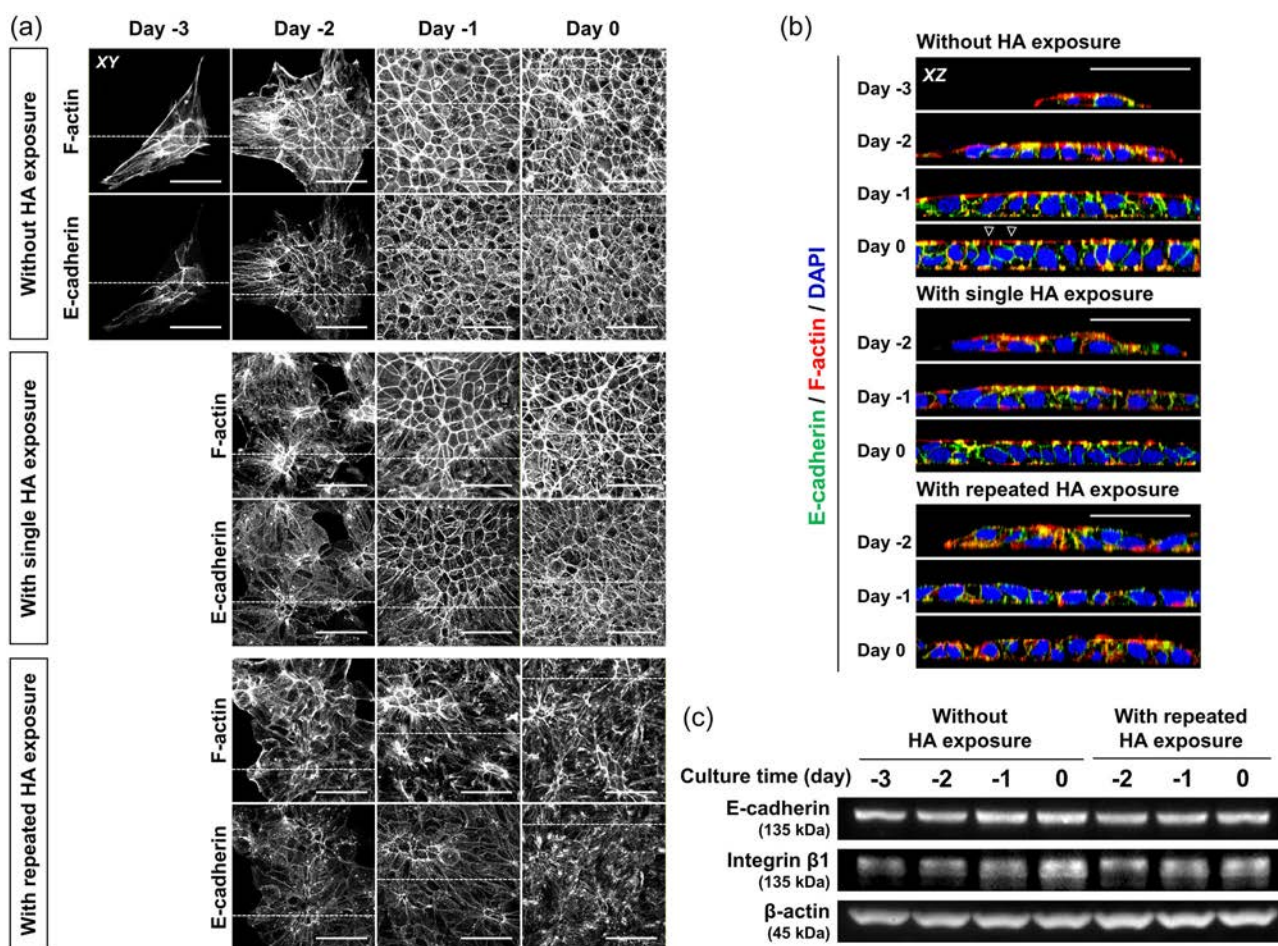


FIGURE 2 HA-mediated regulation of cell-cell adhesion induces rearrangement of actin cytoskeleton in an exposure duration-dependent manner. (a) Fluorescence staining images in the XY plane showing F-actin and E-cadherin in hiPSCs following single and repeated exposure to 10 nM HA. Scale bar, 50 μm. (b) Reconstruction images (XZ plane) showing the F-actin (red) and E-cadherin (green) at the location of the yellow dashed line shown in each XY image in (a). Nuclei (blue) were stained with DAPI. Arrowheads indicate partially overlapped nuclei. Scale bar, 50 μm. (c) Western blot analysis showing levels of E-cadherin and integrin β1 in hiPSC culture with or without HA exposure. β-actin was used as a loading control. The HA was repeatedly exposed to cells from Day -3 to Day 0. DAPI, 4,6-diamidino-2-phenylindole; HA, hemagglutinin; hiPSCs, human induced pluripotent stem cell.

3.3 | Actomyosin cytoskeleton rearrangement synchronizes mechanical memory with YAP acting

To test whether HA-mediated actomyosin cytoskeleton rearrangement affects mechanical memory with YAP activity, we used immunofluorescence staining to examine the cellular localization of YAP. After 3 days of culture (at Day -2), as cells grew as small clusters, YAP was mainly distributed in the nucleus, but mainly accumulated in the nucleus with a lesser cytoplasmic presence by the end of culture (at Day 0), when the cells reached confluence (Figure 3a). Interestingly, YAP was translocated into the cytoplasm region following HA exposure. After repeated exposure to HA, YAP was found distributed in both cytoplasmic and nuclear regions at Day 0. Quantitative analysis of the nuclear-to-cytoplasmic (N/C) ratio of YAP showed its apparent decrease over time in all culture conditions (Figure 3b). In the control culture, the range of distribution of the YAP N/C ratio increased gradually with cell density, resulting in

heterogeneity in mechanical memory via YAP location. HA treatment significantly reduced the YAP N/C ratio over time and became close to 0 at the end of culture (Figure 3c). In addition, the distribution of the YAP N/C ratio had a narrow range compared to that in the control culture. These results indicate that the synchronization effect of HA on YAP localization increased in cells with repeated exposure to HA.

YAP activity is regulated by nuclear-cytoplasmic shuttling through phosphorylation-dependent manner (Wang, Sinnott-Smith, et al., 2016). Western blot analysis demonstrated that HA treatment resulted in increased YAP phosphorylation (Figure 3d). Furthermore, YAP phosphorylation expression levels in hiPSCs were positively correlated with HA exposure duration, but YAP phosphorylation decreased on Day 0, when the cells reached confluence.

To further investigate whether the rearrangement of the actin cytoskeleton and E-cadherin-based adhesion junction of hiPSCs by HA exposure correlates with cytoskeletal contraction, we investigated the phosphorylation of the myosin light chain

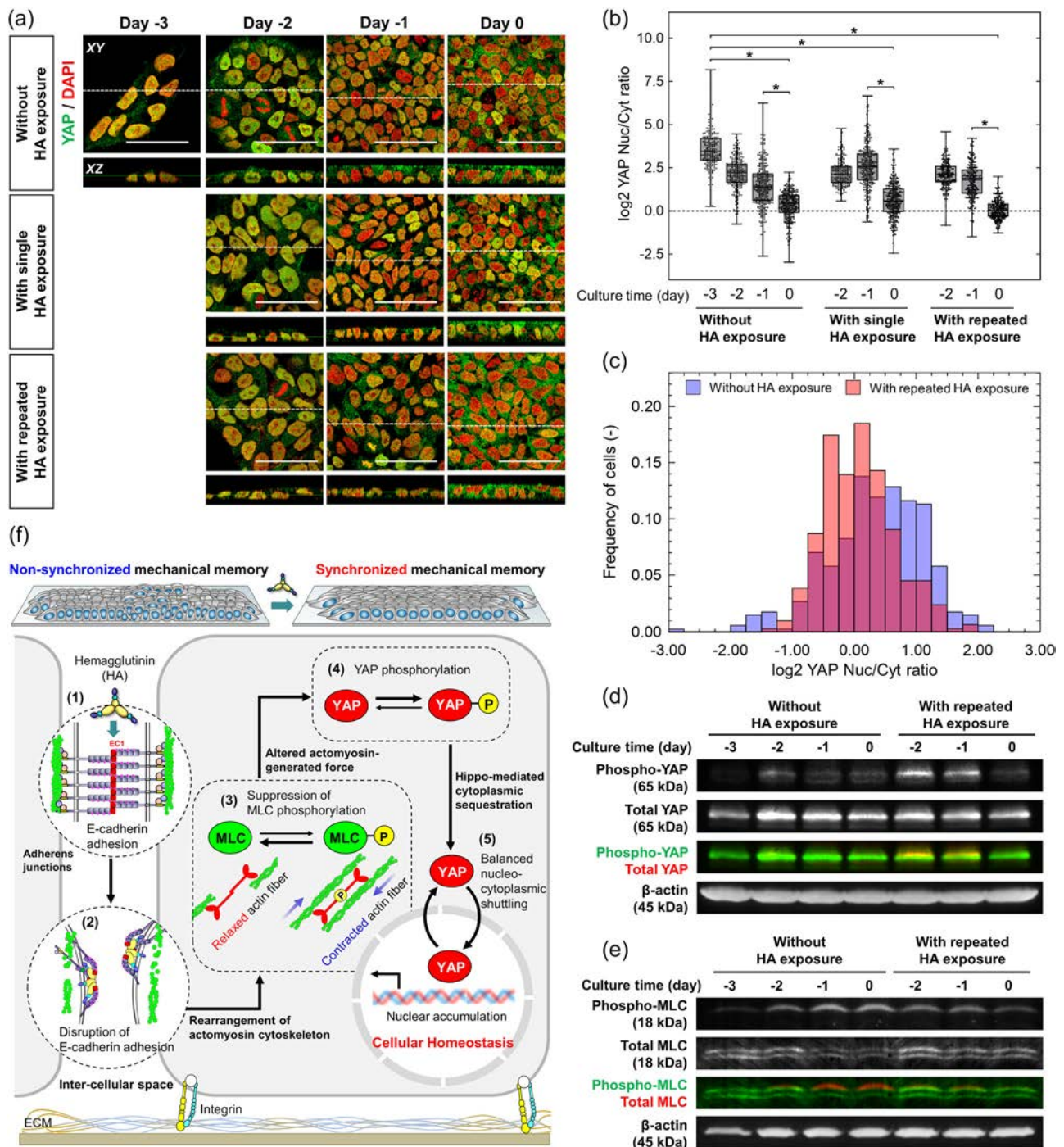


FIGURE 3 Repeated HA exposure efficiently synchronizes the nuclear-cytoplasmic translocation of YAP. (a) Immunofluorescence staining images of YAP in hiPSCs following single and repeated exposure to HA. Single-section images in the XY and XZ planes were displayed in the top and bottom panels, respectively. A white dashed line indicates the location of the XZ image plane; conversely, a green solid line indicates the location of the XY image plane. Nuclei (red) were stained with DAPI. Scale bar, 50 μm. (b) Boxplot (with whiskers showing the minimum and maximum values) of YAP nuclear-to-cytoplasmic (N/C) ratio (log₂) corresponding to quantification of (a) ($n = 206\text{--}355$ cells per conditions). Significance was determined by one-way analysis of variance with Tukey's test (** $p < 0.01$, compared to control). A YAP N/C ratio (log₂) of 0 indicates that the intensity of the YAP signal in the nucleus and cytoplasm is the same. When the YAP N/C ratio (log₂) is >0 , YAP is predominantly nuclear. (c) Frequency of cells showing YAP N/C ratio (log₂) at Day 0 of hiPSC cultures with or without HA exposure corresponding to quantification of (b). The HA was repeatedly exposed to cells from Day -3 to Day 0. (d) Western blot analysis showing levels of phosphorylated YAP and total YAP in hiPSC cultures with or without HA exposure. β-actin was used as a loading control. The HA was repeatedly exposed to cells from Day -3 to Day 0. (e) Western blot analysis showing levels of phosphorylated MLC and total MLC in hiPSC culture with or without HA exposure. β-actin was used as a loading control. The HA was repeatedly exposed to cells from Day -3 to Day 0. (f) Schematic drawing our hypothesis on the mechanism by which HA induces the synchronization of mechanical memory in hiPSC culture. DAPI, 4,6-diamidino-2-phenylindole; HA, hemagglutinin; hiPSCs, human induced pluripotent stem cells; MLC, myosin light chain.

(MLC), which is the main regulatory event leading to actomyosin contractility, by western blot analysis. We found that the levels of MLC phosphorylation were significantly higher after 3 days of culture (at Day -2), and that they were sustained at the end of culture (at Day 0) (Figure 3e). MLC phosphorylation on the other hand, was suppressed during repeated HA exposure. Taken together, these results indicate that cells with repeated HA exposure effectively synchronized mechanical memory via YAP localization. In a YAP phosphorylation-dependent manner, HA induces cytoplasmic YAP translocation (Figure 3f).

3.4 | Synchronized mechanical memory enhances hepatocytes differentiation stability

HiPSCs were treated with different concentrations of HA for 3 days before culturing for 21 days in hepatocyte differentiation medium to test the functional role of synchronized mechanical memory with YAP in regulating cell differentiation (Figure 4a). When the cell colonies were treated with HA, they scattered through migration within the culture vessel compared with the control (Supporting Information: Movie S2 and Figure 4b). Cells showed loosening of cell-cell adhesion and colony compaction in a concentration-dependent manner. The majority of cells in these colonies expressed the pluripotency marker OCT3/4, indicating the undifferentiated state of hiPSCs at the start of differentiation (Figure 5).

To induce direct differentiation of hiPSCs into hepatocytes, we adopted a modified protocol from a previous study (Kajiwara et al., 2012). Hepatocyte differentiation shown by the results of immunofluorescence staining was also confirmed by quantitative RT-PCR analysis of various stage-specific genes. After Day 1 in the control culture, heterogeneous cells with different morphologies were observed (Supporting Information: Movie S2), followed by the formation of a definite endoderm after 3 days (Figures 4c and 5). These cells began to express the definitive endodermal marker SOX17 while decreasing the pluripotency marker SOX2. From Day 3 to Day 10, hepatocyte-like morphology was observed in the second and third stages of differentiation (Supporting Information: Movie S2). However, the swelling area increased from Day 10 and changed into a cystic-like structure, which mostly tended to maintain swelling at various sizes. This structure was also persistently maintained until the end of differentiation. We found that the cells were able to differentiate into hepatocyte-like cells that expressed HNF4a, as well as cholangiocyte-like cells that formed cystic-like structures and expressed SOX9, indicating that the differentiation into hepatocytes was not uniform.

Synchronized hiPSCs treated with HA rapidly acquired cuboidal morphology from Day 3 to Day 21 (Supporting Information: Movie S2). At higher HA concentrations, SOX9 was weakly expressed, whereas HNF4a was strongly expressed in most cells forming cuboidal monolayers (Figure 5). Compared with the control, synchronized hiPSCs with HA showed significantly higher expression of definitive endodermal-specific genes, such as SOX17, at Day 3

(Figure 4c). At Day 21, although insignificant, the expression of hepatocyte-associated genes (*AFP*, *ALB*, *A1AT*, *HNF4a*, *CYP3A4*, and *CYP2C9*) was increased in the synchronized hiPSCs with HA at 10 nM, compared with the control culture. Conversely, the expression of cholangiocyte-related genes (*SOX9* and *CK19*) was significantly downregulated in a concentration-dependent manner by HA. Furthermore, we showed that the earliest distinction between E- and N-cadherin localization occurred during hepatocyte differentiation (Figure 6). When monolayers of differentiated cells were organized at Days 17 and 21, N-cadherin was found to be prominently localized to the cell-cell borders of the hexagonally packed, cuboidal monolayer, and E-cadherin was also detected at regions of cell-cell contact. The localization of E-cadherin to the cell-cell boundaries of differentiating hepatocytes in vitro occurred after that of N-cadherin, indicating that the differentiation progression of hiPSCs into hepatocyte-like cells is mediated by a sequential epithelial-mesenchymal-epithelial transition.

The efficiency and reproducibility of hepatocyte differentiation in relation to the synchronization of undifferentiated hiPSCs were investigated at Days 17 and 21 of differentiation. Immunofluorescence staining demonstrated that the control culture contained a mixture of monolayered areas and proliferative regions containing cystic-like structures, while the synchronized cells with HA formed monolayers without accumulation of cysts at Day 21 (Figure 7a). The cells showed homogeneous expression of ALB and AFP, exhibiting a significant effect on hepatocyte differentiation at higher HA concentrations (10 nM). Further flow cytometry analysis of ALB and AFP expression showed that when HA-synchronized hiPSCs were differentiated, the percentage of ALB/AFP double-positive cells showed significantly higher efficiencies (Figure 7b,c). However, the percentage of ALB/AFP double-negative cells in synchronized hiPSCs was significantly reduced, suggesting that alternative nonhepatocyte differentiation pathways are suppressed.

Intra-run and inter-run variability were evaluated by the percentage of ALB/AFP double-positive cells by flow cytometry and secreted ALB and urea levels by ELISA (Figure 7d,e). In control culture, total cell numbers were significantly higher than that of hiPSCs synchronized with HA on both Days 17 and 21. The percentage of ALB/AFP double-positive cells in control culture were decreased from 38.1% to 11.5% at Day 21, suggesting that the rest of the proliferative population was consisting of transit-amplifying cells. By contrast, the percentage of ALB/AFP double-positive cells in hiPSCs synchronized with HA appeared firstly at Day 17 to be 57.7% and the level reached around 78.2% at Day 21. The percentage of ALB/AFP double-positive cells at Days 17 and 21 in the synchronized cells was 1.52- and 6.79-fold higher than that in the control culture, respectively. In addition, from Day 17 to Day 21, the percentage of ALB-negative/AFP-positive cells in synchronized cells was found not increased, indicating that the HA treatment did not delay or limit the hepatocyte differentiation progression. Albumin secretion in the synchronized cells at Days 17 and 21 was 1.31- and 1.55-fold higher than that in the control culture. In addition, urea production in the synchronized cells at Days 17 and 21 was 1.50- and 1.53-fold higher

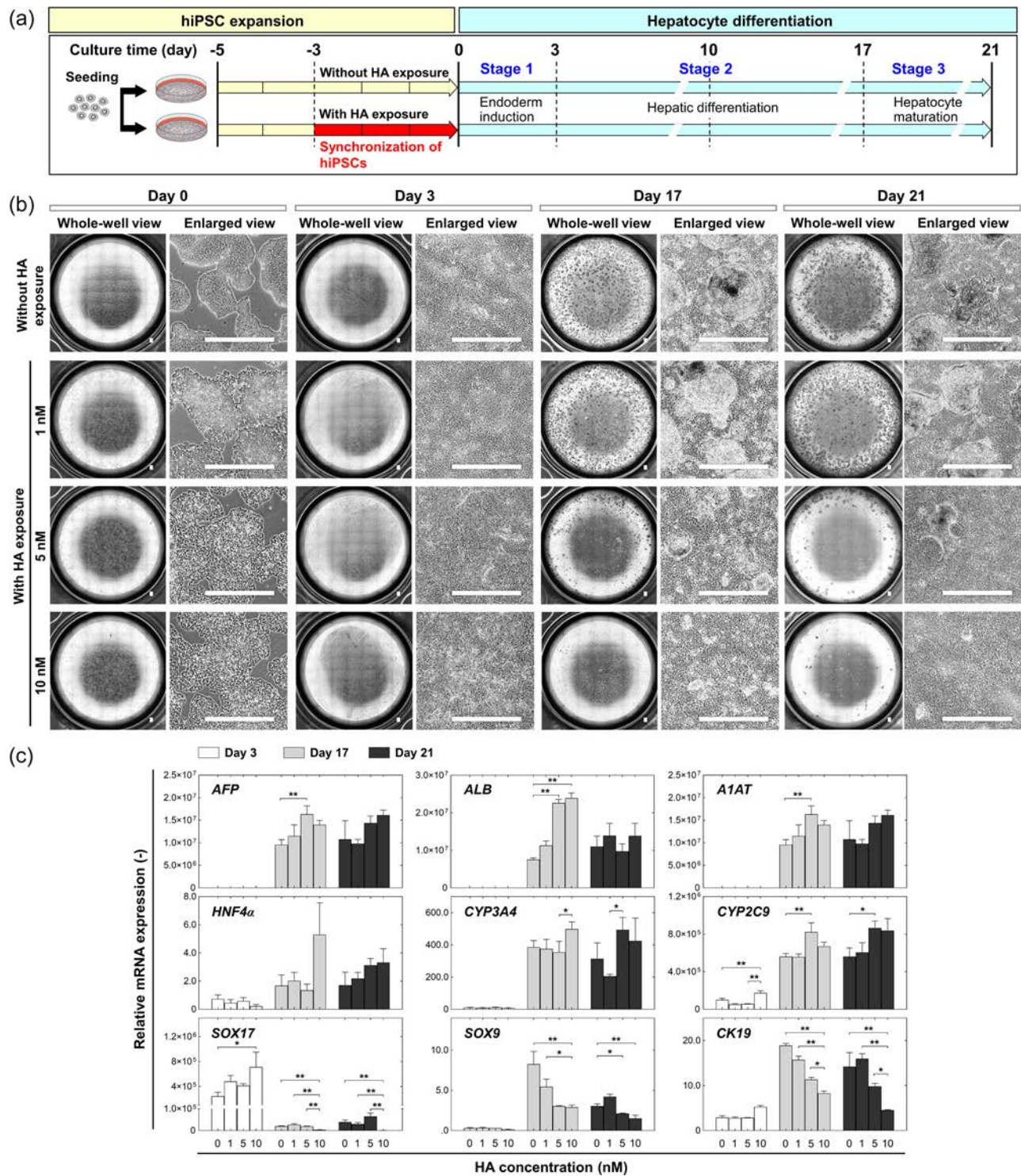


FIGURE 4 HA-mediated synchronization strategy enhances differentiation potential of hiPSCs into hepatocytes. (a) Experimental scheme of cell synchronization using HA and hepatocyte differentiation. (b) Morphological observations of synchronized hiPSCs at different time points during hepatocyte differentiation with different concentrations of HA (0, 1, 5, and 10 nM). The HA was repeatedly exposed from Day -3 to Day 0. Images are shown as the entire culture wells of a six-well plate and enlarged views. Scale bar, 1 mm. (c) Relative mRNA expression of endoderm-associated gene (*SOX17*), hepatocyte-associated genes (*AFP*, *ALB*, *A1AT*, *HNF4 α* , *CYP3A4*, and *CYP2C9*), and cholangiocyte-associated genes (*SOX9* and *CK19*) at Day 3 (open bars), Day 17 (light gray bars), and Day 21 (dark gray bars) during hepatocyte differentiation of synchronized hiPSCs with different concentration of HA (0, 1, 5, and 10 nM). Data is presented as mean \pm SD from three independent experiments. Significance was determined by one-way analysis of variance with Tukey's test (** $p < 0.01$, * $p < 0.05$, compared to control). HA, hemagglutinin; hiPSCs, human induced pluripotent stem cells; n.s., non-significant.

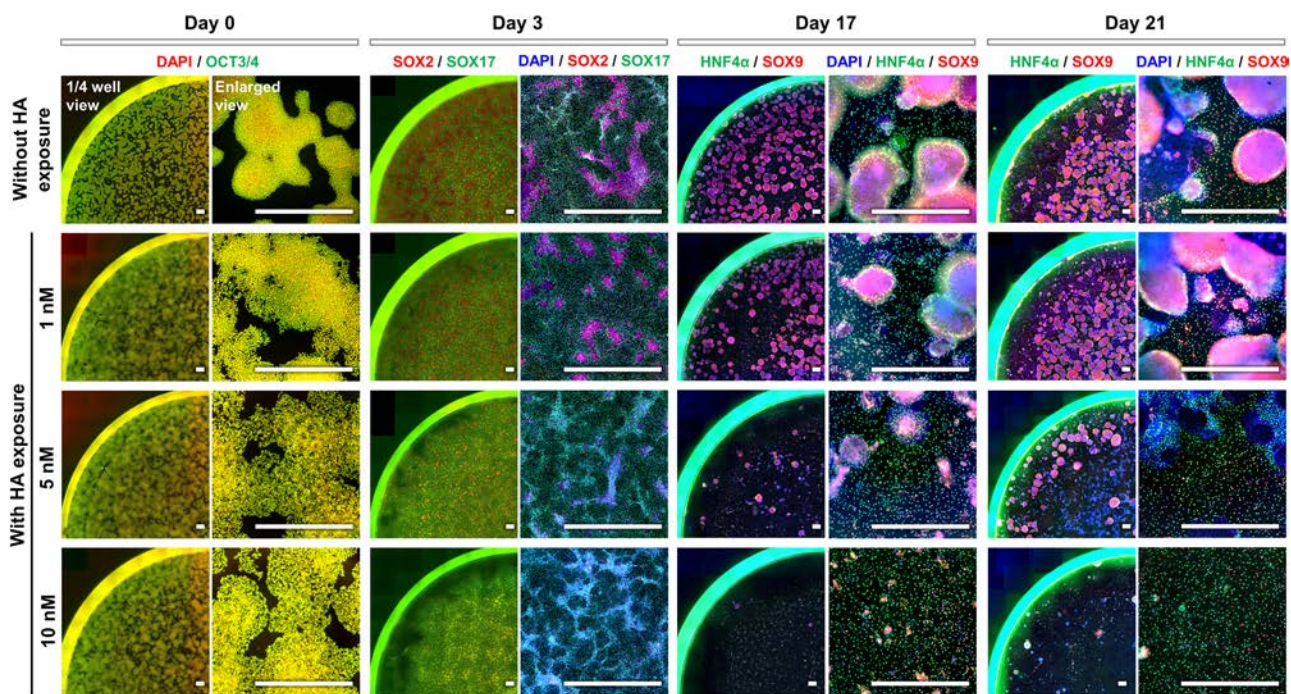


FIGURE 5 HA-mediated synchronization strategy induces highly synchronized hepatocyte differentiation. Immunofluorescence staining images of stage-specific markers during hepatocyte differentiation of synchronized hiPSCs with different concentrations of HA (0, 1, 5, and 10 nM). Stage-specific markers included the pluripotency markers (OCT3/4 and SOX2), endoderm marker (SOX17), hepatocyte marker (HNF4α) and cholangiocyte marker (SOX9). Nuclei were stained with DAPI. Images are shown as the entire culture wells of a six-well plate and enlarged views. Scale bar, 1 mm. DAPI, 4,6-diamidino-2-phenylindole; HA, hemagglutinin; hiPSCs, human induced pluripotent stem cells.

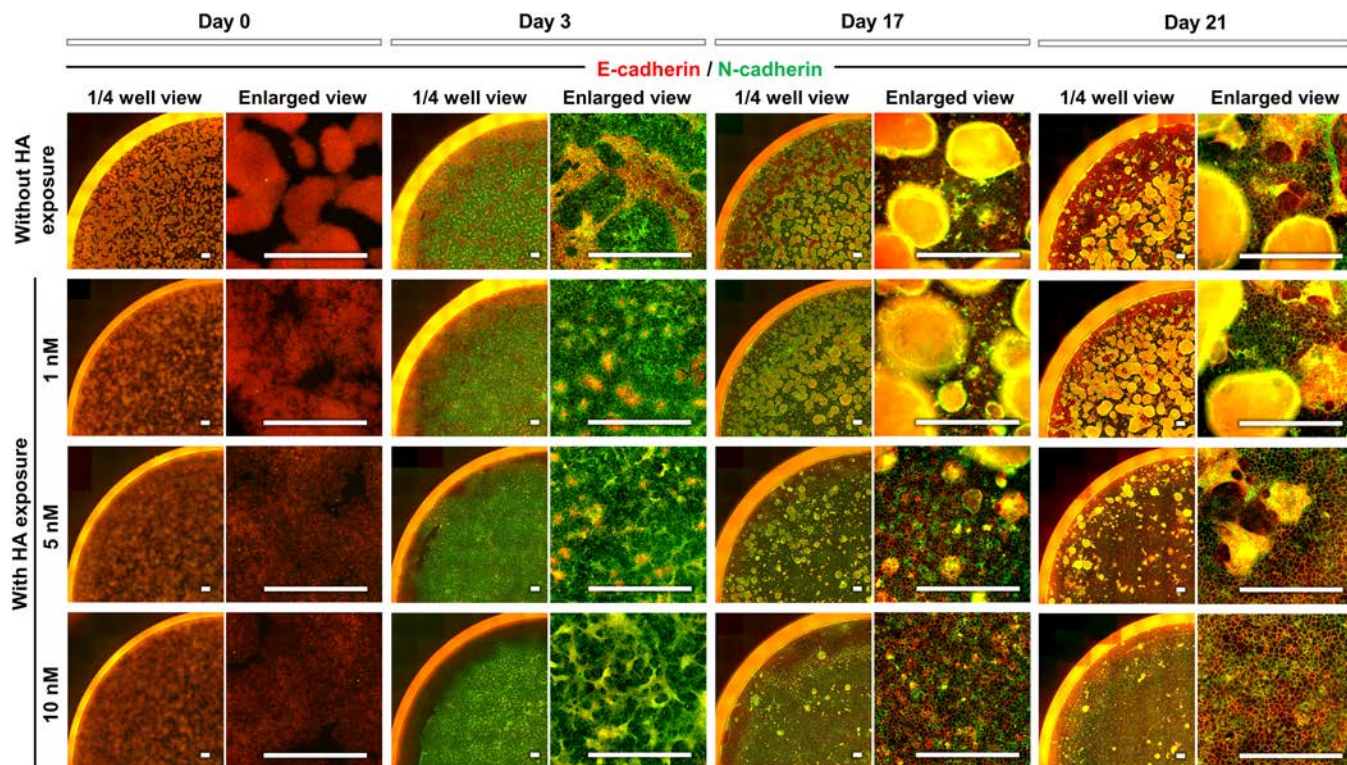


FIGURE 6 Synchronized hiPSCs using HA induce the E-cadherin and N-cadherin switch in hepatocyte differentiation. Immunofluorescence staining of E-cadherin and N-cadherin at different time points before and during hepatocyte differentiation of synchronized hiPSCs with different concentrations of HA (0, 1, 5, and 10 nM). The HA were repeatedly exposed from Day -3 to Day 0. Images are shown as one-quarter of a six-well plate and enlarged views. Scale bar, 1 mm. HA, hemagglutinin; hiPSCs, human induced pluripotent stem cells.

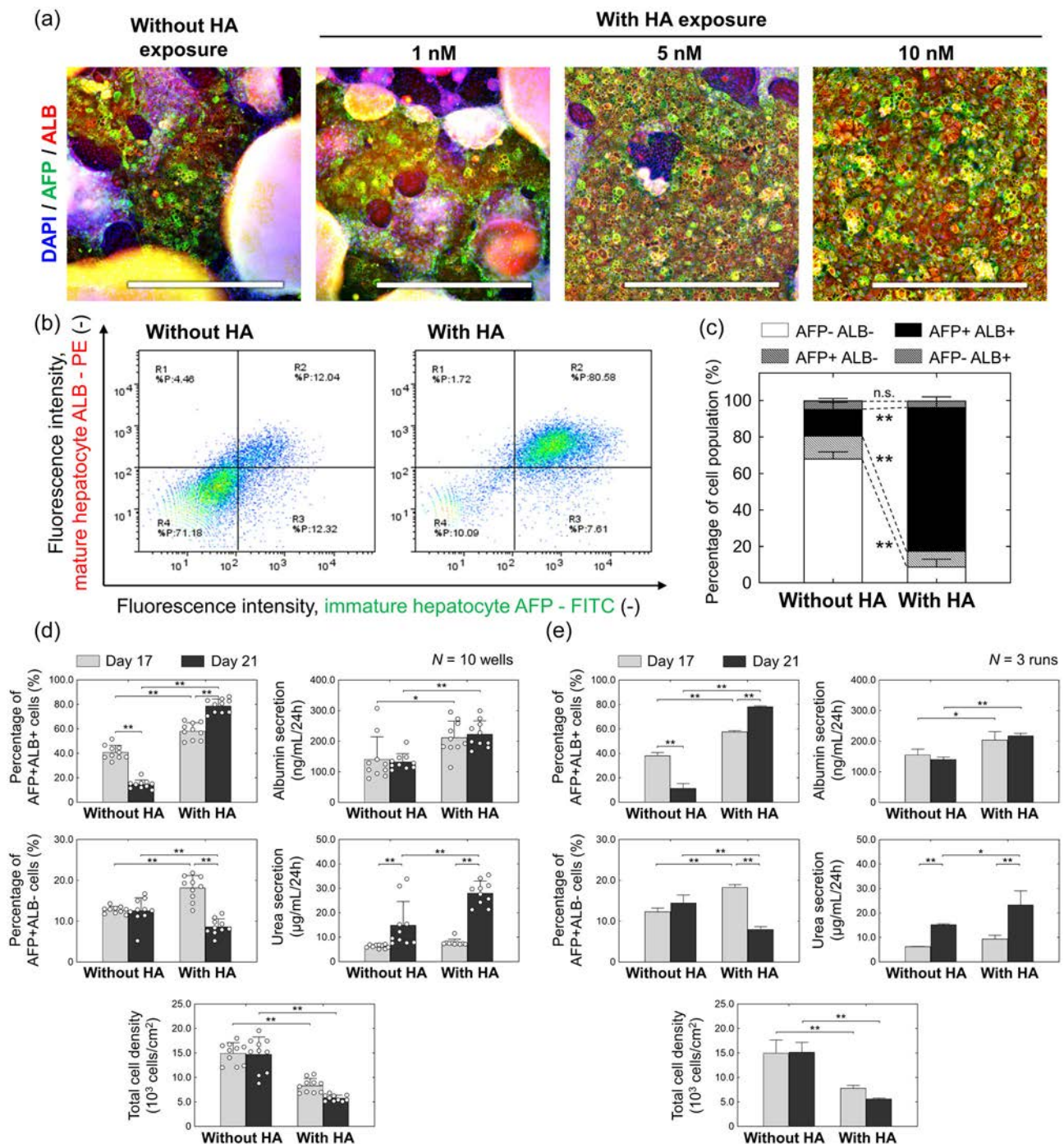


FIGURE 7 HA-mediated synchronization strategy enhances hepatocyte differentiation stability of hiPSCs. (a) Immunofluorescence staining images of the hepatocyte-specific markers (AFP and ALB) during hepatocyte differentiation of synchronized hiPSCs with HA exposure. Nuclei were stained with DAPI. Scale bar, 1 mm. (b) Representative flow cytometry histograms of the hepatocyte-specific markers (AFP and ALB) at Day 21 after differentiation of synchronized hiPSCs with 10 nM HA exposure. (c) Percentage of four different cell populations marked with AFP and ALB at Day 21 after differentiation of synchronized hiPSCs with 10 nM HA exposure. Data is presented as mean \pm SD from 10 culture wells. Significance was determined by Student's *t*-test (n.s., non-significant, ***p* < 0.01, compared to control). (d) Intra-run evaluation of total cell density, percentage of ALB/AFP double-positive cells, and amount of albumin and urea secretion at Days 17 and 21 after differentiation of synchronized hiPSCs with 10 nM HA exposure, from 10 culture wells in a single experimental run. Data is presented as mean \pm SD (*n* = 10). Significance was determined by one-way analysis of variance (ANOVA) with Tukey's test (***p* < 0.01, compared to control). (e) Inter-run evaluation of total cell density, percentage of ALB/AFP double-positive cells, and amount of albumin and urea secretion at Days 17 and 21 after differentiation of synchronized hiPSCs with 10 nM HA exposure, from three experimental runs. Data is presented as mean \pm SD (*n* = 3). Significance was determined by one-way ANOVA with Tukey's test (***p* < 0.01, **p* < 0.05, compared to control). HA, hemagglutinin; hiPSCs, human induced pluripotent stem cells.

TABLE 1 Comparison of intra-run and inter-run coefficient of variation values (CV%) between cultures without and with HA exposure

CV values		Without HA exposure				With HA exposure			
		Total cell density	Percentage of ALB/AFP-double positive cells	Albumin secretion	Urea secretion	Total cell density	Percentage of ALB/AFP-double positive cells	Albumin secretion	Urea secretion
Intra-run CV%	Day 17	8.88	13.63	41.55	11.69	10.51	13.01	22.94	17.13
	Day 21	8.54	17.18	19.62	64.92	7.85	6.19	17.18	17.60
Inter-run CV%	Day 17	17.80	6.89	11.70	0.33	7.00	1.56	13.15	15.92
	Day 21	13.19	32.61	5.23	2.24	2.46	0.79	3.36	24.62

Note: The intra-run and inter-run CV% were calculated from data in Figure 5d,e, respectively. The intra-run CV% is an expression of culture-to-culture consistency calculated from 10 culture wells in a single experimental run. The inter-run CV% is an expression of run-to-run consistency calculated from the three experimental runs.

than that in the control culture. These results indicate a gradual functional maturation from hiPSCs to hepatocyte-like cells. Intra-run and inter-run CV% values obtained in synchronized hiPSCs with HA were lower than those in the control (Table 1). The intra-run CV% values for percentage of ALB/AFP double-positive cells in synchronized hiPSCs with HA were greatly declined from 17.18% to 6.19% at Day 21, compared with that in control culture. The intra-run CV% values for albumin secretion in synchronized hiPSCs with HA were reduced from 19.62% to 17.18%. Importantly, inter-run CV% values obtained in synchronized hiPSCs with HA were greatly reduced. All inter-run CV% values were below 10% at Day 21, resulting in more stable and consistent differentiation across the runs. These results indicate that hiPSC synchronization using HA is a potentially useful culture strategy that is highly consistent in terms of differentiation efficiency across different cultures and runs.

4 | DISCUSSION

In this study, we focused on the mechanisms underlying HA-mediated synchronization of mechanical memory that enhance the hepatocyte differentiation from hiPSCs. We hypothesized that (i) HA-mediated temporal disruption of cell-cell interactions causes spatial rearrangement within cell culture, (ii) actomyosin cytoskeleton rearrangement syncs mechanical memory with YAP acting, and (iii) synchronized mechanical memory improves homogeneous pluripotent cell production. This can enhance the homogeneity and stability of following hepatocyte differentiation, which are associated with synchronization of behavior-driven mechanical memory. We found that loss of E-cadherin and the resulting suppression or weakening of cell-cell adhesion following HA exposure is a crucial step in coordinating temporal and spatial differences in actin filament structure between cells (Figure 2). HA-mediated cell-cell junction relaxation inhibits changes in actomyosin-generating force and, subsequently, the synchronized mechanical memory via YAP acting in hiPSC cultures (Figure 3). These changes would be expected to inhibit abnormal deformation occurring at sites of nucleus-cytoskeletal linkage and cytoskeletal linkage to the ECM and to the adjacent cell. These findings suggest that the importance of synchronized behavior-driven mechanical memory via YAP localization

in maintaining cellular homeostasis through active actin cytoskeleton forces.

Furthermore, we demonstrated that synchronization techniques of cell behaviors using HA can be used to improve the robustness of cell cultures and enhance their further differentiation process (Figures 4 and 7). The HA-mediated synchronization of cell behavior-driven mechanical memory allows higher efficiency and reproducibility of hepatocyte differentiation observed at the end of the differentiation phase (Figure 7). At Day 21, the percentage of ALB/AFP double-positive cells within a run was 6.22-fold higher than those in the control (Figure 7) and exhibited eliminated inconsistencies (intra-run CV% decreased from 17.18% to 6.19%, Table 1). The inter-run CV% values obtained in synchronized hiPSCs with HA were greatly reduced. The inter-run CV% values obtained were all below 10% at Day 21, resulting in more stable and consistent differentiation across runs. The efficiency of HA synchronization could be explained by its effect on homogeneous mechanical memory resulting from changes in cellular behavior during hiPSC culture. Because HA can synchronize cell behavior-driven mechanical memory within a culture, the cellular responses to growth factors supplemented in the differentiation medium may be homogenized, enhancing culture reproducibility.

Although many studies have focused on the fundamental mechanisms underlying cell fate decision-making during stem cell differentiation, the formation of behavior-driven mechanical memory of cultured stem cells and its regulation have been relatively unexplored. Local cell density influences cell fate decision-making between hepatocytes and cholangiocytes during hepatocyte differentiation, supporting previous work suggesting that cell tension modifies cell behavior by altering the context of cell signaling (Graffmann et al., 2018). It was shown that cytoplasmic retention of YAP in high density cultures favors cholangiocyte development, whereas YAP nuclear localization in low seeding density cultures facilitates hepatocyte differentiation. In accordance with previous reports (Graffmann et al., 2018; Zhao et al., 2009), cells were detected in a highly heterogeneous mixed-cell population of hepatocyte-like cells and cholangiocyte-like cells after differentiation induction utilizing nonsynchronized cells in control culture. Consistently, our results indicate that YAP phosphorylation decreased the expression levels of pluripotent markers and increased the expression level of hepatocyte markers in hiPSCs, suggesting

synchronized mechanical memory compromises the cholangiocyte differentiation of hiPSCs and induces their hepatocyte differentiation. While cells change their mechanical properties in response to the surrounding cells, YAP activity can be mechanically regulated downstream of actomyosin contractility, and its transcriptional activity is also weakened due to YAP cytoplasmic translocation (Elosegui-Artola et al., 2017; Fernandez-Gonzalez et al., 2009; Wang et al., 2016b). The actomyosin cytoskeleton plays an important role in the regulation of YAP phosphorylation and localization, and remodeling of the cytoskeleton in association with cell-cell adhesion status is likely a key mechanism responsible for the YAP activity. This implies that the changes in cell behavior during hiPSC culture, which could be explained by several factors including altered cell-substrate and cell-cell adhesion, as well as cell motility, mediate the regulation of YAP and possibly involve the spatiotemporal emergence of cell functional heterogeneity. As a result, our findings demonstrate and validate the utility of HA in exploring the mechanisms by which synchronization of cell behavior-driven mechanical memory within a culture enhances early fate decisions during differentiation. Although it has long been postulated that distinct cell-cell interaction and compression pressure generated by local cell density influence an outcome variety of cellular functions, designing efficient synchronization tools to regulate cell behaviors would serve as a potentially useful strategy for controlling features of cultured cells and improving a desired cell production. In this study, effects of HA administration in dependence on exposure intervals and concentrations indicate that optimization of treatment conditions is prerequisite to ensure its capacity in controlling the cell synchronization and following differentiation homogeneity. Tracking of differentiation events should be taken into considerations when establishing culture methods to verify that there is no disturbance in cell developmental progression. In the synchronized cells with HA, the percentage of ALB/AFP double-positive cells, albumin production, and urea secretion were found significantly improved following the differentiation. To further recapitulate the *in vivo* hepatocyte development, a combination of complex culture dimensionality and biochemical and biophysical stimulation might be applied, and a high-content analysis would be required for characterizing critical features of mature hepatocytes, such as downregulation of AFP, enzymatic activation of several CYP family members, and formation of bile canaliculi, to ensure the functionality and maturation progression. Overall, this study has revealed a novel mechanism for the synchronization of cell behavior-driven mechanical memory in the expansion culture of hiPSCs; extracellular biophysical signals arising from altered cell behavior by HA are translated into biochemical signaling events in the nucleus through mechanotransduction, exerting a significant impact on differentiation efficiency and reproducibility.

5 | CONCLUSION

In this proof-of-principle study, we explored the concept of “synchronization” in the context of cell behavior-driven mechanical memory in hiPSC culture using HA as a culture tool to produce

a homogeneous population of differentiated cells. We showed that temporal disruption of cell-cell interactions by HA results in spatial rearrangement of cells within the culture and the synchronized mechanical memory by repeated HA exposure improves homogeneous pluripotent cell production, suggesting the maintenance of homeostatic mechanical properties in hiPSCs. We were able to demonstrate how hiPSC differentiation protocols may be optimized to control hepatocyte differentiation by identifying molecular mechanisms through which HA synchronization of cell behavior-driven mechanical memory leads to the production of homogeneous hiPSCs. These characteristics resulted in varying recoverability of YAP localization after E-cadherin disruption in undifferentiated hiPSCs and demonstrated that E-cadherin regulation was a fully reversible event. The optimal combination of HA concentration and exposure time was shown to effectively regulate mechanical memory while preserving hiPSC pluripotency. The HA synchronization strategy can expand cells while still allowing them to differentiate into all three germ layers and aid in early lineage specificity, and that pre-preparation of cells can be used to support early differentiation events. These results strongly suggest that improved differentiation stability will necessitate not only controlling the spatio-temporal coordination of cell behaviors, but may also provide unique and powerful opportunities to develop a culture strategy to manipulate stem cell fates.

AUTHOR CONTRIBUTIONS

Mee-Hae Kim: Conceptualization; methodology; formal analysis; investigation; writing. **Naruchit Thanuthanakhun:** Formal analysis; investigation; writing. **Masahiro Kino-oka:** Formal analysis; investigation; writing.

ACKNOWLEDGMENTS

We would like to express our gratitude to Prof. Fujinaga of the Department of Bacteriology, Graduate School of Medical Sciences, Kanazawa University, for helpful discussions on HA. We would also like to express our gratitude to the Cell Manufacturing Systems Engineering (Healios) Joint Research Chair, Osaka University and the Industrial Biotechnology Initiative Division, Institute for Open and Transdisciplinary Research Initiatives, Osaka University. This work was supported by the Project Focused on Developing Key Evaluation Technology: Development of Platform Technology for Drug Discovery through Application of Regenerative Medicine from AMED under Grant Number JP19be0604001.

CONFLICT OF INTEREST

The authors declare no conflict of interest.

DATA AVAILABILITY STATEMENT

The data that supports the findings of this study are available in the Supporting Information of this article. All the data in this manuscript is provided in the Figures/tables submitted for publication.

ORCID

Mee-Hae Kim  <http://orcid.org/0000-0001-5661-9249>

Masahiro Kino-oka  <http://orcid.org/0000-0002-4912-5811>

REFERENCES


- Adewumi, O., Aflatoonian, B., Ahrlund-Richter, L., Amit, M., Andrews, P. W., Beighton, G., Bello, P. A., Benvenisty, N., Berry, L. S., Bevan, S., Blum, B., Brooking, J., Chen, K. G., Choo, A. B., Churchill, G. A., Corbel, M., Damjanov, I., Draper, J. S., Dvorak, P., & Zhang, W. (2007). Characterization of human embryonic stem cell lines by the International Stem Cell Initiative. *Nature Biotechnology*, 25, 803–816. <https://doi.org/10.1038/nbt1318>
- Alisafaei, F., Jokhun, D. S., Shivashankar, G. V., & Shenoy, V. B. (2019). Regulation of nuclear architecture, mechanics, and nucleocytoplasmic shuttling of epigenetic factors by cell geometric constraints. *Proceedings of the National Academy of Sciences*, 116, 13200–13209. <https://doi.org/10.1073/pnas.1902035116>
- Bar-Nur, O., Russ, H. A., Efrat, S., & Benvenisty, N. (2011). Epigenetic memory and preferential lineage-specific differentiation in induced pluripotent stem cells derived from human pancreatic islet beta cells. *Cell Stem Cell*, 9, 17–23. <https://doi.org/10.1016/j.stem.2011.06.007>
- Driscoll, T. P., Cosgrove, B. D., Heo, S. -J., Shurden, Z. E., & Mauck, R. L. (2015). Cytoskeletal to nuclear strain transfer regulates YAP signaling in mesenchymal stem cells. *Biophysical Journal*, 108, 2783–2793. <https://doi.org/10.1016/j.bpj.2015.05.010>
- Dupont, S., Morsut, L., Aragona, M., Enzo, E., Giulitti, S., Cordenonsi, M., Zanconato, F., Le Dıgabel, J., Forcato, M., Bicciato, S., Elvassore, N., & Piccolo, S. (2011). Role of YAP/TAZ in mechanotransduction. *Nature*, 474, 179–183. <https://doi.org/10.1038/nature10137>
- Elosegui-Artola, A., Andreu, I., Beedle, A. E. M., Lezamiz, A., Uroz, M., Kosmalska, A. J., Oria, R., Kechagia, J. Z., Rico-Lastres, P., Le Roux, A. L., Shanahan, C. M., Trepas, X., Navajas, D., Garcia-Manyès, S., & Roca-Cusachs, P. (2017). Force triggers YAP nuclear entry by regulating transport across nuclear pores. *Cell*, 171, 1397–1410.e14. <https://doi.org/10.1016/j.cell.2017.10.008>
- Fernandez-Gonzalez, R., Simoes, S. M., Röper, J. C., Eaton, S., & Zallen, J. A. (2009). Myosin II dynamics are regulated by tension in intercalating cells. *Developmental Cell*, 17, 736–743. <https://doi.org/10.1016/j.devcel.2009.09.003>
- Graffmann, N., Ncube, A., Wruck, W., & Adjaye, J. (2018). Cell fate decisions of human iPSC-derived bipotential hepatoblasts depend on cell density. *PLoS One*, 13, e0200416. <https://doi.org/10.1371/journal.pone.0200416>
- Halder, G., Dupont, S., & Piccolo, S. (2012). Transduction of mechanical and cytoskeletal cues by YAP and TAZ. *Nature Reviews Molecular Cell Biology*, 13, 591–600. <https://doi.org/10.1038/nrm3416>
- Hoffman, L. M., Smith, M. A., Jensen, C. C., Yoshigi, M., Blankman, E., Ullman, K. S., & Beckerle, M. C. (2020). Mechanical stress triggers nuclear remodeling and the formation of transmembrane actin nuclear lines with associated nuclear pore complexes. *Molecular Biology of the Cell*, 31, 1774–1787. <https://doi.org/10.1091/mbc.E19-01-0027>
- Ingber, D. E. (2006). Cellular mechanotransduction: putting all the pieces together again. *The FASEB Journal*, 20, 811–827. <https://doi.org/10.1096/fj.05-5424rev>
- Kajiwara, M., Aoi, T., Okita, K., Takahashi, R., Inoue, H., Takayama, N., Endo, H., Eto, K., Toguchida, J., Uemoto, S., & Yamanaka, S. (2012). Donor-dependent variations in hepatic differentiation from human-induced pluripotent stem cells. *Proceedings of the National Academy of Sciences*, 109, 12538–12543. <https://doi.org/10.1073/pnas.1209979109>
- Kim, M.-H., & Kino-oka, M. (2015). Maintenance of an undifferentiated state of human induced pluripotent stem cells through migration-dependent regulation of the balance between cell-cell and cell-substrate interactions. *Journal of Bioscience and Bioengineering*, 119, 617–622. <https://doi.org/10.1016/j.jbiosc.2014.10.024>
- Kim, M.-H., Masuda, E., & Kino-oka, M. (2014). Kinetic analysis of deviation from the undifferentiated state in colonies of human induced pluripotent stem cells on feeder layers. *Biotechnology and Bioengineering*, 111, 1128–1138. <https://doi.org/10.1002/bit.25188>
- Kim, M.-H., Matsubara, Y., Fujinaga, Y., & Kino-oka, M. (2018). A simple and robust method for culturing human-induced pluripotent stem cells in an undifferentiated state using botulinum hemagglutinin. *Biotechnology Journal*, 13, 1700384. <https://doi.org/10.1002/biot.201700384>
- Kim, M.-H., Sugawara, Y., Fujinaga, Y., & Kino-oka, M. (2017). Botulinum hemagglutinin-mediated selective removal of cells deviating from the undifferentiated state in hiPSC colonies. *Scientific Reports*, 7, 93. <https://doi.org/10.1038/s41598-017-00083-1>
- Kim, M.-H., Thanuthanakhun, N., Fujimoto, S., & Kino-oka, M. (2021). Effect of initial seeding density on cell behavior-driven epigenetic memory and preferential lineage differentiation of human iPSCs. *Stem Cell Research*, 56, 102534. <https://doi.org/10.1016/j.scr.2021.102534>
- Kim, Y., Jang, H., Seo, K., Kim, J. H., Lee, B., Cho, H. M., Kim, H. J., Yang, E., Kim, H., Gim, J. A., Park, Y., Ryu, J. R., & Sun, W. (2022). Cell position within human pluripotent stem cell colonies determines apical specialization via an actin cytoskeleton-based mechanism. *Stem Cell Reports*, 17, 68–81. <https://doi.org/10.1016/j.stemcr.2021.11.005>
- Lee, K., Zhong, X., Gu, S., Krueel, A. M., Dörner, M. B., Perry, K., Rummel, A., Dong, M., & Jin, R. (2014). Molecular basis for disruption of E-cadherin adhesion by botulinum neurotoxin A complex. *Science*, 344, 1405–1410. <https://doi.org/10.1126/science.1253823>
- Li, D., Zhou, J., Wang, L., Shin, M. E., Su, P., Lei, X., Kuang, H., Guo, W., Yang, H., Cheng, L., Tanaka, T. S., Leckband, D. E., Reynolds, A. B., Duan, E., & Wang, F. (2010). Integrated biochemical and mechanical signals regulate multifaceted human embryonic stem cell functions. *Journal of Cell Biology*, 191, 631–644. <https://doi.org/10.1083/jcb.201006094>
- Lian, I., Kim, J., Okazawa, H., Zhao, J., Zhao, B., Yu, J., Chinnaiyan, A., Israel, M. A., Goldstein, L. S., Abujarour, R., Ding, S., & Guan, K. L. (2010). The role of YAP transcription coactivator in regulating stem cell self-renewal and differentiation. *Genes & Development*, 24, 1106–1118. <https://doi.org/10.1101/gad.1903310>
- Nakagawa, M., Taniguchi, Y., Senda, S., Takizawa, N., Ichisaka, T., Asano, K., Morizane, A., Doi, D., Takahashi, J., Nishizawa, M., Yoshida, Y., Toyoda, T., Osafune, K., Sekiguchi, K., & Yamanaka, S. (2015). A novel efficient feeder-free culture system for the derivation of human induced pluripotent stem cells. *Scientific Reports*, 4, 3594. <https://doi.org/10.1038/srep03594>
- Price, C. C., Mathur, J., Boerckel, J. D., Pathak, A., & Shenoy, V. B. (2021). Dynamic self-reinforcement of gene expression determines acquisition of cellular mechanical memory. *Biophysical Journal*, 120, 5074–5089. <https://doi.org/10.1016/j.bpj.2021.10.006>
- Rosowski, K. A., Mertz, A. F., Norcross, S., Dufresne, E. R., & Horsley, V. (2015). Edges of human embryonic stem cell colonies display distinct mechanical properties and differentiation potential. *Scientific Reports*, 5, 14218. <https://doi.org/10.1038/srep14218>
- Shuzui, E., Kim, M.-H., Azuma, K., Fujinaga, Y., & Kino-oka, M. (2019). Maintenance of an undifferentiated state of human-induced pluripotent stem cells through botulinum hemagglutinin-mediated regulation of cell behavior. *Journal of Bioscience and Bioengineering*, 127, 744–751. <https://doi.org/10.1016/j.jbiosc.2018.11.014>
- Shuzui, E., Kim, M.-H., & Kino-oka, M. (2019). Anomalous cell migration triggers a switch to deviation from the undifferentiated state in colonies of human induced pluripotent stems on feeder layers.

- Journal of Bioscience and Bioengineering*, 127, 246–255. <https://doi.org/10.1016/j.jbiosc.2018.07.020>
- Smith, Q., Rochman, N., Carmo, A. M., Vig, D., Chan, X. Y., Sun, S., & Gerecht, S. (2018). Cytoskeletal tension regulates mesodermal spatial organization and subsequent vascular fate. *Proceedings of the National Academy of Sciences*, 115, 8167–8172. <https://doi.org/10.1073/pnas.1808021115>
- Soncini, F., & Ward, C. M. (2011). The function of E-cadherin in stem cell pluripotency and self-renewal. *Genes*, 2, 229–259. <https://doi.org/10.3390/genes2010229>
- Sugawara, Y., Yutani, M., Amatsu, S., Matsumura, T., & Fujinaga, Y. (2014). Functional dissection of the Clostridium botulinum Type B hemagglutinin complex: identification of the carbohydrate and E-cadherin binding sites. *PLoS One*, 9, e111170. <https://doi.org/10.1371/journal.pone.0111170>
- Sun, Y., Villa-Diaz, L. G., Lam, R. H. W., Chen, W., Krebsbach, P. H., & Fu, J. (2012). Mechanics regulates fate decisions of human embryonic stem cells. *PLoS One*, 7, e37178. <https://doi.org/10.1371/journal.pone.0037178>
- Takahashi, K., & Yamanaka, S. (2006). Induction of pluripotent stem cells from mouse embryonic and adult fibroblast cultures by defined factors. *Cell*, 126, 663–676. <https://doi.org/10.1016/j.cell.2006.07.024>
- Thanuthanakhun, N., Kino-oka, M., Borwornpinyo, S., Ito, Y., & Kim, M.-H. (2021). The impact of culture dimensionality on behavioral epigenetic memory contributing to pluripotent state of iPS cells. *Journal of Cellular Physiology*, 236, 4985–4996. <https://doi.org/10.1002/jcp.30211>
- Thomson, J. A., Itskovitz-Eldor, J., Shapiro, S. S., Waknitz, M. A., Swiergiel, J. J., Marshall, V. S., & Jones, J. M. (1998). Embryonic stem cell lines derived from human blastocysts. *Science*, 282, 1145–1147. <https://doi.org/10.1126/science.282.5391.1145>
- Uhler, C., & Shivashankar, G. V. (2017). Regulation of genome organization and gene expression by nuclear mechanotransduction. *Nature Reviews Molecular Cell Biology*, 18, 717–727. <https://doi.org/10.1038/nrm.2017.101>
- Wang, B., Qin, P., Zhao, H., Xia, T., Wang, J., Liu, L., Zhu, L., Xu, J., Huang, C., Shi, Y., & Du, Y. (2016). Substrate stiffness orchestrates epithelial cellular heterogeneity with controlled proliferative pattern via E-cadherin/ β -catenin mechanotransduction. *Acta Biomaterialia*, 41, 169–180. <https://doi.org/10.1016/j.actbio.2016.05.025>
- Wang, J., Sinnett-Smith, J., Stevens, J. V., Young, S. H., & Rozengurt, E. (2016). Biphasic regulation of yes-associated protein (YAP) cellular localization, phosphorylation, and activity by G protein-coupled receptor agonists in intestinal epithelial cells. *Journal of Biological Chemistry*, 291, 17988–18005. <https://doi.org/10.1074/jbc.M115.711275>
- Yang, C., Tibbitt, M. W., Basta, L., & Anseth, K. S. (2014). Mechanical memory and dosing influence stem cell fate. *Nature Materials*, 13, 645–652. <https://doi.org/10.1038/nmat3889>
- Zhang, C., Zhu, H., Ren, X., Gao, B., Cheng, B., Liu, S., Sha, B., Li, Z., Zhang, Z., Lv, Y., Wang, H., Guo, H., Lu, T. J., Xu, F., Genin, G. M., & Lin, M. (2021). Mechanics-driven nuclear localization of YAP can be reversed by N-cadherin ligation in mesenchymal stem cells. *Nature Communications*, 12, 6229. <https://doi.org/10.1038/s41467-021-26454-x>
- Zhao, D., Chen, S., Cai, J., Guo, Y., Song, Z., Che, J., Liu, C., Wu, C., Ding, M., & Deng, H. (2009). Derivation and characterization of hepatic progenitor cells from human embryonic stem cells. *PLoS One*, 4, e6468. <https://doi.org/10.1371/journal.pone.0006468>

SUPPORTING INFORMATION

Additional supporting information can be found online in the Supporting Information section at the end of this article.

Generation of universal natural killer cells from a cryopreserved cord blood mononuclear cell-derived induced pluripotent stem cell library

Wei Du^{1,2,3,4} , Lijuan Cui^{1,3,4}, Jinmei Zhang^{1,3,4}, Hua Zhang^{1,3,4}, Rongzhi Liu^{1,3,4}, Wenling Yang^{1,4} and Yu Zhang^{1,3,4,5}

1 Union Stem Cell & Gene Engineering Co., LTD, Tianjin, China

2 School of Medicine, Nankai University, Tianjin, China

3 Tianjin Key Laboratory of Blood Cell Therapy Technology, China

4 National Stem Cell Product Industrialization Base, State Industrial Base for Stem Cell Engineering Products, Tianjin, China

5 Vcanbio Cell & Gene Engineering Co., Ltd, Tianjin, China

Keywords

cell therapy; cryopreserved cord blood mononuclear cells; induced pluripotent stem cells; natural killer cells

Correspondence

Y. Zhang, Tianjin Key Laboratory of Blood Cell Therapy Technology, SVP&CSO of Vcanbio Cell & Gene Engineering Co., Ltd, Tianjin 300384, China
 E-mail: zhangyu@vcanbio.com

(Received 17 December 2021, revised 8 April 2022, accepted 22 June 2022)

doi:10.1002/2211-5463.13460

Natural killer (NK) cells play a key role in innate immunity and are regarded as a promising candidate for cellular immunotherapy. Natural killer cells may be generated from different sources, including induced pluripotent stem cells (iPSCs); these stem cells produce an abundant amount of NK cells to meet the needs of a wide range of clinical applications. Autologous iPSCs are expensive and labor-intensive to prepare, while allogeneic iPSCs require human leukocyte antigen (HLA) matched cells to avoid the risk of immune rejection. In the current study, we prepared HLA-matched iPSCs using HLA common haplotype homozygous (HLA^h) donors from cryopreserved human cord blood (CB) sourced from the Tianjin Cord Blood Public Bank. This approach was designed to generate a CB-derived iPSC library from HLA^h donors and use it to produce off-the-shelf NK cells. Starting with readily available cryopreserved CB mononuclear cells (cryoCBMCs), we produced cryoCBMC-derived iPSCs (cryoCB-iPSCs). These cryoCB-iPSCs were induced to generate embryoid bodies (EBs) using an improved 3D suspension culture method, and induced NK (iNK) cells were differentiated from EBs. iNK cells expressed specific surface markers of NK cells, exhibited cytotoxicity comparable with NK cells generated from CB (CB-NK) and peripheral blood (PB-NK), and expressed lower levels of KIRs and HLA-DR compared to CB-NK and PB-NK. Taken together, we have shown that an iPSC library can be established from HLA^h cryoCBMCs, and cryoCB-iPSCs can be used to generate a large number of ‘universal’ NK cells for future clinical applications.

There have been many recent developments in immune-cellular therapy targeting cancer, notably in the field of *chimeric antigen receptor T* (CAR-T) cell therapy. To date, five CAR-T products have been

approved by the Food and Drug Administration and two CAR-T products have also been recently launched in China [1]. Natural killer (NK) cells, a unique lymphocyte subgroup, are an important participant of

Abbreviations

CAR-T, chimeric antigen receptor T; CB, cord blood; CB-NK, NK cells generated from CB; cryoCB-iPSCs, cryoCBMCs-derived iPSCs; cryoCBMCs, cryopreserved CB mononuclear cells; EBs, embryoid bodies; HLA, human leukocyte antigen; iNK, induced NK; iPSCs, induced pluripotent stem cells; MHC, major histocompatibility complex; NK cells, natural killer cells; PB-NK, NK cells generated from peripheral blood.

innate immunity and exhibit the capacity to kill virally infected cells and tumor cells. In addition, NK cells exhibit potential value in tumor immunotherapy due to their non-major histocompatibility complex (MHC) restriction and extensive tumor recognition ability [2]. Natural killer cells can recognize and lyse mutated cells with downregulated MHC-I molecules or overexpressed activated NK cell receptors [3,4]. Thus, NK cells, not only in autologous but also allogeneic, can be used to treat cancer without causing serious adverse effects, such as graft-versus-host disease (GvHD), holding promise for significantly broadening the availability of clinical application [5].

At present, there are many clinical studies on the applications of NK cells in tumor therapy [3,5–7]. The clinical application of NK cells usually requires large and repeated doses to achieve therapeutic effects [8,9]. Thus, identifying sources that can be used to mass-produce NK cells to meet clinical requirements has been an active area of research. Indeed, various sources have been tested to generate NK cells, including NK cell lines, peripheral blood-derived NK cells (PB-NK), and cord blood-derived NK cells (CB-NK) [5,10]. Natural killer cell lines are unstable and require irradiation before infusion, and the irradiated cells only survive for 48 h [11]. Due to this limitation, NK cell lines cannot achieve long-term therapeutic effects [12]. PB-NK and CB-NK cells are limited for individual dosing, and generating PB-NK and CB-NK cells is time-consuming and cost-inefficient [10]. Therefore, there is an urgent need to identify an appropriate source to produce a large number of allogeneic NK cells.

Induced pluripotent stem cells (iPSCs) are often generated by the forced expression of relevant pluripotent transcription factors in somatic cells [13]. iPSCs have strong self-renewal ability and exhibit embryonic stem cell (ES)-like pluripotency to differentiate into various functional cell lineages [14]. More interestingly, iPSCs have been reported to have the potential to become standard raw materials to produce a large number of NK cells [15,16]. Further, human CB represents an attractive source of cells for reprogramming iPSCs [17] due to its wide availability, non-invasive acquisition, low risk of viral contamination and mutation, and it is typically already stored in liquid nitrogen for transplantation. Moreover, the most frequent HLA haplotype homozygous (HLA^h) CB selected from public CB bank is an optimal source to produce ‘universal’ iPSCs for a wider range of recipients [18].

In the present study, we designed a strategy to use cryopreserved CB mononuclear cells (cryoCBMCs) to

generate iPSCs (cryoCB-iPSCs). We then improved a method to mass-produce induced NK (iNK) cells derived from cryoCB-iPSCs. We characterized iNK cells by evaluating the expression of surface markers of NK cells and cytotoxicity.

Materials and methods

CryoCB and cryoCBMC isolation

Human cryoCB was obtained from the Tianjin Cord Blood Public Bank. The donors involved in the study were informed and signed written informed consents. This study was conducted in accordance with the Declaration of Helsinki for experiments involving humans and was approved by the ethical advisory board of the Institute of Hematology and Blood Diseases Hospital (YW2018001-EC-1). The CBMC and cryoCBMCs were prepared from fresh and cryopreserved CB, respectively, by Ficoll-Hypaque (G&E Healthcare, Chicago, IL, USA; 17-1440-02) as previously described [19].

Episomal vectors

Oct4-e2a-Sox2 (OS), MYC (M), KLF4 (K), and Bcl-XL (B) were inserted into an EV plasmid backbone, containing Spleen focus-forming virus U3 (SFFV) promoter, Post-transcriptional regulatory element (Wpre), Polyadenylation signal from SV40 virus (SV40PolyA), EBV origin of replication (oriP), and Epstein-Barr nuclear antigen 1 (EBNA1) elements as described previously [20]. All insertions of the cloned vectors were verified by sequencing.

Reprogramming of cryoCBMC to pluripotency

The cryoCBMCs were cultured for 6 days in an erythroid medium as previously described [19]. The 4×10^5 cells were nucleofected with a 1 μ L plasmid mixture (400 ng- μ L⁻¹ OS, 200 ng- μ L⁻¹ M, 200 ng- μ L⁻¹ K, and 100 ng- μ L⁻¹ B), and distributed to one well in a vitronectin-treated 6-well plate and cultured for another 2 days. After 2 days, the culture medium was changed to the induction medium (2 mL-well⁻¹), which contained Knockout™ DMEM/F12 (Gibco, Grand Island, NY, USA; 12660012) with 50 ng-mL⁻¹ basic fibroblast growth factor (Peprotech, Rocky Hill, NJ, USA; 100-18C-10), 13 ng-mL⁻¹ Insulin-Transferrin-Selenium (Gibco; 41400-045), 2 mM L-glutamine (Gibco; 25030081), and 50 mg-mL⁻¹ ascorbic acid (Sigma, St. Louis, MO, USA; 49752-10G). The induction medium was replenished every 2 days, and on day 6, was changed to another induction medium that contained 0.25 mM sodium butyrate (Sigma; B5887-250MG), which was replenished every 2 days until day 12. The resulting iPSCs were cultured *in vitro* nectin-treated 6-well plates and refreshed with mTeSR1 medium (Stemcell, Vancouver, BC, Canada; 85850) every 2 days for long-term culture.

Alkaline phosphate staining and immunocytochemistry

Alkaline phosphatase (AP) staining was performed using an Alkaline Phosphatase Staining Kit II (Stemgent, Cambridge, MA, USA; 00-0055). For detection of pluripotent stem cell marker antigens, cells were fixed with 4% paraformaldehyde in PBS for 10 min at room temperature. After washing with PBS, cells were incubated in 0.25% Triton X-100 (Sigma-Aldrich; X100-1L) for 10 min at room temperature, and then blocked with 5% sheep or donkey serum for 30 min at room temperature. Cells were then incubated with the following primary antibodies SSEA-4 (1 : 100; Invitrogen, Carlsbad, CA, USA; MA1-021X), TRA-1-60 (1 : 50; Invitrogen; MA1-023), Oct-4 (1 : 100; Invitrogen; PA5-27438), SOX2 (1 : 100; Invitrogen; PA1-094X), and Nanog (1 : 100; Invitrogen; 14-5768-82), overnight at 4 °C. Cells were then incubated with appropriate secondary antibodies corresponding to the primary antibody at room temperature for 1 h. The secondary antibodies included Alexa Fluor 594 AffiniPure Donkey anti-mouse IgG (1 : 250; Jackson, Bar Harbor, ME, USA; 715-585-150), Alexa Fluor 488 AffiniPure Donkey anti-rabbit IgG (1 : 250; Jackson; 711-545-152) and Alexa Fluor 594 AffiniPure goat anti-mouse anti-mouse IgG (1 : 250; Jackson; 115-585-075). The nuclei were stained with DAPI (1 : 10; Vector Laboratories, Burlingame, CA, USA; H-1200).

Differentiation capacity of cryoCB-iPSCs *in vitro*

STEMdiff™ Trilineage Differentiation Kit (Stemcell; 5230) was used to differentiate cryoCB-iPSCs into endoderm, mesoderm, and ectoderm. Mesoderm and endoderm lineages were formed on day 5, and ectoderm lineages were formed on day 7. Immunofluorescence staining was used to detect representative markers (AFP3 for mesoderm, 1A4 for endoderm and 10C2 for ectoderm) of cryoCB-iPSCs. The Human Pluripotent Stem Cell Trilineage Differentiation quantitative polymerase chain reaction (qPCR) Array (Stemcell; 7515) was performed to characterize hPSCs and their trilineage differentiation capacity. This qPCR array was designed to detect the gene expression profile of undifferentiated hPSCs and their trilineage derivatives following *in vitro* directed or spontaneous differentiation. Genes were selected based on their demonstrated differential expression in ES and iPSCs compared with hPSC-derived ectodermal, mesodermal, and endodermal lineage cells.

Teratoma formation assay and histological analysis

Approximately 1×10^6 cryoCB-iPSC after 15 passages in culture were harvested with Accutase (Stemcell; 07920) and resuspended in 200 μ L solution that was prepared with Matrigel (Corning, Acton, MA, USA; 354277) and

DMEM/F12 medium (HyClone, Logan, UT, USA; SH30243.01) at a ratio of 1 : 1. These cells were subcutaneously injected into the rear haunch of each NOD/SCID immunodeficient mouse. Two months after implantation, the formed teratomas were removed and sectioned at 7 μ m thickness for hematoxylin and eosin (H&E) staining.

NK cells induced from cryoCB-iPSCs

To produce NK cells from cryoCB-iPSCs, we developed a method for EB formation from 3D cultured iPSCs. In brief, cryoCB-iPSCs (8×10^5 cells·mL⁻¹) were transferred and cultured in non-tissue cultured (TC) treated six-well plates (2 mL mTeSR™ 3D Medium (Stemcell; 03950) per well). Cells were incubated on a shaking table with a rotation speed of 70 r.p.m. at 37 °C, 5% CO₂ for 4 days. Morphological changes of cryoCB-iPSCs were monitored every day. On the fourth day, EBs were approximately spherical with a diameter of 150–250 nm. EBs were then transferred to non-TC treated six-well plates at a density of 300–400 per well. Then the classic two-step differentiation method was used to induce NK (iNK) cells as previously described [16,21]. Single cells in suspension culture were filtered out. EBs were transferred in differentiation medium (APEL™ medium (Stemcell; 05275) and PFHM-II at a proportion of 20 : 1, including VEGF (20 ng·mL⁻¹) and BMP4 (20 ng·mL⁻¹), SCF (40 ng·mL⁻¹), the density was adjusted to 40–60 EBs per well. EBs were then incubated at 37 °C in a 5% CO₂ incubator for 11 days. Blastocyst-like EBs were generated and the APEL differentiation medium was replaced with an AEL differentiation medium (including IL-3 (5 ng·mL⁻¹), IL-15(10 ng·mL⁻¹), FLT3 (10 ng·mL⁻¹), IL-7(20 ng·mL⁻¹), and SCF (20 ng·mL⁻¹)), which led to lymphocyte differentiation. AEL differentiation medium was replaced every week. After 4 weeks, iNK cells were harvested in suspension (Fig. 1).

Flow cytometry

To investigate phenotypic changes during differentiation of cryoCB-iPSCs, FACSCalibur flow cytometry (BD Biosciences, San Diego, CA, USA) was used to characterize cryoCB-iPSCs with antibodies against CD34 (catalog no. Z6410008), CD45 (catalog no. Z6410006), CD3 (catalog no. Z6410026), and CD16 (catalog no. Z6410070; Quantobio, Beijing, China); CD56 (catalog no. 562794), NKp46 (catalog no. 557991), NKp44 (catalog no. 558563), NKpG2D (catalog no. 562064), and CD94 (catalog no. 559876; BD Biosciences). Isotype controls were used to eliminate background due to the nonspecific binding of antibodies to cell surfaces.

Cytotoxicity assay of iNK cells

CD107a expression and intracellular IFN- γ and TNF- α production determined by flow cytometry were used to evaluate the cytotoxicity of iNK cells. In brief, iNK cells

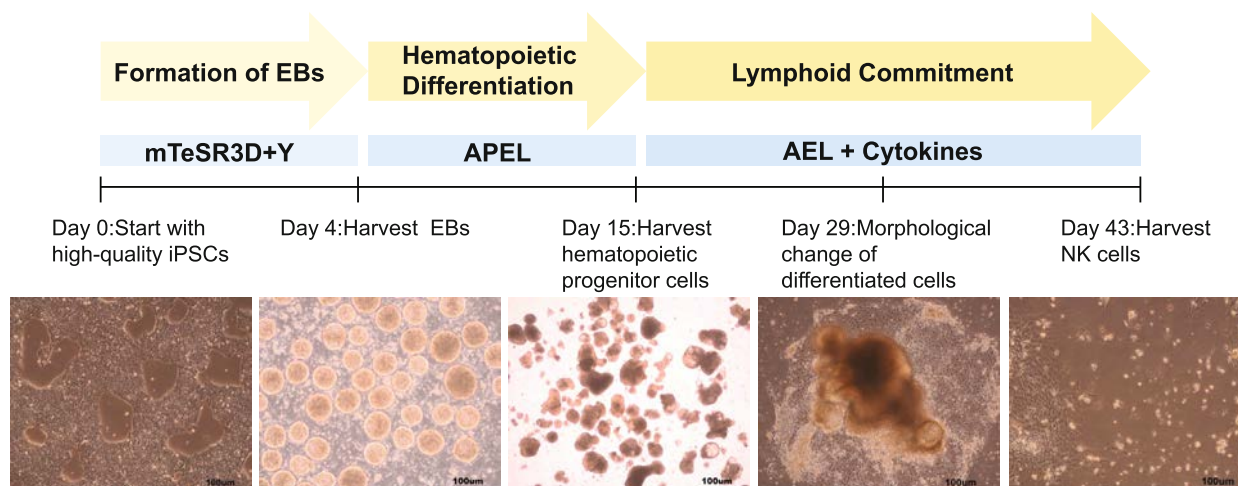


Fig. 1. Schematic representation showing a three-stage protocol for the generation of NK cells from iPSCs.

(i.e., effector cells) were co-cultured with K562 cells (i.e., target cells) at a ratio of 1 : 1. iNK cells that were not co-cultured with target cells were used as a negative control. iNK cells were collected after 5 h incubation and stained with CD56-FITC (catalog no. 562794), CD107a-APC (catalog no. 560664), IFN- γ -PE (catalog no. 559327; BD Biosciences), and TNF- α -APC (catalog no. 502912; Biolegend, San Diego, CA, USA). The expression of CD107A, IFN- γ , and TNF- α was analyzed and compared in iNK cells between the two groups.

To detect direct cytotoxicity of NK cells against target cells, a flow cytometry-based method was used [10,12]. In brief, 0.5×10^5 to 5×10^5 NK cells were cocultured with 5×10^4 carboxyfluorescein diacetate succinimidyl ester (CFSE) – labeled cancer cells at various effector to target (E : T) ratios for 4 h. Samples were then stained on ice with 7-AAD for 10 min. After washing, target cell death was assessed with a flow cytometer by the percentage of 7-AAD-stained cells in the CFSE-positive population. To inhibit the activity of the perforin/granzyme system in NK cells, the co-culture killing assays were performed in the presence of 5/3 mM EGTA/Mg⁺⁺. Target cells (CFSE⁺) were gated, and the percent of 7-AAD⁺ cells was used to calculate NK cell cytotoxicity using the following equation: (Experimental–Spontaneous dead cells/(100–Spontaneous dead cells) \times 100%.

Statistical analysis

All analyses were performed with spss 25.0 software (SPSS Inc., Chicago, IL, USA). Data were expressed as mean \pm standard error of the mean (SEM). ANOVA was used for the comparison of variables among multiple groups. Student *t*-test was used for comparison of variables between two groups. A *P* value < 0.05 was considered statistically significant.

Results

Characterization of cryoCB-iPSCs

The cryoCB-iPSCs were positive for AP staining (Fig. 2A). The expression of pluripotency markers SOX2, OCT3/4, and NANOG were markedly increased in the cryoCB-iPSCs compared with the parental CBMCs, and were comparable to expression in H1 human ES cells as revealed by RT-qPCR (Fig. 2B). Also, pluripotency markers TRA-1-60, SSEA4, NANOG, OCT3/4, and SOX2 were markedly expressed in the cryoCB-iPSCs as revealed by flow cytometry (Fig. 2C). Consistent with the above observations, immunofluorescence staining showed that the cryoCB-iPSCs were positive for typical ES cell markers such as TRA-1-60, SSEA4, NANOG, OCT3/4, and SOX2 (Fig. 2D).

Differentiation of cryoCB-iPSCs

We next examined the differentiation capability of cryoCB-iPSCs using hPSC Trilineage Differentiation qPCR Array, and found that cryoCB-iPSCs could differentiate into ectoderm, mesoderm, and endoderm cells (Fig. 3A). Immunofluorescence staining showed that representative markers, AFP3, 1A4, and 10C2, were positive for mesoderm, endoderm, and ectoderm, respectively (Fig. 3B). We also subcutaneously injected cryoCB-iPSCs into immunosuppressed mice and examined the teratoma formation after 2 months by H&E staining. H&E staining showed that the teratoma contained three germ layer tissues (Fig. 3C).

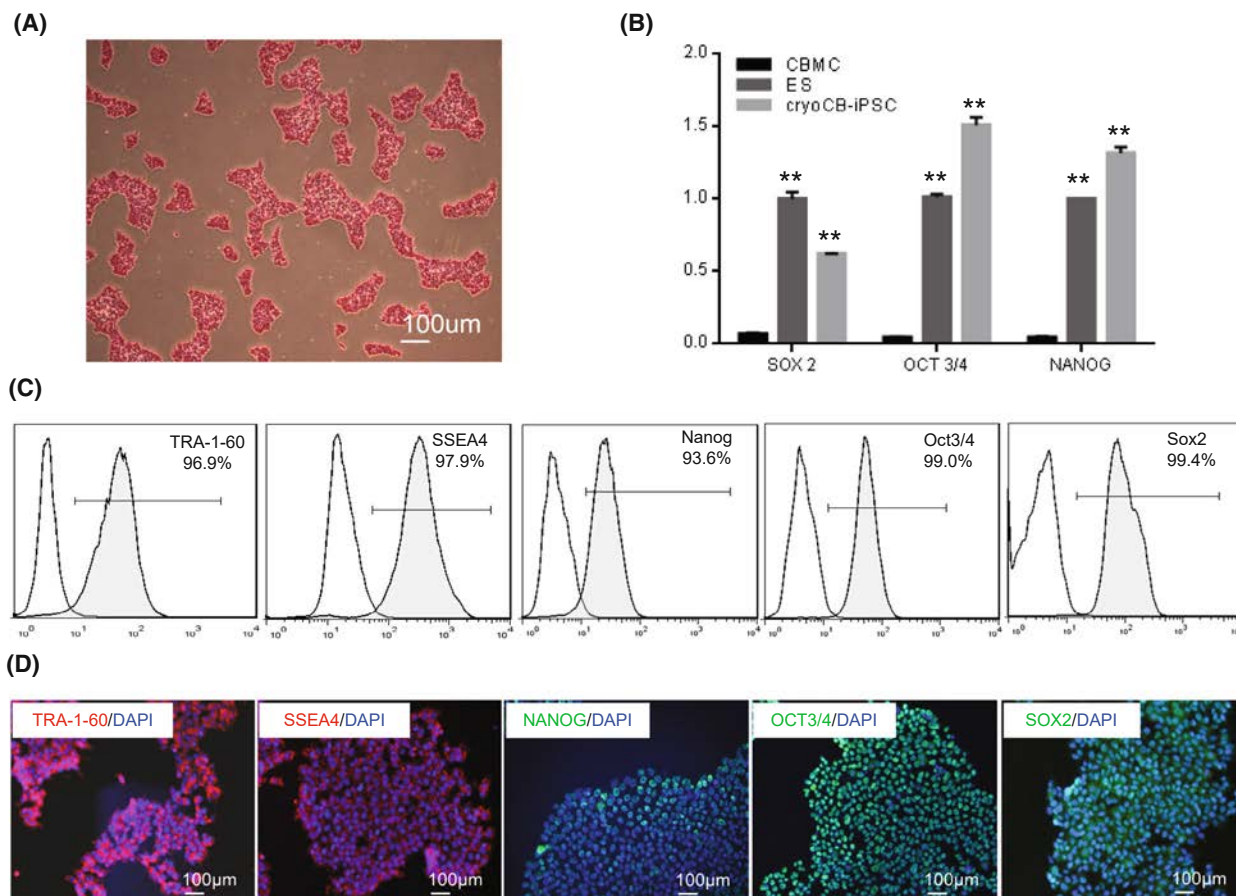


Fig. 2. Characterization of cryoCB-iPSCs. (A) Alkaline phosphatase staining of cryoCB-iPSCs. Scale bar, 100 μ m. (B) Comparison of expression of pluripotency gene, SOX2, OCT3/4, and NANOG, between cryoCB-iPSCs and CBMC-iPSCs and H1 human ES cells ($n = 5$). Data are represented as the mean \pm SEM. $**P < 0.01$ vs. CBMC as determined by Student *t*-test. (C) Flow cytometry analysis of the expression of pluripotency markers, TRA-1-60, SSEA4, NANOG, OCT3/4, and SOX2, on cryoCB-iPSCs. (D) Representative images of immunofluorescence staining showing expression of typical ES cells markers TRA-1-60 (red), SSEA4 (red), NANOG (green), OCT3/4 (green), and SOX2 (green) on cryoCB-iPSCs. Nuclei are stained with DAPI (blue). Scale bar, 100 μ m.

Safety evaluation of cryoCB-iPSCs

We selected three cryoCB-iPSCs and analyzed the changes in average copies of total plasmids. Zero copies of the plasmid were detected in cells from passage 10 of the three cryoCB-iPSCs (Fig. 4A), suggesting that plasmids were depleted from these cells. Karyotype analysis was performed to evaluate the genomic stability of cryoCB-iPSCs at passage 15, and showed a normal karyotype (Fig. 4B), suggesting that long-term cultured cryoCB-iPSCs did not exhibit detectable chromosomal abnormalities.

HLA^{Ah} CB in Tianjin Cord Blood Public Bank

To demonstrate the feasibility of generating a CB-derived HLA^{Ah} iPSC library, we investigated HLA^{Ah}

CB from the Tianjin Cord Blood Public Bank. We found that there were 16 homozygous CBs, including HLA-A, -B, -C, -DR, and -DQ. The genotype frequency of these 16 homozygous CBs was 6.5% in the Chinese population, covering 11.3% of the total Chinese population (Table 1) based on high-resolution analyses of HLA-A, -B, -C, -DR, and -DQ frequencies of 169 995 volunteers from the China Bone Marrow Donor Registry Program [22].

Characteristics of iNK Cells

We first characterized iNK cells by examining the expression of surface markers. Compared to PB-NK and CB-NK cells, iNK cells had the expression of immunoglobulin-like receptors (KIRs), CD16, NKp46,

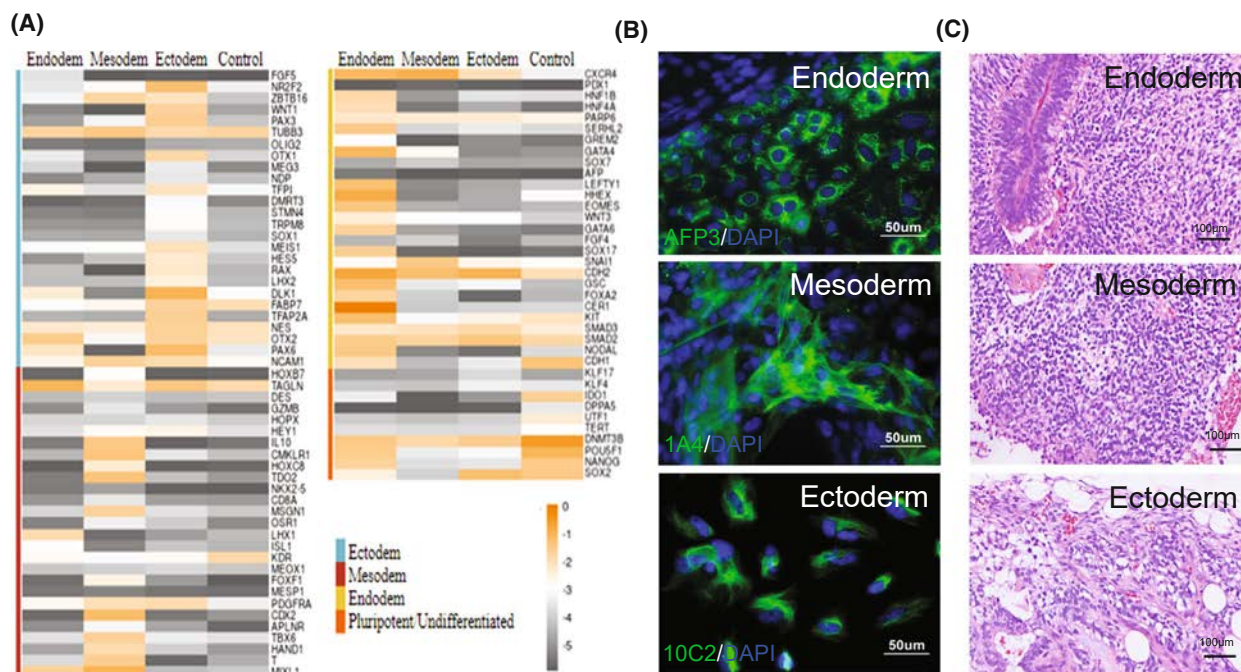


Fig. 3. Differentiation capability of cryoCB-iPSCs. (A) Trilineage differentiation quantitative PCR array of cryoCB-iPSCs. (B) Representative images of immunofluorescence staining of markers of different lineage cells: AFP3 for mesoderm, 1A4 for endoderm, and 10C2 for ectoderm. Scale bar, 50 μ m. (C) Representative images of H&E staining of teratomas containing endoderm, mesoderm, and ectoderm. Scale bar, 100 μ m.

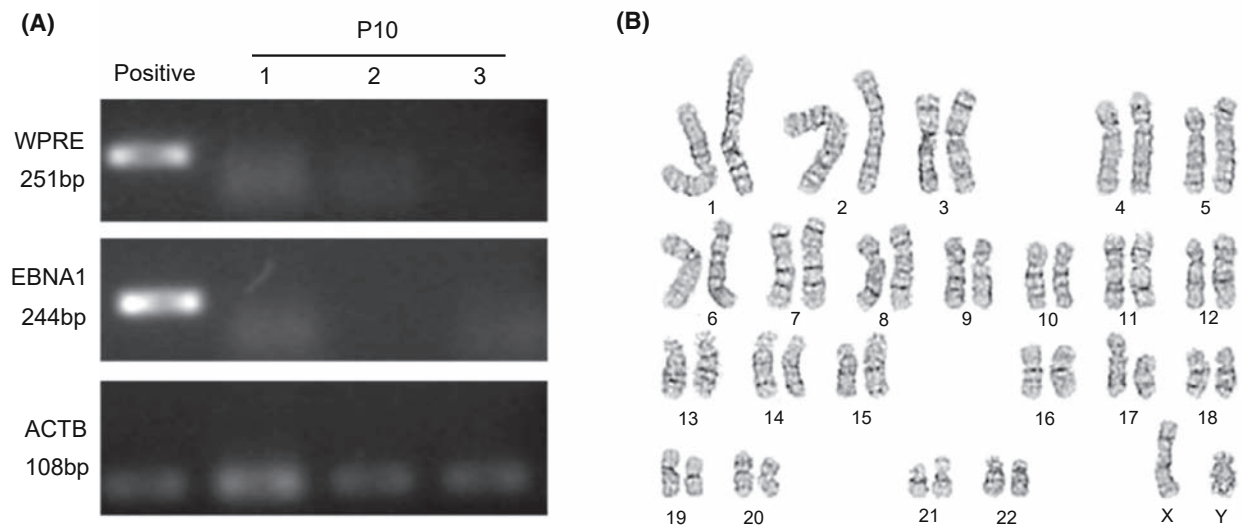


Fig. 4. Safety evaluation of cryoCB-iPSCs. (A) PCR-based detection of vector sequence (EBNA1 and WPRE) was not found in the expanded cryoCB-iPSCs after 10 passages. (B) A representative karyotyping image of a cryoCB-iPSC.

NKp44, CD94, NKG2D, and CD117 indicating that iNK cells can be generated from cryoCB-iPSCs using our EB differentiation method. In addition, we also found that iNK cells expressed lower levels of KIRs and CD16, compared to PB-NK and CB-NK cells (Fig. 5).

Immunogenicity of cryoCB-iPSC and iNK cells

We next examined the expression of HLA-I (A, B, C) and HLA-II (DR) in cryoCB-iPSCs and iNK cells to assess their immunogenicity. The cryoCB-iPSCs and

Table 1. Genotypes and frequency of 16 HLAh cord blood from the Tianjin cord blood public bank.

Numbers	Freq. (%)	HLA-A		HLA-B		HLA-C		HLA-DR		HLA-DQ	
10	37.0023	30:01	30:01	13:02	13:02	06:02	06:02	07:01	07:01	02:02	02:02
4	24.6414	02:07	02:07	46:01	46:01	01:02	01:02	09:01	09:01	03:03	03:03
1	5.7905	02:03	02:03	38:02	38:02	07:02	07:02	16:02	16:02	05:02	05:02
1	3.6439	02:01	02:01	39:01	39:01	07:02	07:02	11:06	11:06	03:01	03:01

ES-H1 had a comparable expression of HLA-I (A, B, C) and HLA-II (DR; Fig. 6A). Compared to CB-NK and PB-NK cells, iNK cells expressed comparable levels of HLA-I (A, B, C) and lower levels of HLA-II (DR) (Fig. 6B). These results demonstrate that iNK cells have low immunogenicity and may become ‘universal’ NK cells.

Cytotoxicity of iNK cells against cancer cells

We investigated the cytotoxicity of the generated NK cells by co-culturing three types of NK cells, iNK, PB-NK, and CB-NK cells, with K562 cells (chronic myeloid leukemia cell line) at a ratio of 1 : 1, respectively, followed by flow cytometry analysis for staining of CD56-FITC, CD107a-APC, and IFN- γ -PE. The NK cells cultured without target cells were used as a control. Compared to CB-NK and PB-NK cells, iNK cells expressed higher levels of CD107a expression and TNF- α secretion, and lower levels of IFN- γ secretion (Fig. 7A–C).

We also evaluated the direct cytotoxicity against cancer cells by assessing cytotoxicity induced by NK cells on K562, MB-MDA-231 (breast cancer cell line), and Raji (lymphoma cell line). iNK cells were able to efficiently kill K562 cells and MB-MDA-231. However, PB-NK cells induced the highest toxicity on Raji

cells compared with iNK or CB-NK cells (Fig. 7D). To determine whether NK-induced cytotoxicity depends on cytotoxic granule release, cytotoxicity was measured in the presence or absence of the Ca⁺⁺ chelator EGTA, which inhibits cytotoxic granule release. EGTA completely blocked cytotoxicity, suggesting that degranulation was required (Fig. 7E).

Discussion

Natural killer cells have marked potential value in tumor immunotherapy due to characteristics such as non-MHC restriction and extensive tumor recognition [3,23]. However, the main problem hindering the clinical application of NK cells is the production of large numbers of NK cells required for therapeutic clinical applications [24,25]. Therefore, there is an urgent need for a method that can be used to mass-produce NK cells [5,25]. To address this unmet need we designed an approach to produce unlimited NK cells from cryoCB-iPSCs. Using an improved EB formation protocol, functional mature NK cells were produced from cryoCB-iPSCs. These iNK cells expressed NK cell-specific surface markers, exhibited cytotoxicity, but had less KIRs and HLA-DR. Therefore, we believe that this approach may be used to generate a large

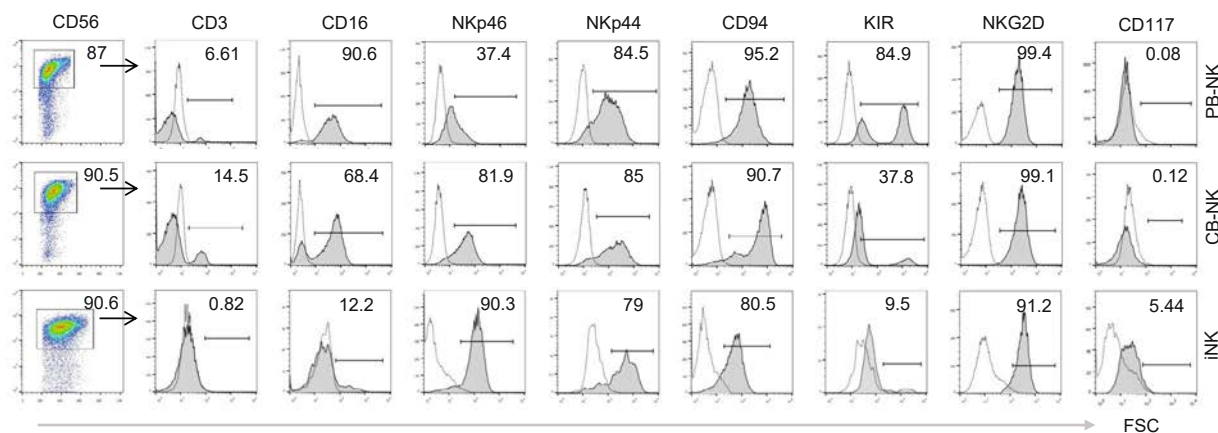


Fig. 5. Detection of surface markers, CD56, CD16, Nkp46, Nkp44, CD94, KIR, NKG2D, and CD117, on PB-NK cells, CB-NK cells, and iNK cells by flow cytometry.

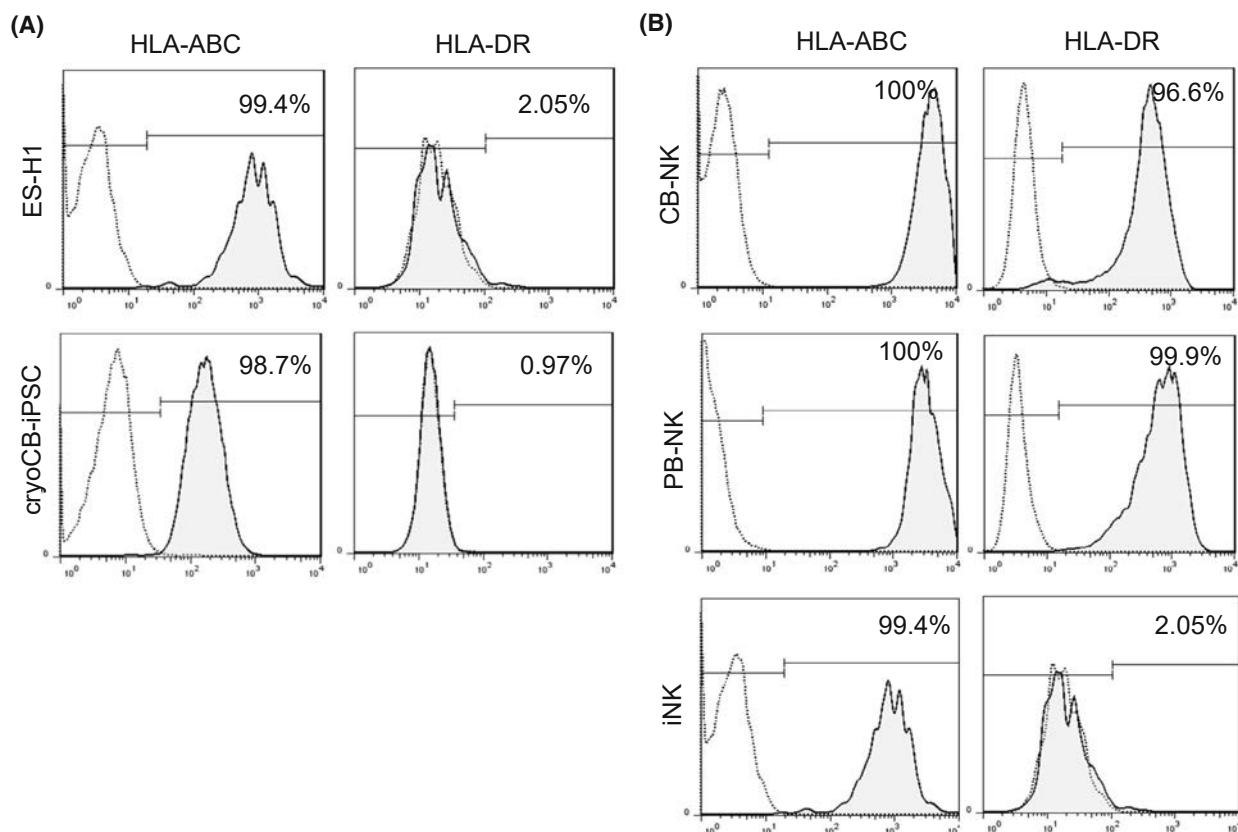


Fig. 6. Immunogenicity of cryoCB-iPSCs and iNK cells. (A) Expression of HLA-I (A, B, C) and HLA-II (DR) in cryoCB-iPSCs and ES-H1 cells. (B) Expression of HLA-I (A, B, C) and HLA-II (DR) in iNK, PB-NK, and CB-NK cells.

number of ‘universal’ functional NK cells, enabling wider clinical application of tumor immunotherapy.

Currently, therapeutic NK cells are primarily derived from NK cell lines, PB and CB. In recent years, accumulating evidence has suggested that iPSCs are a promising source of NK cells [13,26]. For example, iPSC-derived NK cells have been used in several clinical studies to treat tumors [27]. Further, a large number of preclinical and clinical studies using autologous iPSCs-derived functional cells have been used to treat various diseases in regenerative medicine [28]. Notably, autologous iPSCs have been used to produce retinal pigment epithelial cells to treat age-related macular degeneration [29]. Unfortunately generating autologous iPSCs is expensive and labor-intensive which has limited the therapeutic value of this approach.

An alternative strategy is to provide iPSC products using universal HLAh donors. For this purpose, CB represents an excellent source to produce iPSCs compared with adult cells, such as PBMCs and skin fibroblasts [17]. Previous results have shown that iPSCs derived from adult tissues have higher levels of mitochondrial DNA mutations than those derived from

CBMCs [30], suggesting an advantage of using CB cells to generate iPSCs. Moreover, the most common HLA CB can be selected from a CB bank to produce iPSCs for a wider range of applications. As previously reported, high-resolution HLA CB has been used to establish an iPSCs bank, and the 10 most common homozygous iPSC lines, matching 41.07% of the Korean population, have been characterized [18]. Taylor *et al.* [31] showed that 14 high-frequency homozygous iPSC lines could provide HLA-matched donors for 58.11% of the UK population. We assayed HLAh CB from the Tianjin Cord Blood Public Bank and found that there were 16 homozygous CBs, including HLA-A, -B, -C, -DR, and -DQ. The genotype frequency of the 16 homozygous CB was 6.5% in the Chinese population, matching 11.3% of the Chinese population.

KIRs, also known as CD158, are a group of transmembrane glycoproteins that are universally expressed on NK cells and are key regulators of NK cell cytotoxicity [32,33]. The levels of KIR expression on NK cells mediate the cytotoxicity of NK cells, and targeting KIRs has been shown to be a therapeutic approach to improve clinical outcomes. In addition, a

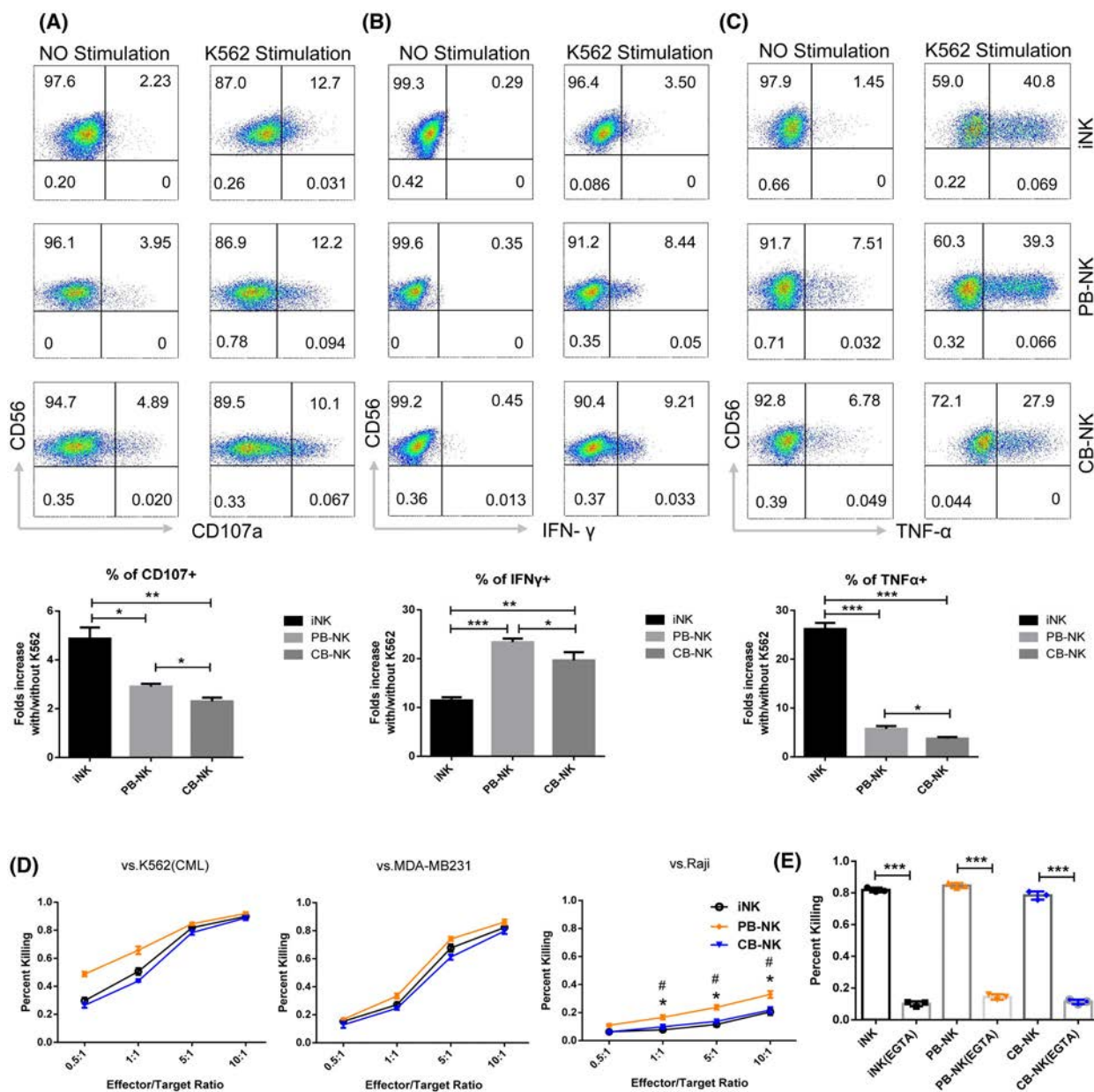


Fig. 7. Functional characterization of iNK cells. (A) Expression of CD107a in iNK, PB-NK, and CB-NK cells ($n = 3$ for each group). Data are represented as the mean \pm SEM. $*P < 0.05$ and $**P < 0.01$ as determined by ANOVA. (B) Expression of IFN- γ in iNK, PB-NK, and CB-NK cells ($n = 3$). Data are represented as the mean \pm SEM. $*P < 0.05$, $**P < 0.01$, and $***P < 0.001$ as determined by ANOVA. (C) Expression of TNF- α in iNK, PB-NK, and CB-NK cells ($n = 3$). Data are represented as the mean \pm SEM. $*P < 0.05$ and $***P < 0.001$ as determined by ANOVA. (D) Cytotoxicity assay against K562, MDA-MB-231, and Raji ($n = 3$). Data are represented as the mean \pm SEM. $*$ or $\#P < 0.05$; $*$: PB-NK vs. iNK; $\#$: PB-NK vs. CB-NK as determined by ANOVA. iNK cells killed K562 cells and MDA-MB-231 cells with comparable capacity as PB-NK and CB-NK cells. PB-NK cells killed Raji cells significantly better than iNK and CB-NK cells. (E) Cytotoxicity assay against K562 (effector/target ratio = 5 : 1) in the presence of EGTA. Data are represented as mean \pm SEM ($n = 3$). Data are represented as the mean \pm SEM. $***P < 0.001$ as determined by Student t -test.

KIR-HLA mismatch donor has to be selected for patients to achieve optimal outcomes [34]. Previously, iPSCs derived from PBMCs were shown to generate KIR-negative NK cells, which may contribute to their

clinical efficacy [12]. Consistent with the observations above, in the present study we also found that cryoCB-iPSCs were able to produce KIRs-negative iNK cells. In addition to the expression of low levels

of KIRs, these iNK cells all expressed typical NK cell surface molecules. Therefore, we hypothesize that our method of using cryoCB-iPSCs to generate a large number of iNK cells is a viable alternative to the traditional methods which will enable additional clinical applications.

Inducing differentiation of iPSCs toward NK cells is a key step in the application of NK cells. One method is to produce CD34⁺ hematopoietic progenitor cells from iPSCs, then promote CD34⁺ hematopoietic progenitor cells to differentiate into NK cells [16,35]. That protocol is complex and reduces the yield of NK cells because of the exclusion of many other hematopoietic progenitors [16,35]. Another method is to form EBs, collect EBs, and then differentiate EBs into NK cells. The traditional method to generate EBs is to inoculate iPSCs with 3000 cells per well into a 96-well plate and then rotate it under appropriate conditions [36]. The generated EBs are then collected and distributed every six spins in one well of a 24-well plate, and differentiated into NK cells. Technically, this method is labor-intensive and difficult to mass-produce NK cells for clinical applications [36]. In the present study, we established an improved protocol for EB formation by transferring cryoCB-iPSCs at a density of 8×10^5 cells·mL⁻¹ to non-TC treated six-well plates with mTeSR™ 3D Medium. These cells were then incubated on a shaking table with a rotation speed of 70 r.p.m. at 37 °C in a 5% CO₂ incubator for 4 days. Embryoid bodies were formed with approximately spherical shapes with a diameter of 150–250 nm on the fourth day. Embryoid bodies were then transferred to non-TC treated six-well plates at a density of 300–400 per well for differentiation into hematopoietic cells. This improved protocol is easy for large-scale production of NK cells, which we believe will meet the needs of various clinical applications.

Conclusion

We report a technique to generate NK cells, that is, ‘from cryoCB to iPSCs, then back to NK cells’, and characterized the resulting NK cells. We found that these iNK cells were similar to those generated from other sources with regard to surface marker expression and functions such as cytotoxicity. Our work demonstrates that this technique is a viable approach to mass-producing NK cells for various clinical applications.

Acknowledgements

This work was supported by Tianjin Science and Technology Research Program, Innovation Platform

Program (18PTSJYC00070); Tianjin Science and Technology Research Program, Overseas R&D Center Program (16PTWYHZ00030); and Tianjin Postdoctoral Support Program (TJQYBSH2018030). We greatly appreciate Medjaden Inc. for the scientific editing of this manuscript.

Conflict of interest

The authors declare no conflict of interest.

Author contributions

Conceptualization, WD and YZ; Funding acquisition, WD and YZ; Methodology, WD, LC, JZ, HZ and RL; Supervision, WY and YZ; Writing – original draft, WD and LC; Writing – review and editing, YZ.

Data availability statement

The authors confirm that all of the data supporting the findings of the present study are available within the article.

References

- Xiao X, Huang S, Chen S, Wang Y, Sun Q, Xu X, et al. Mechanisms of cytokine release syndrome and neurotoxicity of CAR T-cell therapy and associated prevention and management strategies. *J Exp Clin Cancer Res.* 2021;**40**:367.
- Vivier E, Tomasello E, Baratin M, Walzer T, Ugolini S. Functions of natural killer cells. *Nat Immunol.* 2008;**9**:503–10.
- Shimasaki N, Jain A, Campana D. NK cells for cancer immunotherapy. *Nat Rev Drug Discov.* 2020;**19**:200–18.
- Morvan MG, Lanier LL. NK cells and cancer: you can teach innate cells new tricks. *Nat Rev Cancer.* 2016;**16**:7–19.
- Myers J, Miller J. Exploring the NK cell platform for cancer immunotherapy. *Nat Rev Clin Oncol.* 2020;**18**:85–100.
- Liu E, Marin D, Banerjee P, Macapinlac HA, Thompson P, Basar R, et al. Use of CAR-transduced natural killer cells in CD19-positive lymphoid tumors. *N Engl J Med.* 2020;**382**:545–53.
- Dolstra H, Roeven MWH, Spanholtz J, Hangalapura BN, Tordoir M, Maas F, et al. Successful transfer of umbilical cord blood CD34(+) hematopoietic stem and progenitor-derived NK cells in older acute myeloid leukemia patients. *Clin Cancer Res.* 2017;**23**:4107–18.
- Minetto P, Guolo F, Pesce S, Greppi M, Obino V, Ferretti E, et al. Harnessing NK cells for cancer treatment. *Front Immunol.* 2019;**10**:2836.

- 9 Li Y, Hermanson D, Moriarity B, Kaufman D. Human iPSC-derived natural killer cells engineered with Chimeric antigen receptors enhance anti-tumor activity. *Cell Stem Cell*. 2018;**23**:181–92.e5.
- 10 Zhu H, Blum RH, Bjordahl R, Gaidarova S, Rogers P, Lee TT, et al. Pluripotent stem cell-derived NK cells with high-affinity noncleavable CD16a mediate improved antitumor activity. *Blood*. 2020;**135**:399–410.
- 11 Klingemann H, Boissel L, Toneguzzo F. Natural killer cells for immunotherapy – advantages of the NK-92 cell line over blood NK cells. *Front Immunol*. 2016;**7**:91.
- 12 Zeng J, Tang SY, Toh LL, Wang S. Generation of "Off-the-Shelf" natural killer cells from peripheral blood cell-derived induced pluripotent stem cells. *Stem Cell Reports*. 2017;**9**:1796–812.
- 13 Takahashi K, Tanabe K, Ohnuki M, Narita M, Ichisaka T, Tomoda K, et al. Induction of pluripotent stem cells from adult human fibroblasts by defined factors. *Cell*. 2007;**131**:861–72.
- 14 Glicksman M. Induced pluripotent stem cells: the most versatile source for stem cell therapy. *Clin Ther*. 2018;**40**:1060–5.
- 15 Knorr DA, Kaufman DS. Pluripotent stem cell-derived natural killer cells for cancer therapy. *Transl Res*. 2010;**156**:147–54.
- 16 Knorr D, Ni Z, Hermanson D, Hexum M, Bendzick L, Cooper L, et al. Clinical-scale derivation of natural killer cells from human pluripotent stem cells for cancer therapy. *Stem Cells Transl Med*. 2013;**2**:274–83.
- 17 Haase A, Olmer R, Schwanke K, Wunderlich S, Merkert S, Hess C, et al. Generation of induced pluripotent stem cells from human cord blood. *Cell Stem Cell*. 2009;**5**:434–41.
- 18 Lee S, Huh JY, Turner DM, Lee S, Robinson J, Stein JE, et al. Repurposing the Cord Blood Bank for Haplobanking of HLA-homozygous iPSCs and their usefulness to multiple populations. *Stem Cells*. 2018;**36**:1552–66.
- 19 Su RJ, Neises A, Zhang XB. Generation of iPSCs from human peripheral blood mononuclear cells using episomal vectors. *Methods Mol Biol*. 2016;**1357**:57–69.
- 20 Wen W, Zhang JP, Xu J, Su RJ, Neises A, Ji GZ, et al. Enhanced generation of integration-free iPSCs from human adult peripheral blood mononuclear cells with an optimal combination of episomal vectors. *Stem Cell Reports*. 2016;**6**:873–84.
- 21 Ng E, Davis R, Stanley E, Elefanty A. A protocol describing the use of a recombinant protein-based, animal product-free medium (APEL) for human embryonic stem cell differentiation as spin embryoid bodies. *Nat Protoc*. 2008;**3**:768–76.
- 22 Zhou X, Zhu F, Li J, Mao W, Zhang D, Liu M, et al. High-resolution analyses of human leukocyte antigens allele and haplotype frequencies based on 169,995 volunteers from the China Bone Marrow Donor Registry Program. *PLoS ONE*. 2015;**10**:e0139485.
- 23 Chester C, Fritsch K, Kohrt HE. Natural killer cell immunomodulation: targeting activating, inhibitory, and co-stimulatory receptor signaling for cancer immunotherapy. *Front Immunol*. 2015;**6**:601.
- 24 Lapteva N, Szmania S, van Rhee F, Rooney C. Clinical grade purification and expansion of natural killer cells. *Crit Rev Oncog*. 2014;**19**:121–32.
- 25 Zhu H, Kaufman DS. An improved method to produce clinical-scale natural killer cells from human pluripotent stem cells. *Methods Mol Biol*. 2019;**2048**:107–19.
- 26 Takahashi K, Yamanaka S. Induction of pluripotent stem cells from mouse embryonic and adult fibroblast cultures by defined factors. *Cell*. 2006;**126**:663–76.
- 27 Karagiannis P, Kim S-I. iPSC-derived natural killer cells for cancer immunotherapy. *Mol Cells*. 2021;**44**:541–8.
- 28 Kikuchi T, Morizane A, Doi D, Magotani H, Onoe H, Hayashi T, et al. Human iPS cell-derived dopaminergic neurons function in a primate Parkinson's disease model. *Nature*. 2017;**548**:592–6.
- 29 Souied E, Pulido J, Staurengi G. Autologous induced stem-cell-derived retinal cells for macular degeneration. *N Engl J Med*. 2017;**377**:792.
- 30 Malik N, Rao MS. A review of the methods for human iPSC derivation. *Methods Mol Biol*. 2013;**997**: 23–33.
- 31 Taylor C, Peacock S, Chaudhry A, Bradley J, Bolton E. Generating an iPSC bank for HLA-matched tissue transplantation based on known donor and recipient HLA types. *Cell Stem Cell*. 2012;**11**:147–52.
- 32 Thielens A, Vivier E, Romagné F. NK cell MHC class I specific receptors (KIR): from biology to clinical intervention. *Curr Opin Immunol*. 2012;**24**:239–45.
- 33 Parham P. MHC class I molecules and KIRs in human history, health and survival. *Nat Rev Immunol*. 2005;**5**:201–14.
- 34 Leung W. Infusions of allogeneic natural killer cells as cancer therapy. *Clin Cancer Res*. 2014;**20**:3390–400.
- 35 Woll PS, Martin CH, Miller JS, Kaufman DS. Human embryonic stem cell-derived NK cells acquire functional receptors and cytolytic activity. *J Immunol*. 2005;**175**:5095–103.
- 36 Tabatabaei-Zavareh N, Vlasova A, Greenwood CP, Takei F. Characterization of developmental pathway of natural killer cells from embryonic stem cells in vitro. *PLoS ONE*. 2007;**2**:e232.

RESEARCH ARTICLE

Production of homogenous size-controlled human induced pluripotent stem cell aggregates using ring-shaped culture vessel

Fuad Gandhi Torizal^{1,2}  | Seong Min Kim² | Ikki Horiguchi³ | Kousuke Inamura¹ | Ikumi Suzuki⁴ | Takashi Morimura⁴ | Masaki Nishikawa¹ | Yasuyuki Sakai^{1,2}

¹Department of Chemical Systems Engineering, Graduate School of Engineering, The University of Tokyo, Bunkyo-ku, Japan

²Department of Bioengineering, Graduate School of Engineering, The University of Tokyo, Bunkyo-ku, Japan

³Department of Biotechnology, Graduate School of Engineering, Osaka University, Suita, Japan

⁴Division of Biotechnology Industrial Equipments, Fukoku Ltd, Saitama, Japan

Correspondence

Fuad Gandhi Torizal, Department of Chemical Systems Engineering, Graduate School of Engineering, The University of Tokyo, Bunkyo-ku, Japan.

Email: t_gandhi@chemsys.t.u-tokyo.ac.jp

Abstract

Aggregate size is an important parameter that determines the cell fate and quality of the resulting human-induced pluripotent stem cells (hiPSCs). Nowadays, large-scale suspension culture is a common method for scaling-up the bio-manufacturing of hiPSCs to realize their practical application. However, this culture system exhibits a complex hydrodynamic condition resulting from the different mixing conditions of culture media, which potentially produce non-uniform aggregates, which may decrease the quality of the cell yield. Here, we performed expansion in a ring-shaped culture vessel and compared it with three other suspension-based culture systems to evaluate the uniformity and characteristics of hiPSC aggregates. Morphologically, the hiPSC aggregates formed and expanded in the ring-shaped culture vessel, resulting in small and uniform aggregates compared to the other culture systems. This aggregate population showed a decent mass transfer required for the exchange of biochemical substances, such as nutrients, growth factors, oxygen, and waste metabolic products, inside the aggregates. Thus, better metabolic performance and pluripotency markers were achieved in this system. Interestingly, all culture systems used in this study showed different tendencies in embryoid body differentiation. The smaller aggregates produced by sphere ring and dish bag tended to differentiate toward ectodermal and mesodermal lineages, while predominantly larger aggregates from the 6-well plates and spinner flask exhibited more potential for endodermal lineage. Our study demonstrates the production of a decent homogenous aggregate population by providing equal hydrodynamic force through the ring-shaped culture vessel design, which may be further upscaled to produce a large number of hiPSCs for clinical applications.

KEYWORDS

aggregates size, differentiation potential, hiPSCs, pluripotency, ring-shaped culture vessel

1 | INTRODUCTION

Human-induced pluripotent stem cells (hiPSCs) exhibit potential for various applications in regenerative medicine, such as transplantation. To realize this application, a sufficient number of hiPSC-derived cells are required to regenerate large organs. For example, 6×10^8 beta cells are required for pancreatic islet transplantation (Zweigerdt, 2009) and 6×10^{10} liver cells are required to regenerate 30% of the liver (Bianconi et al., 2013). To meet this demand, suspension-based large-scale expansion of hiPSCs needs to be performed.

Appropriate modulation of stem cell aggregation may offer enormous potential for future applications in stem cell-based therapies. In addition to biological factors, culture vessel design may affect the biomanufacturing process in hiPSC expansion. Currently, several culture systems, such as stirred bioreactor (Fridley et al., 2010; Olmer et al., 2012) or orbital rotary culture (Carpenedo et al., 2007; Fridley et al., 2010; Sargent et al., 2010), have been developed to establish a system that provides a decent culture environment to achieve a large number of cell yields, sustain self-renewal properties, and maintain pluripotency during hiPSC expansion. However, these culture systems often produce non-uniform aggregate populations. These non-uniform aggregates may result in heterogeneity among the cell yields due to a concentration gradient that limits the transfer of nutrients and toxic metabolic products inside different regions of the larger aggregates. To some extent, the large diameter of aggregates may cause a necrotic core or spontaneous differentiation, which may not be appropriate for practical applications.

The centrifugal force in the conventional orbital culture creates a circular flow that causes the phenomenon of aggregate accumulation in the central part of the culture vessel, known as “Einstein's tea leaf paradox,” (Horiguchi et al., 2019; Yogananda & Einstein, 2000) which causes inhomogeneous aggregation of the hiPSCs. To address this problem, we developed a ring-shaped culture bag that excludes the central area of the culture, avoiding undesirable aggregate accumulation in the central part. This culture design approach successfully created an equal hydrodynamic condition to control the size of the aggregates and maintain their uniformity both in aggregate formation and during the expansion period. Our study demonstrated the feasibility of producing homogenous hiPSC aggregates for various applications in regenerative medicine.

2 | MATERIALS AND METHODS

2.1 | Monolayer cell culture

The hiPSC cell line, TkDN4-M, was provided by Stem Cell Bank, Center for Stem Cell Biology and Regenerative Medicine, The

University of Tokyo, Japan (Takayama et al., 2010). The cells were cultured and maintained in a vitronectin-coated tissue culture dish using Essential 8 (E8) culture medium (Life Technologies) with daily medium replacement.

2.2 | Observation of the movement of aggregates

HiPSCs in monolayer were harvested using 0.5 mM ethylenediaminetetraacetic acid (EDTA) in phosphate-buffered saline (PBS) (FUJIFILM WAKO Pure Chemical) for 5–10 min of incubation, followed by a gentle dissociation with E8 medium sprayed using a micropipette. The single cells were then filtered through a 40 μ m cell strainer (Corning), and the filtered cells were resuspended in the growth medium. The cell aggregates were produced by inoculating 5×10^5 cells/mL density (2×10^6 single-cell suspension in 4 ml E8 medium (Life Technologies)) containing 10 μ M Y27632 at day 0 (FUJIFILM WAKO Pure Chemical) per well in non-treated 6-well plates (Iwaki). The cells were grown in 90 rpm suspension culture for another 3 days with daily E8 medium replacement without Y27632. The cell aggregates were fixed by replacing the culture medium with 4 ml of 4% paraformaldehyde overnight, followed by staining with 4 ml Quick-CBB Plus (FUJIFILM WAKO Pure Chemical) for 24 h. To observe the pattern of aggregate movement during dynamic suspension culture operations, the stained aggregates were suspended in Dulbecco's modified Eagle's medium (DMEM)/Ham's F-12 culture medium without phenol red (FUJIFILM Wako Pure Chemical) and inserted into each dynamic culture system. Images and videos were recorded using a DSLR camera (Canon).

2.3 | Aggregates expansion in the suspension culture vessel

The hiPSCs in monolayer were harvested using 0.5 mM EDTA in PBS and incubated for 5–10 min following gentle dissociation with E8 medium spraying using a micropipette. Subsequently, the single-cell suspension was produced by passing the harvested cell suspension through a 40 μ m cell strainer. To generate the hiPSC aggregates, 2×10^5 cells/mL were inoculated with 20 ml of E8 medium containing 2% free fatty acid-bovine serum albumin (BSA-FFA) (FUJIFILM WAKO Pure Chemical) and 10 μ M Y27632 (FUJIFILM WAKO Pure Chemical) in each culture system with optimum rotational speed, as shown in Figure 1a,b. Medium replacement was performed on days 2 and 4 with 20 ml of E8 medium, without BSA-FFA and Y27632.

2.4 | Morphological observation

Each of the aggregate populations produced by the different culture systems was moved into 12-well plates under a light microscope. The

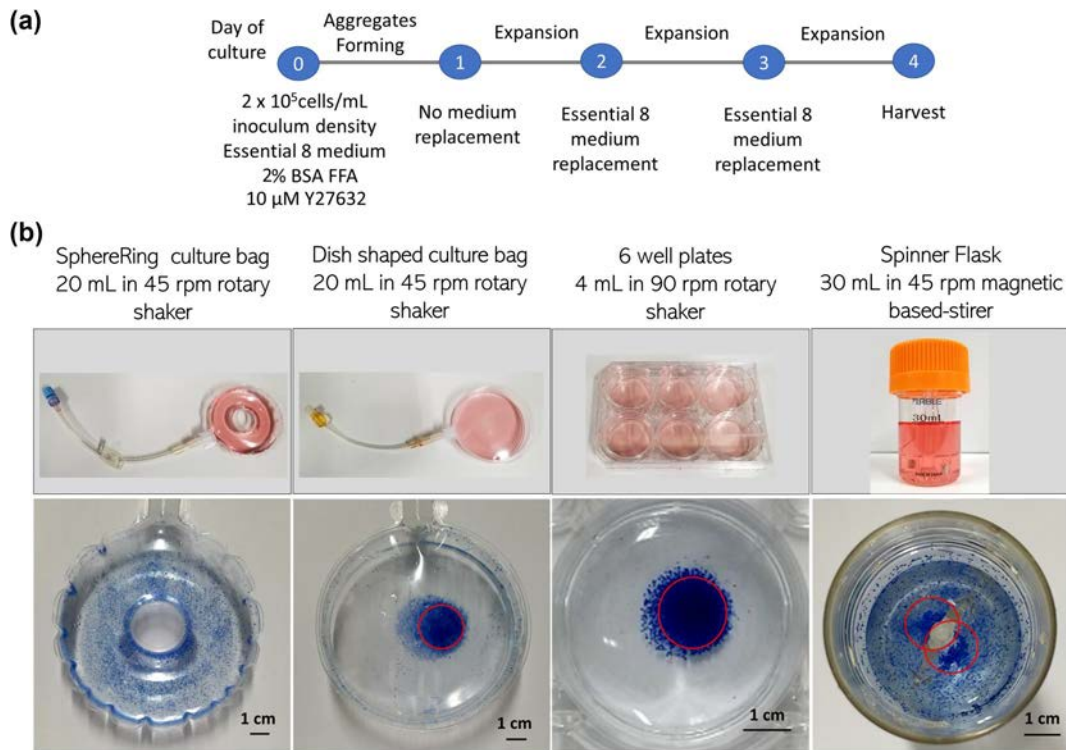


FIGURE 1 Culture platform used in this study. (a) Expansion procedure in all of the culture systems; (b) Aggregates movement in different culture systems. Red circle shows the gathered aggregates as a pattern of a non-uniform hydrodynamic condition among the area inside each of the culture vessels [Colour figure can be viewed at wileyonlinelibrary.com]

image of the aggregate colony was taken using a microscope (Olympus), and its diameter was analyzed using FIJI/ImageJ software (Schindelin et al., 2012) (National Institutes of Health).

2.5 | Aggregates counting and size measurement of aggregates population

The aggregate suspension was transferred into a 50 ml tube and placed under static conditions until all of the aggregates were sedimented at the bottom of the tube. The medium supernatant was aspirated until it remained at approximately 5 ml. Afterward, the remaining aggregate suspension was transferred into 6-well plates which were previously marked with 5 mm × 5 mm square patterns by a permanent marker on the outer transparent bottom surface, followed by aggregate counting under a light microscope. The images of the aggregates were captured using a light microscope and approximately 500 aggregates were measured by image analysis using FIJI/ImageJ software (Schindelin et al., 2012) (National Institutes of Health).

2.6 | Determination of cell number

The aggregates were collected by centrifugation at 1000 rpm for 3–5 min. The culture medium was aspirated, and the aggregates were incubated with Accutase solution (Stemcell Technologies) for 30 min

at 37°C, followed by aggregate dissociation by gentle pipetting. The cell number was determined using a hemocytometer (TATAI).

2.7 | Lactate dehydrogenase (LDH) assay

The culture medium was isolated every 24 h and analyzed using an LDH assay kit (FUJIFILM WAKO Pure Chemical) according to the manufacturer's instructions. The number of injured cells was calibrated using the serial number of diluted cells that were intentionally injured by PBS-Tween 20.

2.8 | Glucose and lactate measurement

The culture medium was isolated every 24 h, and the concentrations of glucose and lactate were measured using an OSI BF-48AS Bio-analyzer (Oji Scientific Instrument).

2.9 | Hematoxylin-eosin staining of cross-sectioned aggregates

Aggregate populations were collected and fixed with 4% para-formaldehyde (FUJIFILM WAKO Pure Chemical) in PBS for 1 h at room temperature, followed by incubation in 30% PBS-sucrose

solution (FUJIFILM WAKO Pure Chemical) at 4°C overnight. The aggregates were placed in a cryomold and embedded with Tissue-Tek OCT compound (Sakura) at -80°C until hardening. Thin sections (10 µm) were prepared using a cryostat (Leica Biosystems) and mounted onto glass slides for hematoxylin-eosin staining.

2.10 | Terminal deoxyribonucleotidyl transferase (TdT)-mediated dUTP nick-end labeling (TUNEL) assay

The TUNEL assay was performed on aggregates obtained from each culture system. As a positive control, the aggregates were treated with a daily medium containing 500 ng/ml doxorubicin hydrochloride for 72 h to induce apoptosis. The aggregates were fixed with 4% paraformaldehyde for at least 30 min. After washing with PBS, the aggregates were permeabilized with 1 ml of 1% Triton X for 1 h in an orbital shaker at room temperature. Then, triton x was removed and washed with PBS, followed by incubation with ice-cold 70% ethanol for a minimum of 30 min at -20°C. Apoptotic cells were identified using the in situ direct DNA fragmentation assay kit (Abcam). Then, 70% ethanol was removed, and the aggregates were washed twice using 1 ml of the wash buffer. After washing, the aggregates were incubated with the staining solution included in the kit (containing 100 µl TdT reaction buffer, 7.5 µl TdT enzyme, 80 µl fluorescein isothiocyanate (FITC)-dUTP, and 322.5 µl ddH₂O) for 60–120 min at 37°C in a rotary shaker. The two times rinsing step was repeated twice by adding 1 ml of rinse buffer to each tube, followed by 3 min centrifugation at 100 rpm. The supernatant was removed by aspiration. HiPSC aggregates were then incubated with propidium iodide/RNase A solution (0.5 ml) in the dark at room temperature for 30–60 min. Apoptotic cells inside the aggregates were analyzed by fluorescence microscopy.

2.11 | FITC penetration assay

To evaluate the penetration capability of the molecules into the aggregates, approximately 100 aggregates were isolated from each culture system. These aggregates were cultured in each well of 6-well plates at 90 rpm in a rotary shaker using E8 medium containing 20 µg/ml of 4 kDa FITC dextran (Sigma Aldrich). Fluorescence imaging of FITC penetration was performed using an FV1200 confocal microscope (Olympus) after 24 h.

2.12 | Alkaline phosphatase activity

To detect the activity of intracellular alkaline phosphatase, aggregates were harvested and stained with an AP staining kit II (Stemgent), with several modifications for aggregate staining using gentle rotational agitation. After washing with 1 × PBST, the aggregates

were incubated with 2 ml fixed solution in 6-well plates at room temperature for 30 min, washed with 1 × PBST, and incubated at room temperature with 3 ml AP substrate solution in the dark for 90 min. The stained aggregates were washed with PBS and observed under a light microscope (Olympus).

2.13 | Flow cytometry analysis

HiPSC aggregates were dissociated by 30 min of incubation in Accutase solution (Stemcell Technologies) at 37°C. Afterward, the aggregates were dissociated by gentle pipetting, and single-cell suspensions were obtained by physical dissociation using a 40 µm cell strainer (Corning, New York, USA) and counted using a hemocytometer. Cells (10⁶) were fixed with 1 ml of 4% paraformaldehyde and stained with Alexa Fluor conjugated-stage-specific embryonic antigen (SSEA)-4 antibody (Biolegend). Flow cytometry analysis was performed using a Coulter Epics Flow Cytometer (Beckman Coulter). All antibodies used in this analysis are listed in Table S1.

2.14 | Immunocytochemistry

The aggregates were fixed with 4% paraformaldehyde overnight at 4°C. The aggregates were then permeabilized with 1% Triton X (Thermo Fisher Scientific) for 1 h, followed by 1 h incubation with gelatin blocking buffer solution containing 1% PBS-Tween (Nacalai Tesque) at room temperature. To detect the protein targets, the aggregates were moved into 48-well plates and incubated with 1 µg/ml primary antibodies for 4 days, followed by incubation with 1 µg/ml secondary antibodies for 2 days. This incubation was performed by shaking the plates with a rotary shaker at 4°C. The aggregates were incubated with 1:1000 nuclear staining 4', 6-diamidino-2-phenylindole (DAPI) (Dojindo) and 1:1000 actin filament phalloidin for 30–40 min before observation. Fluorescence imaging was performed using an FV1200 confocal microscope (Olympus), and image-based quantification was performed using FIJI/ImageJ software (Schindelin et al., 2012) (National Institutes of Health). All the antibodies used in this analysis are described in Table S1 in supporting information.

2.15 | Gene expression analysis by quantitative polymerase chain reaction (qPCR)

Total RNA was isolated and purified using TRIzol reagent (Life Technologies), followed by cDNA synthesis using ReverTra Ace qPCR RT Master Mix (Toyobo). qPCR analysis was performed using StepOnePlus quantitative reverse transcription-polymerase chain reaction (qRT-PCR) (Thermo Fisher Scientific) with Thunderbird SYBR qPCR Mix (Toyobo), following the manufacturer's instructions. The primer sequences used in this analysis are listed in Table S2 in supporting information.

2.16 | Spontaneous differentiation assay

Approximately 100 hiPSC aggregates were transferred into 6-well plates and the culture medium was replaced with DMEM/F12 (Life Technologies) supplemented with 10% fetal calf serum (FUJIFILM WAKO Pure Chemical) in static suspension culture for 7 days. The gene expression levels of the three germ layer markers were measured using qRT-PCR. The primer sequences used in this analysis are listed in Table S2 in supporting information.

2.17 | Analysis of the genetic abnormality

Genomic DNA was purified using the Genomic DNA Purification Kit (StemCell Technologies). Genetic abnormalities were evaluated using the hPSC Genetic Analysis kit (StemCell Technologies) according to the manufacturer's instructions. Amplification and analysis were performed using StepOnePlus qPCR (Thermo Fisher Scientific). Genetic abnormalities could be detected when the copy number of Chr 1q-20q was less than 1.8 or more than 2.2 with a p -value < 0.05.

2.18 | Statistical analysis

Statistical analysis was performed using GraphPad Prism software v.8.3.0 (GraphPad Software). Statistical significance was determined by one-way analysis of variance with Tukey's multiple comparison test. The results are presented as the mean \pm standard error (SE). The value of $p < 0.05$ was considered to represent a statistically significant difference.

3 | RESULTS

3.1 | The effect of hydrodynamic condition on the morphology of aggregates

Based on the evaluation of the hydrodynamic condition by stained aggregates, each culture system showed a different pattern of aggregate movement in the culture vessel area. The localization of the stained aggregate population during dynamic suspension revealed an unequal distribution of the aggregate population among the culture vessel area, which largely depended on the mixing methods (Figure 1b; Video S1). Meanwhile, the sphere ring vessel showed a well-mixed distribution of the aggregates during rotational culture (Figure 1b; Video S1).

In our study, BSA-FFA was included in the first two days of culture to control aggregation and reduce excess agglomeration in all culture systems (Horiguchi & Sakai, 2016). A small and uniform population of cell aggregates was better achieved during aggregate formation in the sphere ring culture system (Figure 2a). This phenomenon occurred because of the design that prevents the tendency of aggregate accumulation in the center area of the culture vessel

during rotational culture, as shown in the dish bag and conventional six well culture vessel. The tendency to gather at the center area of the round vessel by the centrifugal force is also known as the Einstein tea leaves phenomenon. In contrast, the spinner flask generated a low number of non-uniform populations of cell aggregates in size, which consisted of predominantly darker large aggregates (Figure 2a), which may be related to the hydrodynamic condition, which shows a number of aggregate accumulations that are gathered near the impeller axis (Video S1).

3.2 | Effect of different hydrodynamic conditions on aggregates formation and cellular injury

A higher number of small and homogenous aggregate populations was produced during the expansion period in the sphere ring (Figure 2a). Exclusion of the central area in the sphere ring vessel caused the aggregates to migrate through the intermediate and outer areas, which have longer distances per rotational period. This condition creates a dynamic culture environment that allows a higher number of aggregates with a small and homogenous population compared to other culture systems (Figure 2a,b). However, a lower number of viable cells resulted in this system during initial aggregate formation. This condition may be caused by the higher shear stress-induced cell injury compared to the other culture systems in this study (Figure 2c,d). This culture system produced a lower fold expansion compared to the other culture systems used in this group (Figure 2d). The impact of shear stress was confirmed by higher cellular injury, as determined by the amount of intracellular lactate dehydrogenase in the medium leaking from the cell membrane rupture (Figure 3a).

3.3 | Cellular metabolism of hiPSCs during expansion

Although the total glucose concentration in the culture medium was depleted over time due to cellular consumption, its concentration was still sufficient to support the feeding of the proliferated hiPSCs until day four (Figure 3b). The total lactate concentration was maintained at a concentration lower than 1.5 g/L, which was previously studied by Ouyang et al. (2006) as a critical concentration limit that can disrupt cell viability and pluripotency in PSC spheroids by decreasing the pH of the culture medium (Figure 3c). This condition indicated that lactate stress did not interfere much in all culture systems used in this study.

Lower cell number resulted from the aggregates formed in the sphere ring culture bag. Nevertheless, they exhibit a relatively high glucose consumption and even higher lactate secretion compared to the aggregates produced in other culture systems (Figure 4d,e). The higher production of lactate per unit glucose of hiPSCs expanded in the sphere ring indicated a better cellular metabolism of hiPSC aggregates (Figure 4f). The exchange of nutrients and toxic byproducts may be better achieved in smaller aggregates than in larger ones.

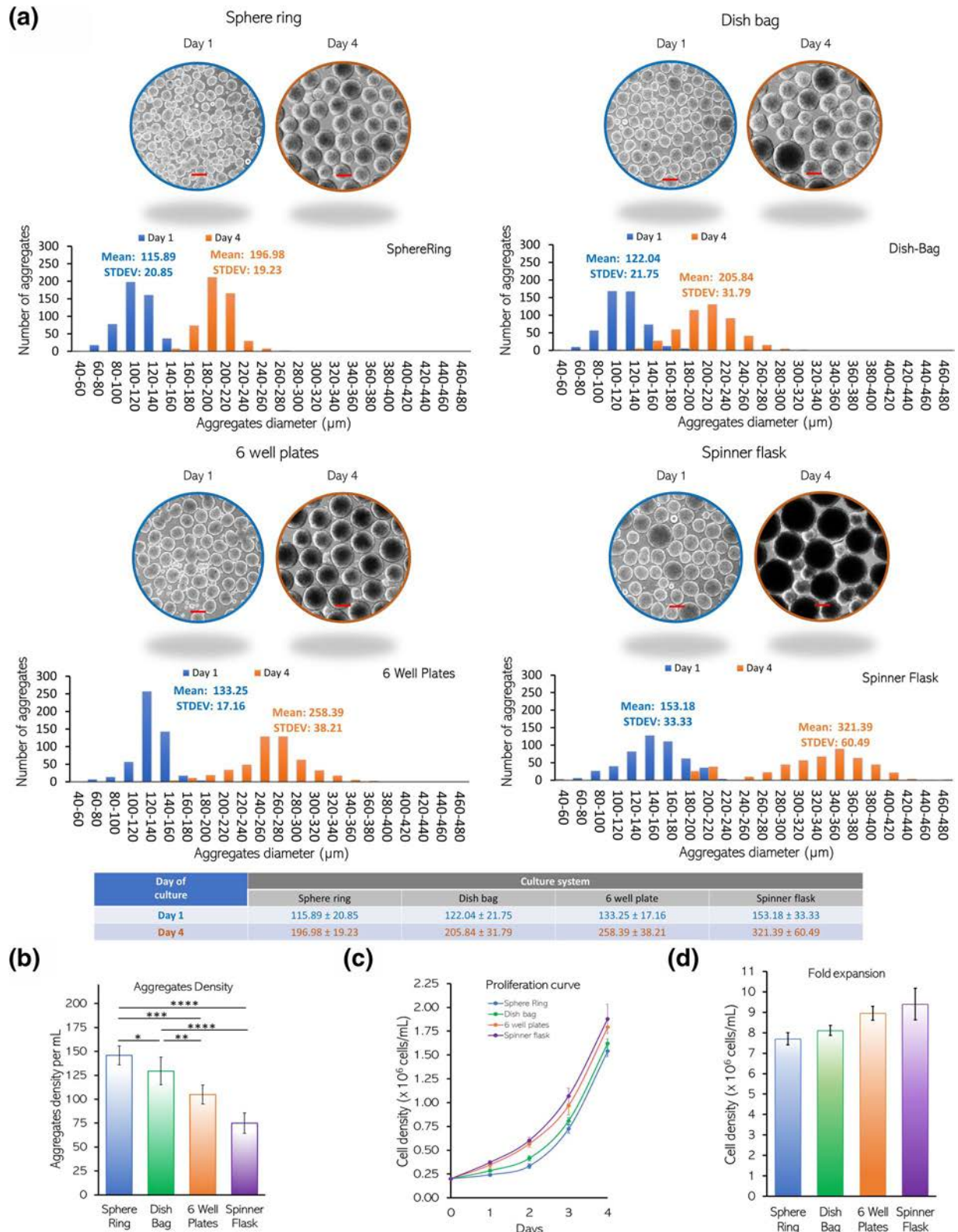


FIGURE 2 Resulting aggregates morphology and growth pattern in different culture platforms. (a) Distribution of the size of aggregates during aggregates formation (blue) and at the end of expansion (orange). The average and standard deviation was calculated from 500 aggregates from each individual culture system (Scale bar: 200 μm). (b) Post-expansion aggregates density (c) Proliferation curve during hiPSCs expansion (d) Fold expansion after 4 days of culture [Colour figure can be viewed at wileyonlinelibrary.com]

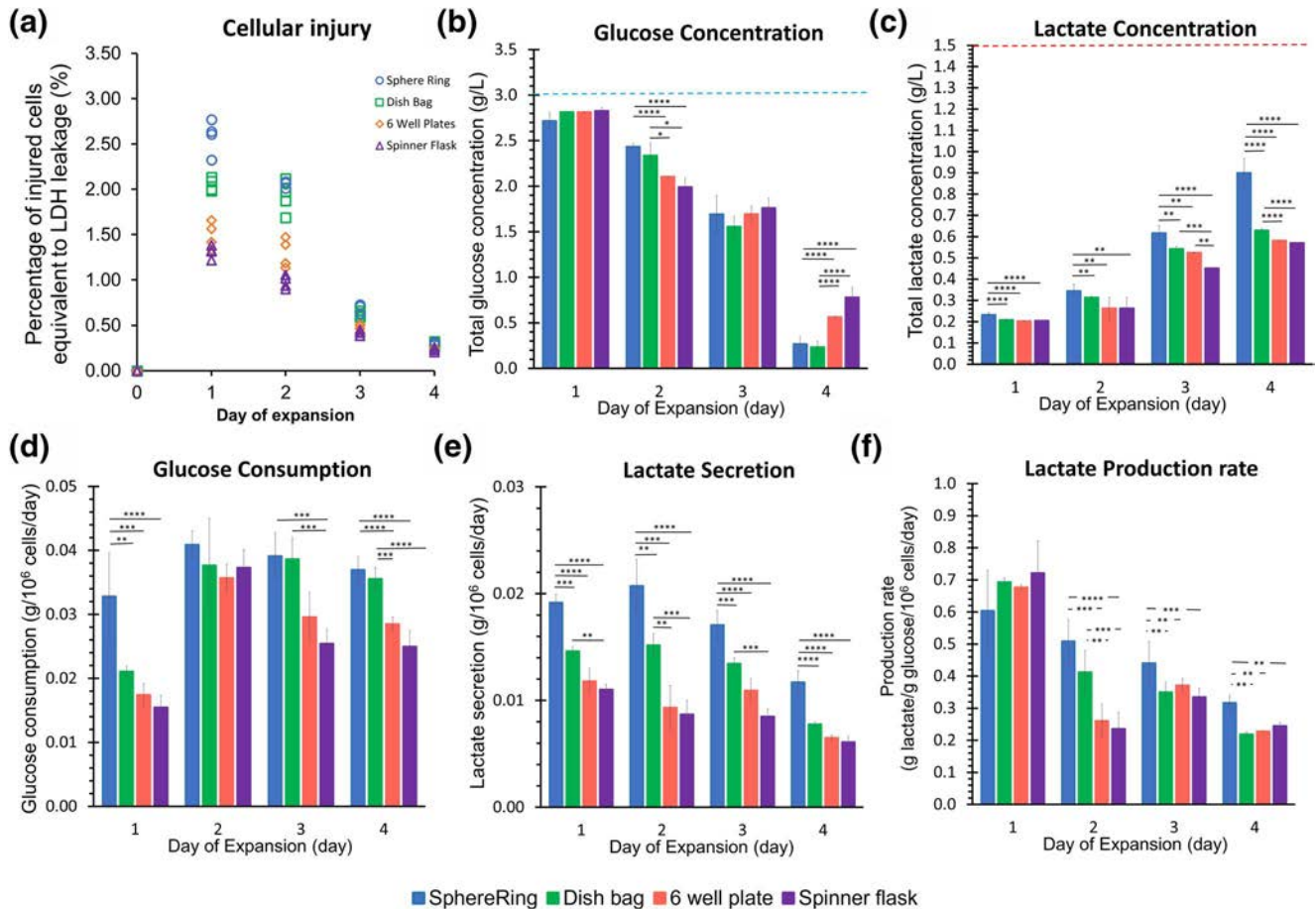


FIGURE 3 Shear-stress-induced cellular injury and kinetics of cellular metabolism. (a) Cellular injury relative to lactate dehydrogenase (LDH) leakage. Concentration of (b) glucose and (c) lactate in the culture medium. Glucose concentration in E8 medium indicated by blue line and critical lactate concentration limit described by Ouyang, et al. indicated by red line. To observe the metabolic activity, (d) glucose consumption and (e) lactate secretion per cell during the expansion period were calculated. (f) Lactate production per unit glucose consumption ($N = 4$ biological replicates). Mean \pm standard deviation are indicated in each graph. Statistical significance: **** $p < 0.0001$; *** $p < 0.001$; ** $p < 0.01$; * $p < 0.05$ [Colour figure can be viewed at wileyonlinelibrary.com]

3.4 | Mass transfer limitation in aggregates of different sizes

Based on the histological analysis, staining, and apoptosis assays, the aggregates expanded in all of the culture systems and did not show any necrotic core or apoptotic cells (Figure 5a,b). Nevertheless, further evaluation is necessary to characterize their capability to transfer large molecules that are required for maintaining pluripotency during the expansion period (Tchoryk et al., 2019). Accordingly, we observed an increasing gradient concentration of 4 kDa FITC during 24 h of culture, along with an increase in the aggregate diameter. In larger aggregates resulting from the spinner flask, FITC was deposited on the outer and middle layers of the aggregate (Figure 5c). Additionally, the darker part shows the limitation of the FITC penetration into the core of the large aggregate, which may limit the penetration and exposure of large molecules, such as growth factors, into the core of the aggregate. This result indicated a potential mass transfer limitation of the relatively higher molecular weight of macromolecule growth factors that were included in the

medium formulation in this study (Chen et al., 2011), such as insulin (5.74 kDa), transferrin (80 kDa), TGF β 1 (25 kDa), and FGF2 (18 kDa).

3.5 | Pluripotency preservation, differentiation potential, and genomic stability of resulting hiPSCs

In the expanded aggregates under all culture systems, we found a similar activity of alkaline phosphatase as a basic marker for the identification of the high metabolic activity of PSCs (Figure 5a). Pluripotency markers, such as SSEA3/4, octamer-binding transcription factor (OCT)-4, and SRY-box transcription factor 2 (SOX2), were highly expressed in the hiPSC aggregates expanded in the sphere ring culture system (Figure 5b-d). We hypothesized that the higher expression of pluripotency markers in sphere rings may be related to the better mass transfer of nutrients, toxic metabolic byproducts, and growth factors in smaller aggregates.

For further analysis, we performed immunocytochemistry of actin filaments. The filament was upregulated in larger aggregates

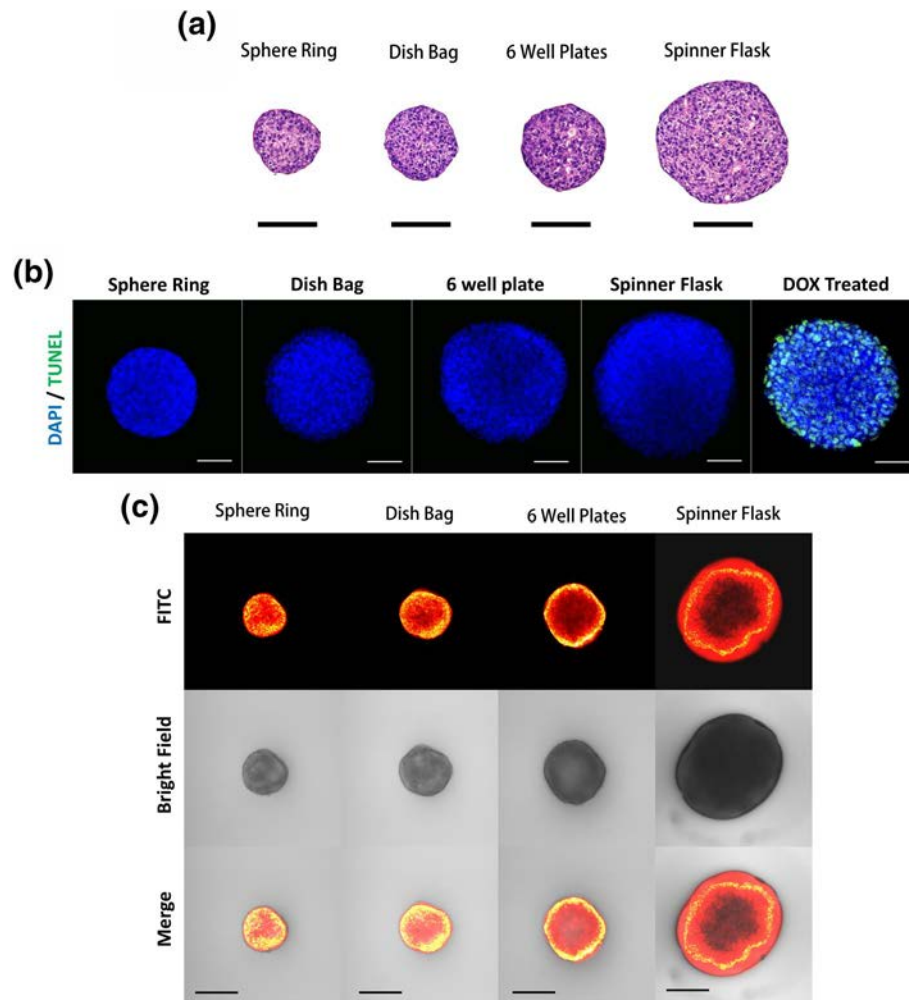


FIGURE 4 Limitation of mass transfer inside the aggregates: (a) Hematoxylin-eosin staining showing that there is no necrotic core in all of the samples (Scale bar: 200 μ m). (b) Apoptotic cells (green) were not detected in aggregates expanded in the culture systems after the culture period, compared to the apoptosis-induced aggregates by doxorubicin treatment used as the positive control. (c) The difference of 4 KDa fluorescein isothiocyanate (FITC) molecule permeability showing an increasing limitation of molecule penetration into the core of large aggregates. Highest FITC intensity showed in yellow, medium FITC intensity showed in red, and the lowest FITC intensity showed by the dark area (Scale bar: 200 μ m). DAPI, 6-diamidino-2-phenylindole [Colour figure can be viewed at wileyonlinelibrary.com]

generated from the spinner flask, as shown in Figure 5c. This condition may create strong adhesiveness between cells inside the aggregates, which can increase the compactness of the aggregates. Additionally, the proliferated area was reduced in the central parts of these compact aggregates, which was likely triggered by their mass transfer limitation. This condition was confirmed by the reduction of the proliferation marker Ki67 and its localization in the peripheral area of the aggregates (Figure 5e).

The differentiation capacity was evaluated by spontaneous differentiation assays of embryoid bodies derived from hiPSCs from each culture system after the expansion period (Figure 6a). The results showed that the embryoid bodies derived from sphere rings and dish bags tended to differentiate into ectodermal and endodermal lineages. On the contrary, the larger embryoid bodies resulting from 6-well plates and spinner flask showed their tendency to differentiate into endoderm lineage rather than ectodermal and mesodermal lineages.

To confirm the possible chromosomal abnormality that may be affected by various culture conditions, genomic analysis was performed on the aggregate population after the expansion period (Figure 6b). The results showed that hiPSCs expanded in all culture systems and were able to maintain genomic stability during the culture period.

4 | DISCUSSION

In this study, we successfully achieved decent aggregate uniformity by modulating the homogenous hydrodynamic conditions in a ring-shaped culture vessel. To meet the ideal criteria for hiPSC bio-manufacturing, a small and uniform aggregate population must be generated at the initial expansion stage. The optimum hydrodynamic exposure is required to support normal growth and produce

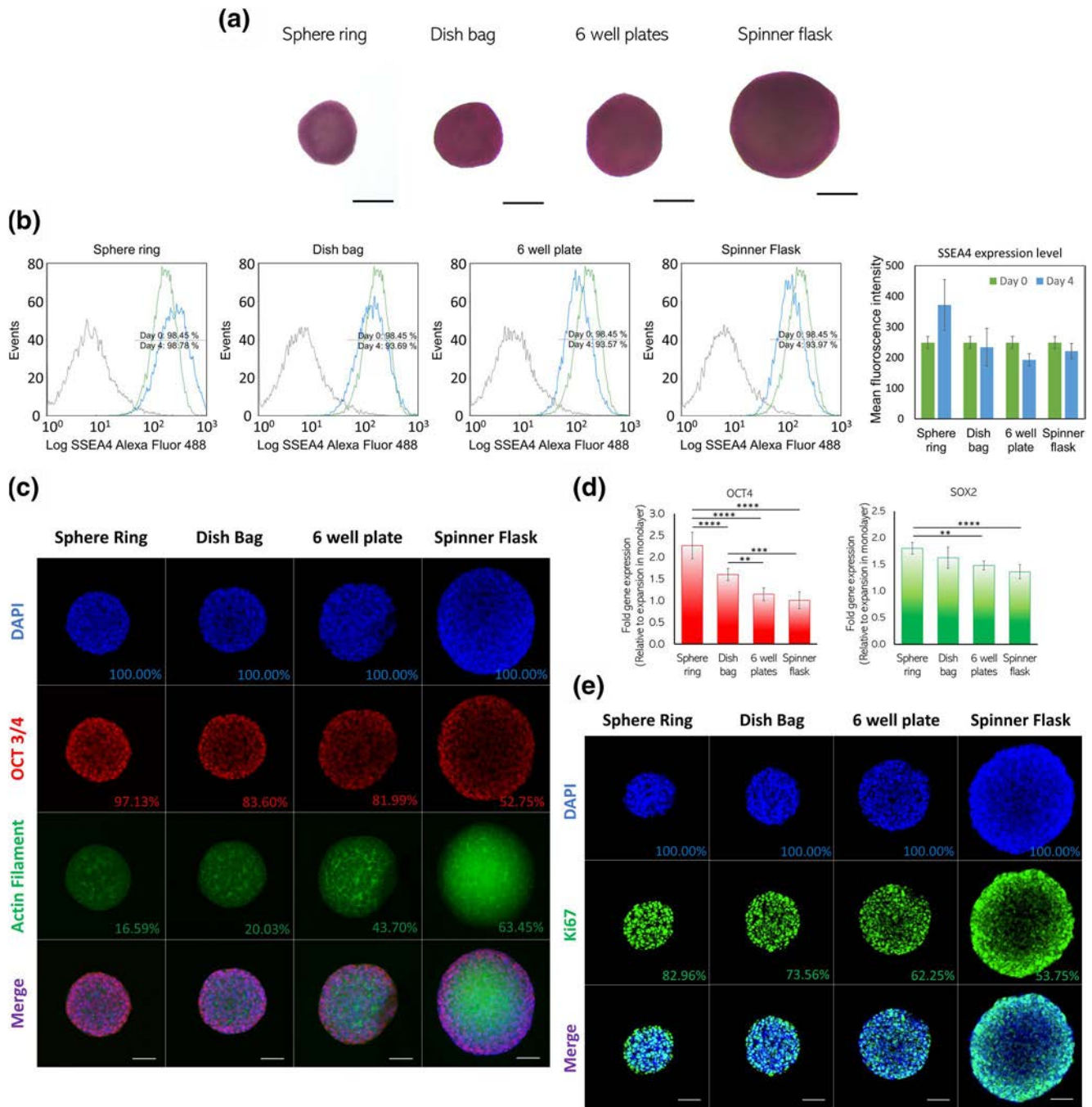


FIGURE 5 Characterization of human-induced pluripotent stem cells (hiPSCs) aggregates. (a) All aggregates showed a similar level of alkaline phosphatase activity (Scale bar: 200 μ m) (b) Flow cytometry assays for stage-specific embryonic antigen 4 (SSEA4) and mean fluorescence intensity. SSEA4 expression is shown in green (day 0) and blue (day 4). The mean fluorescence intensity \pm standard deviation are indicated in the graph. (c) Immunocytochemistry of octamer-binding transcription factor (OCT)-3/4 and actin filament (Scale bar: 100 μ m) (d) Higher level of pluripotency marker OCT4 and SOX2 was observed in hiPSCs expanded in Sphere ring ($N = 4$ biological replicates). (e) Expression of proliferation marker, Ki67. Mean \pm standard deviation are indicated in each graph. The percentage indicates the expression level relative to nuclear staining with 4', 6-diamidino-2-phenylindole (DAPI). Statistical significance: **** $p < 0.0001$; *** $p < 0.001$; ** $p < 0.01$; * $p < 0.05$ [Colour figure can be viewed at wileyonlinelibrary.com]

undifferentiated hiPSCs for translational applications, as shown in Figure 6c. This proper condition is very important for controlling the size of the aggregates, mainly during the aggregate formation period.

Several mixing conditions in various dynamic culture vessels were introduced to reduce the concentration gradient of nutrients or waste metabolic products in the culture area and enhance the oxygen exchange in the culture medium. This condition can be

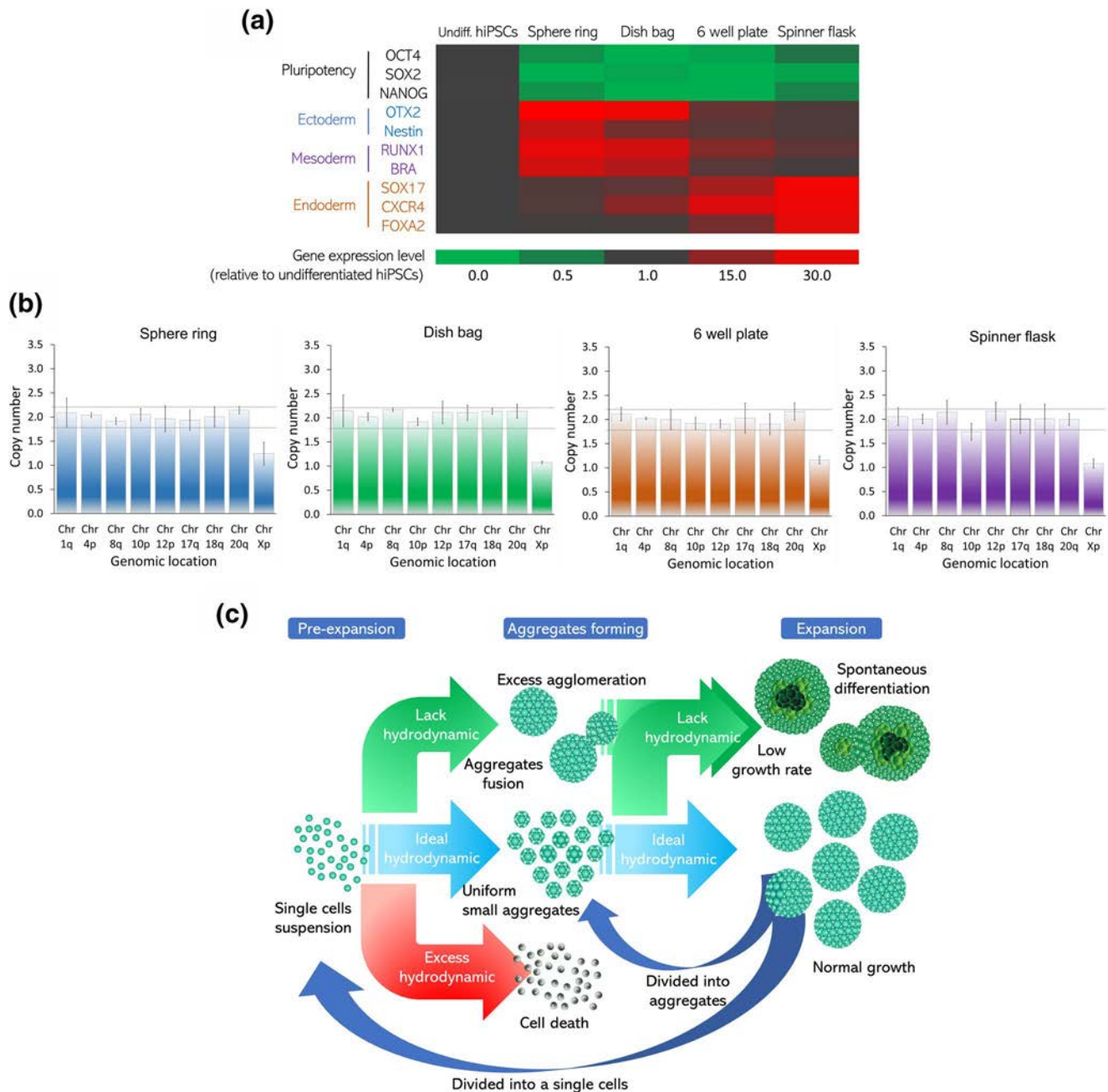


FIGURE 6 Differentiation potential and genetic stability of resulting aggregates. (a) Heat map chart of pluripotency and three germ layer marker gene expression levels after spontaneous differentiation relative to the undifferentiated hiPSCs ($N = 3$ biological replicates). (b) Chromosomal abnormality was not detected from the hiPSCs expanded in all of the culture systems ($N = 3$ biological replicates). A copy number <1.8 or >2.2 with a p -value ≤ 0.05 (range showed by dotted line) indicates the presence of chromosomal abnormality in the culture. The sex chromosome is shown by the copy number of one or two in Chr Xp. (c) Schematic illustration showing the possible detrimental effect of improper hydrodynamic conditions in pluripotent stem cells (PSCs) suspension culture. The lack of hydrodynamic conditions may cause excess agglomeration, which results in large aggregates. At some extent, these large aggregates tend to exhibit a mass transfer limitation of nutrients, oxygen, and toxic metabolic products, causing a low growth rate and spontaneous differentiation. On the contrary, uniform small aggregates were formed in ideal hydrodynamic conditions. This condition also supported normal growth without any mass transfer limitation during the expansion period as well as division into smaller aggregates or single cells. The excess hydrodynamic condition may induce a higher cellular death rate in the aggregates formation period [Colour figure can be viewed at wileyonlinelibrary.com]

achieved via internal agitation, using a spinner flask, or external agitation, using a rotational-based culture system. The hydrodynamics within the culture vessel largely depend on the design of the

culture vessel and its volume (Kehoe et al., 2010; Kinney et al., 2011; Sargent et al., 2010). In addition, this factor can be used to control the aggregation. A lower hydrodynamic force may result

in excess aggregation, whereas a strong hydrodynamic force can induce cellular damage. The excessive amount of both conditions may lead to the spontaneous differentiation of hiPSC aggregates (Leung et al., 2011) (Figure 6c).

Based on the results, the hiPSC aggregates formed by the spinner flask showed a diverse aggregate diameter, which predominantly consisted of large aggregates. Because internal agitation was achieved by an impeller, the formation of intense turbulence resulted in a localized shear and non-uniform distribution of the hydrodynamic force in the different mixing areas during the initial aggregation (Video S1). The horizontal impeller axis area could provide less hydrodynamic mixing, which potentially produces larger aggregates compared to the peripheral area (Verma et al., 2019). These large aggregates often result in the transfer limitation of small molecule nutrients, toxic metabolic byproducts, and macromolecule growth factors into their core (Namepe et al., 2017). Moreover, this non-uniform level of exposure between the aggregate regions may cause heterogeneous cell properties, spontaneous differentiation, or even necrotic cores within multicellular aggregates during the culture period. As an alternative, a bioreactor with a vertical impeller axis, such as a vertical wheel bioreactor (Borys et al., 2021) might be used to generate more uniform aggregates. However, this culture system may result in higher mechanical stress owing to the extensive friction between the impeller and suspended aggregates.

The aggregates formed and expanded in the conventional external agitation-based culture vessel, such as culture dishes or well plates in a rotary shaker, also showed a larger aggregate population and variability in size. A previous study by Filipovic et al. (2016) showed that the different mixing zones are distinct among different regions of culture vessels, based on the distance from the central area of this type of agitation, promoting aggregate heterogeneity within a different area of culture vessel (Ozturk, 1996) during aggregates formation and expansion. Additionally, these aggregates tended to gather in the central area during rotary orbital culture, as shown by the Einstein tea leaves effect.

In contrast, the aggregates generated and expanded in the sphere ring showed a small and homogenous population of aggregates. This ring-shaped bag was able to hinder the effect of Einstein tea leaves by blocking the central area, where the aggregates are often accumulated. In addition, the exclusion of the central area promoted an equal distribution of hydrodynamic force among culture vessel areas. This control is important to avoid excessive agglomeration, which may result in the complicated problem found in other types of rotation-based culture systems in this study.

The results show that the different aggregation control in various types of culture systems in this study generally affected various biological properties of hiPSCs. In general, small aggregates resulting from the sphere ring show better pluripotency and enhanced metabolism due to their equal exposure to nutrients, growth factors, and toxic byproduct removal. In contrast, larger aggregates with darker morphology exhibited more actin filaments. Despite the absence of a necrotic core in all groups, pluripotency and proliferation can be affected by the limited mass transfer of important molecules in large

aggregates (Bauwens et al., 2008; Torizal et al., 2019; Van Winkle et al., 2012). Based on a previous study, the actin filament may indicate the formation of strong matrix interactions that can increase the cell-cell adhesiveness and rigidity of the aggregates (Bayir et al., 2019; Smyrek et al., 2019; Tsai et al., 2015). The increase in their compactness may contribute to the additional barrier for the penetration of several important molecules into the aggregate core, which is required for pluripotency. As a result, the proliferation area marked by Ki67 was limited to the outer layer of the large aggregates due to a lack of nutrient supply in the central area. Different aggregate sizes also displayed a tendency to differentiate. Our results correspond with those of a previous study showing that large aggregates may exhibit higher differentiation potential into the endodermal lineage and its derivatives (Torizal et al., 2019).

Another important factor that influences the differentiation tendency is the exposure to higher shear force, which may induce differentiation into ectoderm and mesoderm lineages. Several studies have reported that higher exposure to shear force may promote differentiation into ectodermal and mesodermal lineages and repress endodermal transcription factors (Vosough, 2013; Wolfe et al., 2012). Additionally, the low stiffness indicated by fewer actin filaments may promote ectodermal differentiation via the modulation of Yes-associated protein 1 (YAP1) (Kaitsuka & Hakim, 2021). Although spontaneous differentiation may occur during expansion due to the mass transfer limitation, high cellular adhesive affinity mediated by actin can spontaneously induce differentiation and direct the differentiation of PSCs into the endodermal lineage (Tse et al., 2021).

The aggregation control of hiPSCs cultured in a spherical ring showed a decent performance. However, the additional hydrodynamic shear stress increased in this system compared to the other culture systems. Consequently, the initial cell number resulting from aggregate formation was relatively lower than that of other culture systems due to additional cellular injury during the aggregate formation period. To solve this problem, it may be necessary to add agents, such as gellan gum, which can adjust the viscoelasticity of the medium. In a previous study, this viscoelastic agent showed a good effect in controlling the aggregation and creating a low shear stress culture environment (Horiguchi et al., 2020; Otsuji et al., 2014; Torizal et al., 2021). The synergistic combination of this agent and sphere ring culture system can be potentially applied to achieve uniform aggregates with minimum shear stress. Therefore, this type of culture vessel design can be further expanded to up-scale the production of homogenous hiPSC aggregates. Currently, the 200 ml scale sphere ring was manufactured and showed a good aggregate population for HEK293 cells. To obtain the optimum conditions for its application in hiPSCs, the rotational speed needs to be carefully optimized according to the diameter of the culture vessel. For example, reduction of the rotational speed is necessary when employing expansion with larger diameters of this culture platform to provide a mild mixing of the cell suspension. These improvements may provide a feasible solution for the production of uniform hiPSC aggregates at a manufacturing scale for various applications.

5 | CONCLUSION

In this study, we successfully demonstrated a suitable culture design approach for the mass production of homogenous hiPSC aggregates with decent pluripotency. This culture vessel can also be enlarged to accommodate a larger volume to produce a higher number of hiPSCs for translational regenerative medicine.

ACKNOWLEDGMENT

None. No funding to declare.

CONFLICT OF INTEREST

The authors declare no competing interest in this research.

AUTHOR CONTRIBUTION

Yasuyuki Sakai, Masaki Nishikawa, Ikki Horiguchi, and Fuad Gandhi Torizal designed the experimental project. Fuad Gandhi Torizal and Seong Min Kim performed the culture experiments. Fuad Gandhi Torizal and Kousuke Inamura performed the data analysis. Ikumi Suzuki and Takashi Morimura designed and provide the sphere ring vessel. Fuad Gandhi Torizal, Seong Min Kim, Masaki Nishikawa, and Yasuyuki Sakai writing the manuscript.

DATA AVAILABILITY STATEMENT

The datasets generated and/or analyzed during the current study are available from the corresponding author on reasonable request.

ORCID

Fuad Gandhi Torizal  <https://orcid.org/0000-0003-1194-531X>

REFERENCES

- Bauwens, C. L., Peerani, R., Niebruegge, S., Woodhouse, K. A., Kumacheva, E., Husain, M., & Zandstra, P. W. (2008). Control of human embryonic stem cell colony and aggregate size heterogeneity influences differentiation trajectories. *Stem Cells*, *26*(9), 2300–2310. <https://doi.org/10.1634/stemcells.2008-0183>
- Bayir, E., Sendemir, A., & Missirlis, Y. F. (2019). Mechanobiology of cells and cell systems, such as organoids. *Biophysics Review*, *11*(5), 721–728. <https://doi.org/10.1007/s12551-019-00590-7>
- Bianconi, E., Piovesan, A., Facchin, F., Beraudi, A., Casadei, R., Frabetti, F., Vitale, L., Pelleri, M. C., Tassani, S., Piva, F., Perez-Amodio, S., Strippoli, P., & Canaider, S. (2013). An estimation of the number of cells in the human body. *Annals of Human Biology*, *40*(6), 463–471. <https://doi.org/10.3109/03014460.2013.807878>
- Borys, B. S., Dang, T., So, T., Rohani, L., Revay, T., Walsh, T., Thompson, M., Argiropoulos, B., Rancourt, D. E., Jung, S., Hashimura, Y., Lee, B., & Kallos, M. S. (2021). Overcoming bioprocess bottlenecks in the large-scale expansion of high-quality hiPSC aggregates in vertical-wheel stirred suspension bioreactors. *Stem Cell Research & Therapy*, *12*(1), 1–19. <https://doi.org/10.1186/s13287-020-02109-4>
- Carpenedo, R. L., Sargent, C. Y., & McDevitt, T. C. (2007). Rotary suspension culture enhances the efficiency, yield, and homogeneity of embryoid body differentiation. *Stem Cells*, *25*(9), 2224–2234. <https://doi.org/10.1634/stemcells.2006-0523>
- Chen, G., Gulbranson, D. R., Hou, Z., Bolin, J. M., Ruotti, V., Probasco, M. D., Smuga-Otto, K., Howden, S. E., Diol, N. R., Propson, N. E., Wagner, R., Lee, G. O., Antosiewicz-Bourget, J., Teng, J. M. C., & Thomson, J. A. (2011). Chemically defined conditions for human iPSC cell derivation and culture. *Nature Methods*, *8*(5), 424–429. <https://doi.org/10.1038/nmeth.1593>
- Filipovic, N., Ghimire, K., Saveljic, I., Milosevic, Z., & Ruegg, C. (2016). Computational modeling of shear forces and experimental validation of endothelial cell responses in an orbital well shaker system. *Computer Methods in Biomechanics and Biomedical Engineering*, *19*(6), 581–590. <https://doi.org/10.1080/10255842.2015.1051973>
- Fridley, K. M., Fernandez, I., Li, M.-T. A., Kettlewell, R. B., & Roy, K. (2010). Unique differentiation profile of mouse embryonic stem cells in rotary and stirred tank bioreactors. *Tissue Engineering Part A*, *16*(11), 3285–3298. <https://doi.org/10.1089/ten.TEA.2010.0166>
- Horiguchi, I., & Sakai, Y. (2016). Serum replacement with albumin-associated lipids prevents excess aggregation and enhances growth of induced pluripotent stem cells in suspension culture. *Published online*, *32*, 1009–1016. <https://doi.org/10.1002/btpr.2301>
- Horiguchi, I., Suzuki, I., Morimura, T., & Sakai, Y. (2019). An orbital shaking culture of mammalian cells in O-shaped vessels to produce uniform aggregates. *Journal of Visualized Experiments*, *2019*(143), 2–6. <https://doi.org/10.3791/57922>
- Horiguchi, I., Torizal, F. G., Nagate, H., Inose, H., Inamura, K., Hirata, O., Hayashi, H., Horikawa, M., & Sakai, Y. (2020). Protection of human induced pluripotent stem cells against shear stress in suspension culture by Bingham plastic fluid. *Biotechnology Progress*, *37*, 1–8. <https://doi.org/10.1002/btpr.3100>
- Kaitsuka, T., & Hakim, F. (2021). Response of pluripotent stem cells to environmental stress and its application for directed differentiation. *Biology*, *10*(2), 1–16. <https://doi.org/10.3390/biology10020084>
- Kehoe, D. E., Jing, D., Lock, L. T., & Tzanakakis, E. S. (2010). Scalable stirred-suspension bioreactor culture of human pluripotent stem cells. *Tissue Engineering Part A*, *16*(2), 405–421. <https://doi.org/10.1089/ten.tea.2009.0454>
- Kinney, M. A., Sargent, C. Y., & McDevitt, T. C. (2011). The multi-parametric effects of hydrodynamic environments on stem cell culture. *Tissue Engineering Part B Reviews*, *17*(4), 249–262. <https://doi.org/10.1089/ten.teb.2011.0040>
- Leung, H. W., Chen, A., Choo, A. B. H., Reuveny, S., & Oh, S. K. W. (2011). Agitation can induce differentiation of human pluripotent stem cells in microcarrier cultures. *Tissue Engineering Part C Methods*, *17*(2), 165–172. <https://doi.org/10.1089/ten.tec.2010.0320>
- Nampe, D., Joshi, R., Keller, K., zur Nieden, N. I., & Tsutsui, H. (2017). Impact of fluidic agitation on human pluripotent stem cells in stirred suspension culture. *Biotechnology and Bioengineering*, *114*, 2109–2120. <https://doi.org/10.1002/bit.26334>
- Olmer, R., Lange, A., Selzer, S., Kasper, C., Haverich, A., Martin, U., & Zweigerdt, R. (2012). Suspension culture of human pluripotent stem cells in controlled, stirred bioreactors. *Tissue Engineering Part C Methods*, *18*(10), 772–784. <https://doi.org/10.1089/ten.tec.2011.0717>
- Otsuji, T. G., Bin, J., Yoshimura, A., Tomura, M., Tateyama, D., Minami, I., Yoshikawa, Y., Aiba, K., Heuser, J. E., Nishino, T., Hasegawa, K., & Nakatsuji, N. (2014). A 3D sphere culture system containing functional polymers for large-scale human pluripotent stem cell production. *Stem Cell Reports*, *2*(5), 734–745. <https://doi.org/10.1016/j.stemcr.2014.03.012>
- Ouyang, A., Ng, R., & Yang, S.-T. (2006). Long-term culturing of undifferentiated embryonic stem cells in conditioned media and three-dimensional fibrous matrices without extracellular matrix coating. *Stem Cells*, *25*(2), 447–454. <https://doi.org/10.1634/stemcells.2006-0322>
- Ozturk, S. S. (1996). Engineering challenges in high density cell culture systems. *Cytotechnology*, *22*, 3–16. <https://doi.org/10.1007/BF00353919>
- Sargent, C. Y., Berguig, G. Y., Kinney, M. A., Hiatt, L. A., Carpenedo, R. L., Berson, R. E., & McDevitt, T. C. (2010). Hydrodynamic modulation of embryonic stem cell differentiation by rotary orbital suspension

- culture. *Biotechnology and Bioengineering*, 105(3), 611–626. <https://doi.org/10.1002/bit.22578>
- Schindelin, J., Arganda-Carreras, I., Frise, E., Kaynig, V., Longair, M., Pietzsch, T., Preibisch, S., Rueden, C., Saalfeld, S., Schmid, B., Tinevez, J.-Y., White, D. J., Hartenstein, V., Eliceiri, K., Tomancak, P., & Cardona, A. (2012). Fiji: An open-source platform for biological-image analysis. *Nature Methods*, 9(7), 676–682. <https://doi.org/10.1038/nmeth.2019>
- Smyrek, I., Mathew, B., Fischer, S. C., Lissek, S. M., Becker, S., & Stelzer, E. H. K. (2019). E-cadherin, actin, microtubules and FAK dominate different spheroid formation phases and important elements of tissue integrity. *Biol Open*, 8(1). <https://doi.org/10.1242/bio.037051>
- Takayama, N., Nishimura, S., Nakamura, S., Shimizu, T., Ohnishi, R., Endo, H., Yamaguchi, T., Otsu, M., Nishimura, K., Nakanishi, M., Sawaguchi, A., Nagai, R., Takahashi, K., Yamanaka, S., Nakauchi, H., & Eto, K. (2010). Transient activation of C-myc expression is critical for efficient platelet generation from human induced pluripotent stem cells. *Journal of Experimental Medicine*, 207(13), 2817–2830. <https://doi.org/10.1084/jem.20100844>
- Tchoryk, A., Taresco, V., Argent, R. H., Ashford, M., Gellert, P. R., Stolnik, S., Grabowska, A., & Garnett, M. C. (2019). Penetration and uptake of nanoparticles in 3D tumor spheroids. *Bioconjugate Chemistry*, 30(5), 1371–1384. <https://doi.org/10.1021/acs.bioconjchem.9b00136>
- Torizal, F. G., Choi, H., Shinohara, M., & Sakai, Y. (2021). Efficient high-density hiPSCs expansion in simple dialysis device. *Methods in Molecular Biology*, 2454. https://doi.org/10.1007/7651_2021_391
- Torizal, F. G., Kimura, K., Horiguchi, I., & Sakai, Y. (2019). Size-dependent hepatic differentiation of human induced pluripotent stem cells spheroid in suspension culture. *Regenerative Therapy*, 12, 66–73. <https://doi.org/10.1016/j.reth.2019.04.011>
- Tsai, A. C., Liu, Y., Yuan, X., & Ma, T. (2015). Compaction, fusion, and functional activation of three-dimensional human mesenchymal stem cell aggregate. *Tissue Engineering Part A*, 21(9–10), 1705–1719. <https://doi.org/10.1089/ten.tea.2014.0314>
- Tse, J. D., Moore, R., Meng, Y., Tao, W., Smith, E. R., & Xu, X. X. (2021). Dynamic conversion of cell sorting patterns in aggregates of embryonic stem cells with differential adhesive affinity. *BMC Developmental Biology*, 21(1), 1–15. <https://doi.org/10.1186/s12861-020-00234-0>
- Van Winkle, A. P., Gates, I. D., & Kallos, M. S. (2012). Mass transfer limitations in embryoid bodies during human embryonic stem cell differentiation. *Cells Tissues Organs*, 196(1), 34–47. <https://doi.org/10.1159/000330691>
- Verma, R., Mehan, L., Kumar, R., Kumar, A., & Srivastava, A. (2019). Computational fluid dynamic analysis of hydrodynamic shear stress generated by different impeller combinations in stirred bioreactor. *Biochemical Engineering Journal*, 151, 107312. <https://doi.org/10.1016/j.bej.2019.107312>
- Vosough, M., Omidinia, E., Kadivar, M., Shokrgozar, M.-A., Pournasr, B., Aghdami, N., & Baharvand, H. (2013). Generation of functional hepatocyte-like cells from human pluripotent stem cells in a scalable suspension culture. *Stem Cells and Development*, 22(20), 2693–2705. <https://doi.org/10.1089/scd.2013.0088>
- Wolfe, R. P., Leleux, J., Nerem, R. M., & Ahsan, T. (2012). Effects of shear stress on germ lineage specification of embryonic stem cells. *Integr Biol (United Kingdom)*, 4(10), 1263–1273. <https://doi.org/10.1039/c2ib20040f>
- Yogananda, C. S., & Einstein, A. (2000). The cause of the formation of meanders in the courses of rivers and of the so-called Baer's law. *Resonance*, 5(3), 105–108. <https://doi.org/10.1007/bf02839006>
- Zweigerdt, R. (2009). Large scale production of stem cells and their derivatives. *Advances in Biochemical Engineering*, 123, 127–141. <https://doi.org/10.1007/10>

SUPPORTING INFORMATION

Additional supporting information may be found in the online version of the article at the publisher's website.

August 2022

Keywords or phrases:

iPSC, Stem Cells, Differentiation, Pluripotency, Flow Cytometry, Live-Cell Imaging, Spheroids, 3D Culture, 2D Culture

Characterization and Optimization of Induced Pluripotent Stem Cell Culture Using Advanced Flow Cytometry and Live-Cell Analysis

Daryl Cole¹, Kirsty McBain¹, Nina Senutovitch² and Nicola Bevan¹¹Sartorius UK Ltd., Units 2 & 3 The Quadrant, Newark Close, Royston Hertfordshire SG8 5HL UK²Sartorius Corporation, 5700 Pasadena Avenue NE, Albuquerque, NM 87113 USA

Correspondence

Email: daryl.cole@sartorius.com

Introduction

In 2006, Japanese researchers published an important discovery outlining a method for creating induced pluripotent stem cells (iPSCs) from primary mouse fibroblasts by activating the expression of key transcription factors.¹ Since this discovery, the field of stem cell biology has rapidly expanded and iPSCs form the basis of many new areas of research. They are intrinsically valuable due to their unique characteristics and the control they afford to researchers and clinicians over the building blocks of the body. The major benefits of the use of iPSCs are the number of different cell types that can be differentiated from them and their capacity for infinite expansion.² This flexibility provides many opportunities for the development of specific cell and tissue models both in 2D and 3D for pharmacological testing,³ cancer research,⁴ organoid modeling of tissues,⁵ and neurodevelopmental biology.⁶ In addition, iPSCs are increasingly used in translational applications, targeting eventual use in the clinic via autologous cell therapies and for individualized medicine approaches.⁷ Increasingly, there is a need to improve the culture and expansion methods of iPSCs away from 2D plate-based methods and towards more physiologically relevant methods such as 3D culture. In particular, 3D suspension cultures, such as cell aggregates and spheroids, can maintain greater cell-to-cell contact, produce endogenous extracellular matrix to promote growth conditions similar to *in vivo*, and are readily available for downstream applications.⁸

Find out more: www.sartorius.com

Some limitations are inherent in any system, however, and iPSCs are high maintenance, expensive, and require constant monitoring to ensure they maintain pluripotency, viability, and homogeneity.⁹ Long-term culture of iPSCs can result in genotypic and phenotypic heterogeneity, even in a cell line derived from a single source cell; therefore, it is vital that methods for monitoring, detecting, and reducing heterogeneity in iPSC lines are developed.¹⁰

Increasing use of stem cells in both clinical and research settings necessitates fast, reliable, and relatively inexpensive solutions for the growth, characterization, and maintenance of this valuable biological resource.

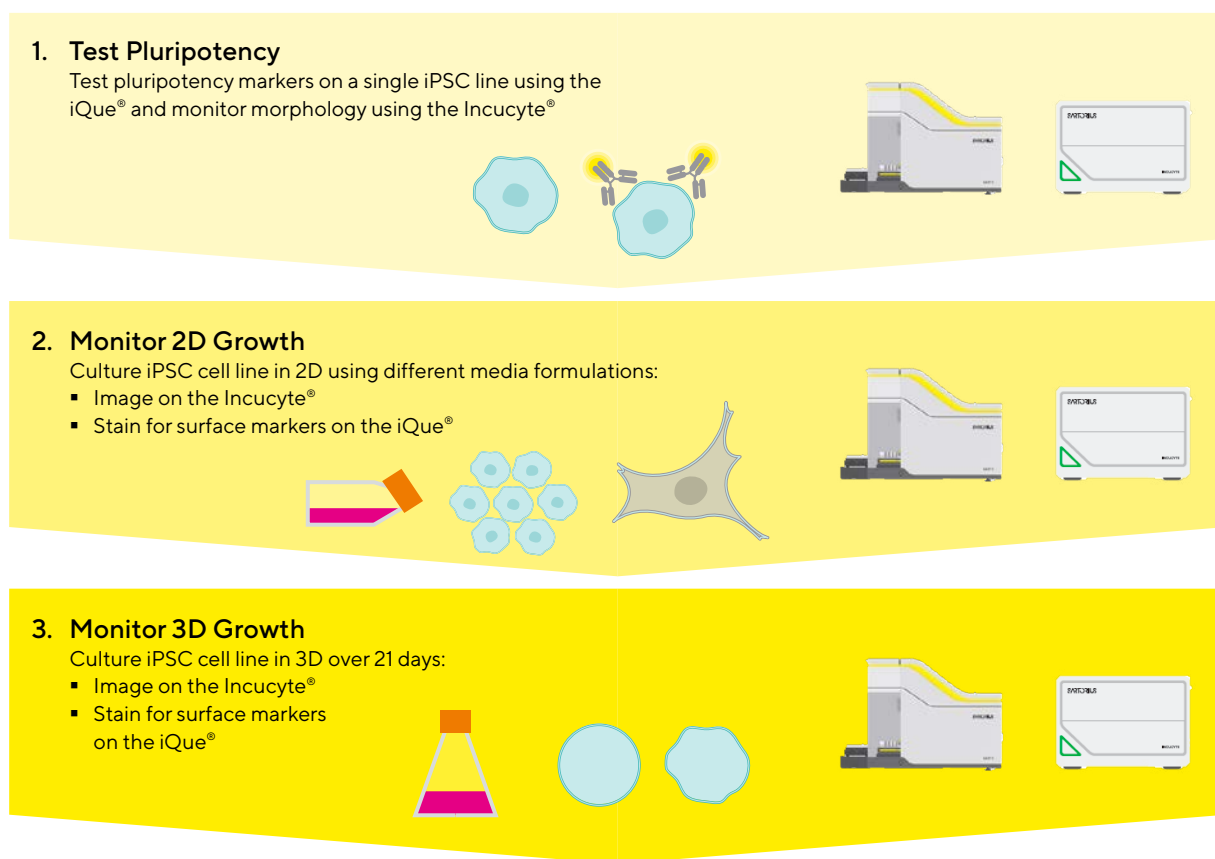
Conventional methods for monitoring iPSC characteristics during culture, such as traditional flow cytometry, can:

- Be labor-intensive and time-consuming, requiring multiple steps including fixation, staining, and washing
- Require large sample volumes, necessitating the use of more precious cells and expensive consumables
- Demand in-depth manual manipulation and analysis of raw data and require compensation optimization
- Often use low-throughput solutions, increasing the time to results

This application note describes methods for the characterization, successful maintenance, scale up, and selection of ideal iPSCs in a combined workflow approach using real-time imaging on the Incucyte® Live-Cell Analysis System for easy morphological analysis and rapid expression profiling using minimal sample volumes (10 µL) on the iQue® Advanced Flow Cytometry platform.

Figure 1

Schematic Highlighting the Combined iQue® and Incucyte® Workflow for iPSC Line Selection and Differentiation Monitoring



Note. Using a combination of two Sartorius instruments, researchers can test iPSC pluripotency and monitor iPSC growth both in 2D and 3D culture, as illustrated above.

Methods

The following methods describe the processes used to characterize and monitor healthy, pluripotent iPSCs grown in 2D and 3D using a combined workflow for the Incucyte® Live-Cell Analysis System and the iQue® Advanced Flow Cytometry platform. Figure 1 outlines the key steps during this workflow.

Cell Culture and Maintenance

Control Cell Line Culture

THP-1 cells (human monocyte derived from an acute monocytic leukemia patient) were grown in suspension at a density of 1×10^5 /mL. NCCIT cells (human developmentally pluripotent cell line derived from a mediastinal mixed germ cell tumor) were grown in 2D monolayers until 70–80% confluent before passaging and use in experiments. Both lines were grown in RPMI 1640 medium supplemented with 10% FBS, L-glutamine 2 mM, Penicillin/Streptomycin 100 µg/mL.

Thawing and Culturing iPSC Lines (2D)

A single iPSC line (ATCC-DYS0100 cells derived from human foreskin fibroblasts) was thawed and plated onto Vitronectin XF™ (1:25 dilution in CellAdhere™ Dilution Buffer) precoated 6-well plates at a seeding density of 1×10^6 /well in 1 mL growth medium (mTESR™ Plus) supplemented with Y-27632 (ROCK inhibitor, 10 µM) and incubated at 37 °C. iPSCs were monitored using the Incucyte® system to assess confluency, colony formation, and general cell morphology and health. The confluence of colonies was analyzed using the integrated Incucyte® AI confluence software algorithm. Passages were performed every 3–4 days at approximately 60–70% confluence using Gentle Cell Dissociation Reagent and replated at 1×10^5 /well. Medium changes were performed daily, with a two-day duration over weekends. For the non-optimized iPSC culture, cells were grown as above except for using RPMI 1640 medium supplemented with 10% FBS, L-glutamine 2 mM, Penicillin/Streptomycin 100 µg/mL.

Culturing iPSC Lines (3D)

Once healthy colonies had been established, iPSCs were transferred from 2D culture into 125 mL Erlenmeyer flasks at a density of 1.5×10^5 /mL in 20 mL StemScale™ PSC Suspension Medium supplemented with Y-27632 (10 µM) and incubated at 37 °C on a shaker at 70 rpm. 3D spheroid size and shape were monitored at regular intervals by taking 1 mL samples from the flask and plating into 24-well plates for analysis using the Incucyte®. Passaging was performed

at least once a week using Accutase® once spheroid sizes reached a limit of 400 µm. Medium changes were performed every other day, with a two-day duration over the weekend.

Characterization and Monitoring of Pluripotency

Pluripotency Characterization: iQue®

iPSCs were dissociated to single cells during passage and at specified timepoints using Gentle Cell Dissociation Reagent for 2D culture and Accutase® for 3D culture. Single-cell suspensions were stained with cell surface marker antibodies (in PBS + 2% FBS) for one non-pluripotent marker, SSEA-1, and two pluripotency markers, SSEA-4 and TRA-1-60, in addition to the iQue® Membrane Integrity (B/Red) Dye, for viability analysis. Cells were seeded at 2×10^4 /well in a V-bottom 96-well plate; they were stained with the cocktail of antibodies described, centrifuged (300 x g, 5 sec), briefly shaken using the iQue® plate station (2000 rpm, 20 sec), and incubated at RT in the dark for 30 min. PBS + 2% FBS (100 µl) was added to each well and centrifuged (300 x g, 5 min), supernatant was aspirated, plate shaken (3000 rpm, 60 sec), and the samples resuspended in PBS + 2% FBS (20 µL), prior to being analyzed on the iQue®. Analysis of data was performed using the iQue Forecyt® software after compensation had been optimized for each of the antibodies.

Monitoring Pluripotency and Cell Health: Incucyte®

During the experiments, iPSCs were monitored for changes in morphology and confluency associated with pluripotency using the Incucyte® Live-Cell Analysis System. 2D-cultured iPSC lines were monitored by high definition (HD) phase contrast at 4-hour intervals using a repeating scan schedule at 10X. Nuclear to cytoplasmic ratios were calculated by staining iPSC nuclei using the Incucyte Nuclight® Rapid Red Reagent (1:1000) and measuring the cytoplasmic area (confluence mask) and the nuclear area (fluorescence mask) using basic masking on the Incucyte® Live-Cell Analysis System to quantify pluripotency/normal iPSC morphology.

3D-cultured iPSC spheroids were sampled every day and plated into 24-well plates for analysis on the Incucyte® system using a one-off scan at 10X. Spheroid diameter was measured, and the circularity of each spheroid was analyzed as a morphological marker of pluripotency.

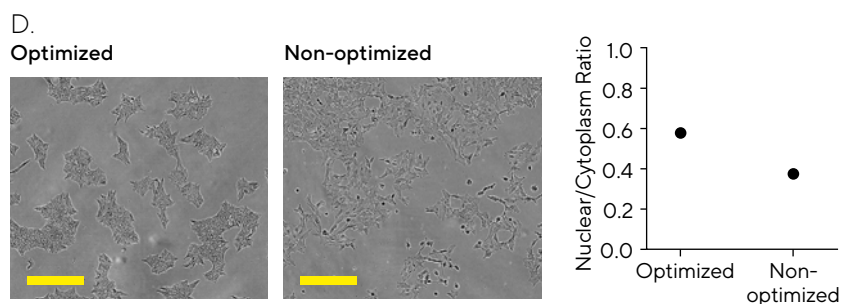
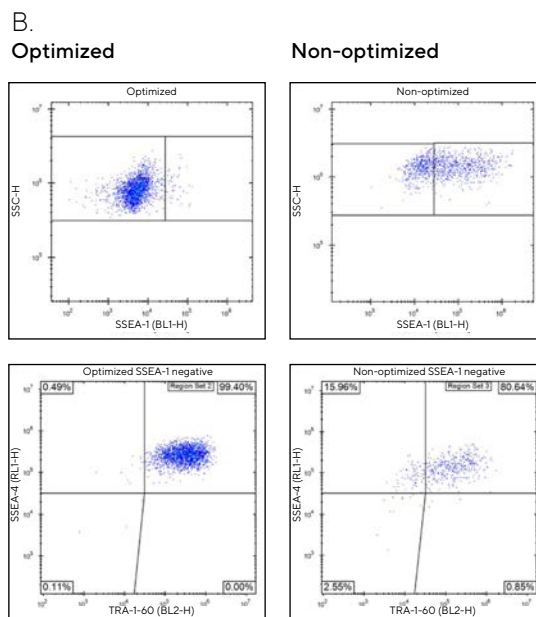
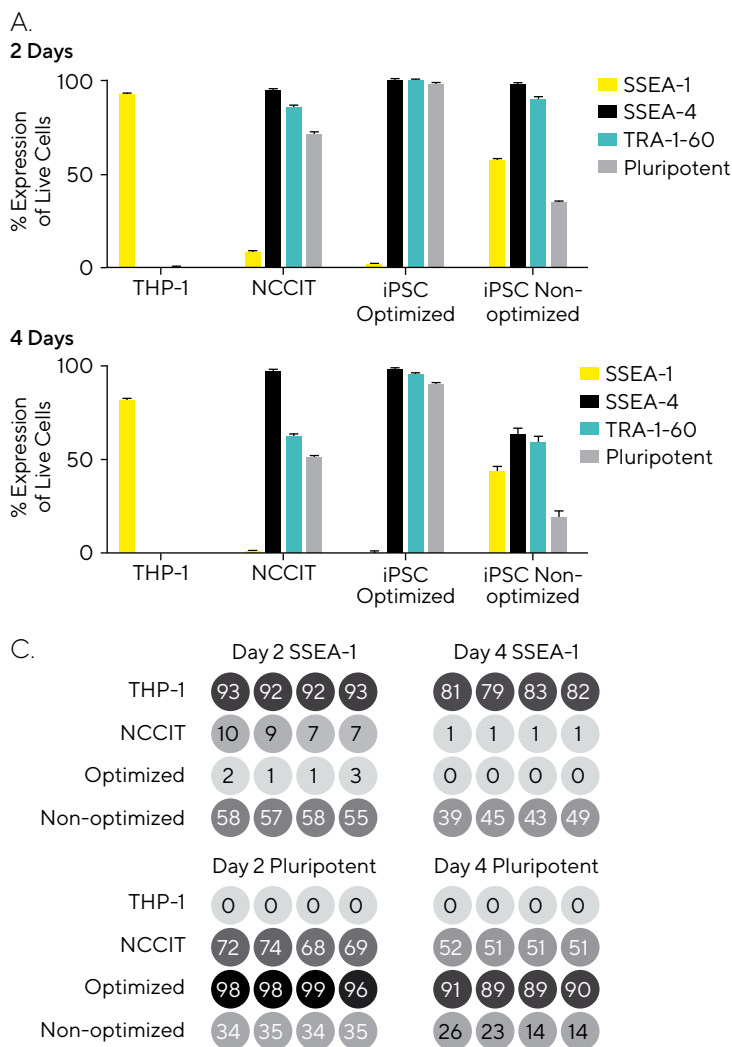
Results

iPSCs require highly specific growth conditions to maintain pluripotency and viability. Determining optimal conditions for their growth and expansion in 2D and 3D during the development of new reagents, techniques, and experimental research can be time-consuming and cost-prohibitive. The data presented here showcase the benefits of using the Incucyte® Live-Cell Analysis platform in conjunction with the iQue® Advanced Flow Cytometry system to monitor the culture of iPSCs during optimization of growth conditions for high levels of pluripotency.

Optimization of Growth Conditions for Successful 2D iPSC Propagation

Using a single iPSC line grown in 2D, we tested the effects of a non-optimized growth condition on the phenotypic presentation of cell surface markers and morphology over the course of two timepoints, 2- and 4-days post-treatment. iPSCs were grown in their usual optimized conditions until colonies formed, at which point they were challenged by changing their medium from mTESR Plus (optimized) to RPMI 1640 with supplements (non-optimized). Control cells, THP-1 and NCCIT, represented a non-pluripotent control line and a line expressing pluripotent surface

Figure 2
Evaluate Optimal Media Formulation to Retain Pluripotency in 2D-Cultured iPSCs



Note. iPSCs were grown in optimized (mTESR Plus) and non-optimized (RPMI) media to induce 'differentiation' for 2 and 4 days (\pm SEM, $n = 4$) (A). Prior to treatment with experimental growth conditions, iPSCs were grown under optimized conditions until medium-sized colonies formed at approximately 3–4 days from initial seeding at 100K cells per well of a 6-well plate. 'Pluripotent' are a population of SSEA-1 negative cells that are positive for both SSEA-4 and TRA-1-60, representing pluripotent cells. (B) Dot plots showing the raw data collected by the iQue® system at 2 days comparing the optimized and non-optimized iPSCs, note the shift in SSEA-1 expression in the non-optimized iPSCs and the subsequent losses in pluripotency marker expression ($n = 4$). (C) Percentage expression 'heatmaps' produced in the iQue Forecyt® software showing the changes in marker expression over 2 and 4 days of 'differentiation' of iPSCs ($n = 4$). (D) iPSCs grown in optimized and non-optimized growth conditions display distinct morphological differences linked to differentiation which can be imaged and analyzed effectively using the Incucyte® (representative images taken at 10X magnification). Graphed quantification of the Nuclear/Cytoplasm ratio analyzed in the Incucyte® from the representative images, right. Scale bar indicates 400 μ m.

markers, respectively. Cells were imaged using the Incucyte® Live-Cell Analysis System and surface markers were analyzed using the iQue® Advanced Flow Cytometry platform.

Analysis shown in Figure 2 highlights the rapid loss of pluripotency in iPSCs when they are grown in non-optimized conditions. This is illustrated by the increase in non-pluripotent marker SSEA-1 expression ($57.5 \pm 0.7\%$) as early as 2 days post-treatment (Figure 2A). Further, we observe decreases in the expression of pluripotency markers SSEA-4 ($97.3 \pm 0.8\%$), TRA-1-60 ($89.8 \pm 0.9\%$), and pluripotent population ($34.6 \pm 0.3\%$), with this decrease amplified after 4 days of treatment (SSEA-4 $63.4 \pm 2.9\%$, TRA-1-60 $58.9 \pm 2.9\%$, pluripotent population $19.3 \pm 3.0\%$). When we compare this data to the optimized iPSCs, where we see no marked differences in expression profile over the time course of these studies ($95 \pm 0.4\%$ for pluripotent markers and less than $1.8 \pm 0.5\%$ for SSEA-1, with one exception being the pluripotent marker at 4 days $89.6 \pm 0.6\%$), there is a clear deviation from the pluripotent profile, i.e. increased SSEA-1 and reduced SSEA-4, TRA-1-60, and combined pluripotency marker expression.

In Figure 2B, (dot plots taken directly from iQue Forecyt® software) there is a clear shift of the population from the Optimized 1.63 % SSEA-1 positive to the Non-optimized 57.5 % SSEA-1 positive (top two dot plots). The lower plots further demonstrate the shift away from pluripotency marker expression in the Non-optimized conditions, where the Optimized iPSCs present a compact population in the upper right quadrant of the plot (SSEA-4+, TRA-1-60+), while the Non-optimized iPSCs present a much more spread population shifting into the TRA-1-60 negative portion of the plot. Heatmaps produced in iQue Forecyt® software present the same data for SSEA-1 and pluripotent expression for the two timepoints, highlighting the flexibility of this platform (Figure 2C).

Incucyte® images of the iPSCs at Day 2, show a marked difference in morphology between the Optimized and Non-optimized conditions. iPSCs grown in Optimized conditions form tightly packed colonies with clearly defined edges, that 'glow' under phase images. By contrast, Non-optimized iPSCs are much more spread out and no longer form colonies, they are beginning to resemble fibroblast cells (Figure 2D). Quantification of these morphological differences was performed using the adherent cell by cell scan at 10X magnification, and nuclear and cytoplasm area measurements were made using the Basic Analyzer and AI Confluence analysis using the following equation to

provide a Nuclear/Cytoplasm ratio, a standard measurement used when studying iPSCs.

$$\frac{\text{total nuclei area}}{\text{total cytoplasmic area}} = \text{nuclear cytoplasm ratio}$$

The more iPSC-like, and thus pluripotent, a cell is, the higher the Nuclear/Cytoplasm ratio. The graph in Figure 2D illustrates the reduction in this ratio in the Non-optimized conditions, from 0.6 to 0.4.

Optimization of Growth Conditions for Successful 3D iPSC Propagation

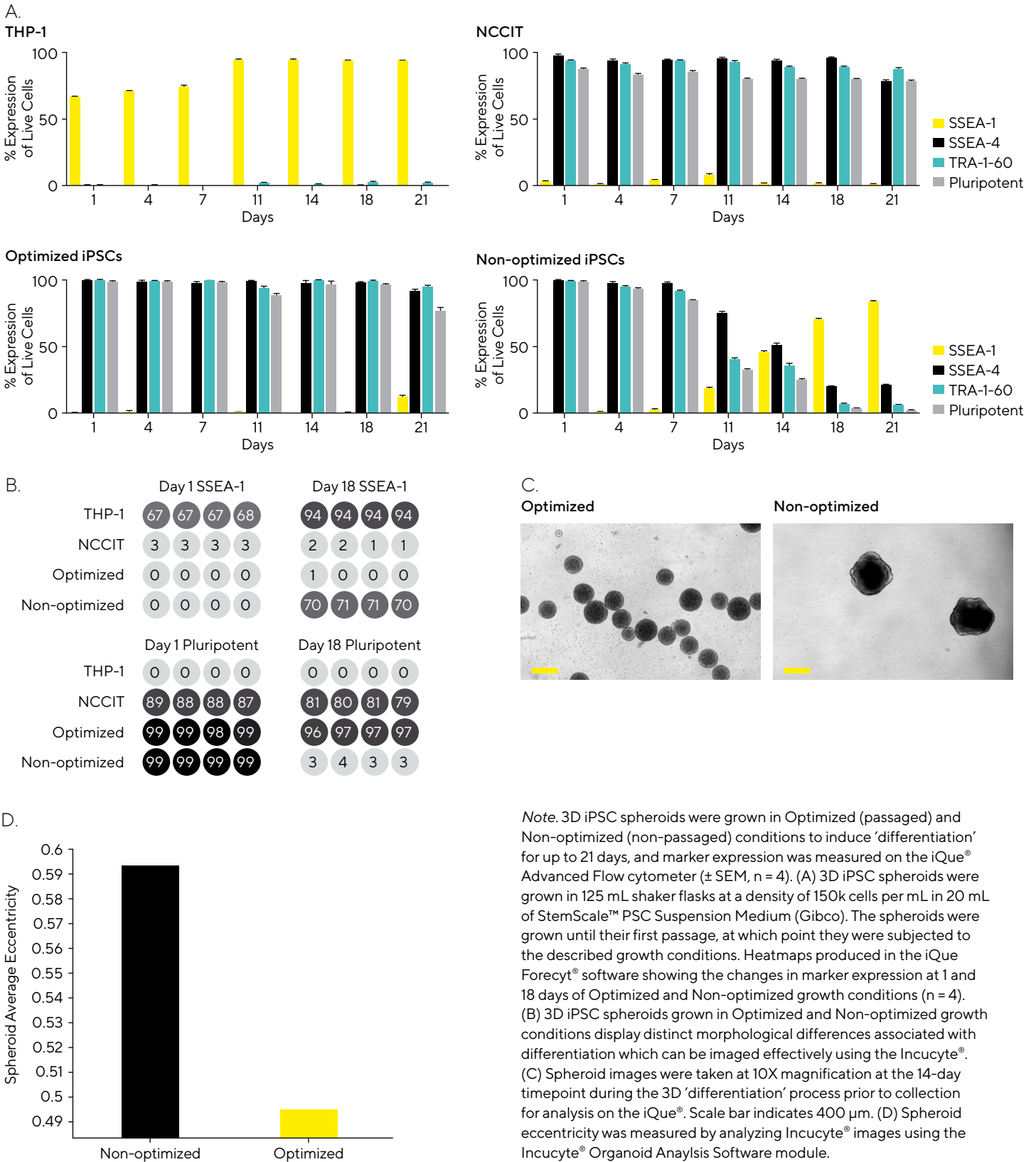
Scaling up iPSC culture requires changes to the conditions under which the cells are grown. Due to the relative flexibility of iPSCs, they can be grown in both 2D and 3D, facilitating scale-up in bioreactors of good quality iPSC lines for a range of downstream processes.

Transferring the culture of the iPSC line used in the 2D experiments to a 3D culture, we investigated the effects of Non-optimized growth conditions on the expression of surface markers for pluripotency and the formation of 3D spheroids over 7 timepoints covering a total of 21 days. iPSCs were grown in 2D culture for at least 2 passages before transfer into 3D culture for at least 1 passage before they were seeded and subjected to Optimized (passaging at each timepoint) and Non-optimized (no passaging) conditions over the time course. Control cells, THP-1 and NCCIT represented a non-pluripotent control line and a line expressing pluripotent surface markers, respectively. Cells were imaged using the Incucyte® Live-Cell Analysis System and surface markers were analyzed using the iQue® Advanced Flow Cytometry platform.

When iPSCs are grown as 3D spheroids, marker expression analysis, Figure 3A, shows that dramatic changes in phenotype only began to present on Day 11 in Non-optimized conditions, where we saw an increase in SSEA-1 expression ($18.5 \pm 0.39\%$) and a reduction in pluripotent marker expression, SSEA-4 ($75.2 \pm 1.2\%$), TRA-1-60 ($40.5 \pm 0.5\%$), and pluripotent ($32.9 \pm 0.5\%$). This trend continued until the endpoint at Day 21 where we observed a final SSEA-1 expression of $83.5 \pm 0.7\%$, SSEA-4 at $20.7 \pm 0.3\%$, TRA-1-60 at $5.9 \pm 0.1\%$, and the pluripotent population at $2.2 \pm 0.1\%$. This data indicates a loss of pluripotency throughout the time course when we contrast the results with the expression profile of our Optimized iPSCs, which stay consistently pluripotent until Day 21. At this timepoint, we start to see an increase in SSEA-1 expression ($12.4 \pm 0.6\%$) and a decrease in the pluripotency markers, SSEA-4 ($91.1 \pm 1.8\%$), and the pluripotent population ($76.5 \pm 2.6\%$). Although there are fluctuations across the time course in the expression profile, Day 21 is increased over the observed variation, suggesting a 21-day cut-off point for successful culture of 3D iPSC spheroids in the system we used.

Figure 3

Determine Optimal Cell Culture Conditions for Improved 3D Spheroid Cell Culture



Note. 3D iPSC spheroids were grown in Optimized (passaged) and Non-optimized (non-passaged) conditions to induce ‘differentiation’ for up to 21 days, and marker expression was measured on the iQue[®] Advanced Flow cytometer (\pm SEM, n = 4). (A) 3D iPSC spheroids were grown in 125 mL shaker flasks at a density of 150k cells per mL in 20 mL of StemScale[™] PSC Suspension Medium (Gibco). The spheroids were grown until their first passage, at which point they were subjected to the described growth conditions. Heatmaps produced in the iQue Forecyt[®] software showing the changes in marker expression at 1 and 18 days of Optimized and Non-optimized growth conditions (n = 4). (B) 3D iPSC spheroids grown in Optimized and Non-optimized growth conditions display distinct morphological differences associated with differentiation which can be imaged effectively using the Incucyte[®]. (C) Spheroid images were taken at 10X magnification at the 14-day timepoint during the 3D ‘differentiation’ process prior to collection for analysis on the iQue[®]. Scale bar indicates 400 μ m. (D) Spheroid eccentricity was measured by analyzing Incucyte[®] images using the Incucyte[®] Organoid Analysis Software module.

Heatmaps produced in iQue Forecyt® software present the same data for SSEA-1 and pluripotent expression for two representative timepoints at Day 1 and Day 18, providing a snapshot of the changes in expression during the experiment (Figure 2C).

3D iPSC spheroids were sampled at each timepoint, plated into a 24-well plate, and visualized in the Incucyte® Live-Cell Analysis System (Figure 3C). The images show the morphological differences after 18 days between the Optimized (top) and Non-optimized (bottom) culture conditions. When 3D iPSC spheroids are grown in Optimized conditions, we observe a very distinct, compact spheroid with high levels of circularity, compared to the Non-optimized conditions, in which the spheroids are much larger, far less compact, and lack the circularity of the Optimized spheroids (0.59 vs 0.49 eccentricity, respectively, Figure 3D).

Conclusions

iPSCs are a valuable resource in many areas of research and clinical development; however, they require highly specific conditions for optimal growth to maintain pluripotency, viability, and propagation potential. These requirements are often expensive and culture methods can be time intensive, requiring complicated techniques. We have shown that by using Sartorius platforms we can successfully characterize iPSCs and monitor their pluripotency with ease via surface marker expression and morphological status, both in 2D and 3D, using the iQue® Advanced Flow Cytometer and the Incucyte® Live-Cell Analysis platform. The key advantages of using this combined workflow over conventional methods are:

- Streamlined processes and data analysis save time and reagent costs to reduce attrition due to low-quality cell products
- Miniaturization reduces antibody reagent costs and saves sample for downstream expansion, characterization, and differentiation
- Low sample requirements provide greater resources for multiple replicates easily processed using a plate-based format
- Monitoring iPSC lines throughout the time course provide greater insights into morphology and pluripotency changes over time
- Rapid protocols require no fixation in a single wash workflow for pluripotent surface markers

The data presented here highlight the advantages of using a streamlined workflow combining multiple Sartorius systems for the characterization and optimization of iPSC culture in 2D and 3D for several applications including drug development, disease modeling, and clinical therapy research.

References

1. Takahashi K, Yamanaka S. Induction of pluripotent stem cells from mouse embryonic and adult fibroblast cultures by defined factors. *Cell*. 2006 Aug 25;126(4):663-76. DOI: 10.1016/j.cell.2006.07.024. Epub 2006 Aug 10. PMID: 16904174.
2. Liu G, David BT, Trawczynski M, Fessler RG. Advances in pluripotent stem cells: History, mechanisms, technologies, and applications. *Stem Cell Rev Rep*. 2020 Feb;16(1):3-32. DOI: 10.1007/s12015-019-09935-x. PMID: 31760627; PMCID: PMC6987053.
3. Gutbier S, Wanke F, Dahm N, et al. Large-scale production of human iPSC-derived macrophages for drug screening. *Int J Mol Sci*. 2020 Jul 7;21(13):4808. DOI: 10.3390/ijms21134808. PMID: 32645954; PMCID: PMC7370446.
4. Karagiannis P, Kim SI. iPSC-Derived natural killer cells for cancer immunotherapy. *Mol Cells*. 2021 Aug 31;44(8):541-548. DOI: 10.14348/molcells.2021.0078. PMID: 34373366; PMCID: PMC8424143.
5. Silva AC, Matthys OB, Joy DA, et al. Co-emergence of cardiac and gut tissues promotes cardiomyocyte maturation within human iPSC-derived organoids. *Cell Stem Cell*. 2021 Dec 2;28(12):2137-2152.e6. DOI: 10.1016/j.stem.2021.11.007. PMID: 34861147.
6. Benito-Kwiecinski S, Lancaster MA. Brain organoids: Human neurodevelopment in a dish. *Cold Spring Harb Perspect Biol*. 2020 Aug 3;12(8):a035709. DOI: 10.1101/cshperspect.a035709. PMID: 31767649; PMCID: PMC7397826.
7. Song B, Cha Y, Ko S, et al. Human autologous iPSC-derived dopaminergic progenitors restore motor function in Parkinson's disease models. *J Clin Invest*. 2020 Feb 3;130(2):904-920. DOI: 10.1172/JCI130767. PMID: 31714896; PMCID: PMC6994130.
8. Centeno EGZ, Cimarosti H, Bithell A. 2D versus 3D human induced pluripotent stem cell-derived cultures for neurodegenerative disease modelling. *Mol Neurodegener*. 2018 May 22;13(1):27. DOI: 10.1186/s13024-018-0258-4. PMID: 29788997; PMCID: PMC5964712.
9. Doss MX, Sachinidis A. Current challenges of iPSC-based disease modeling and therapeutic implications. *Cells*. 2019 Apr 30;8(5):403. DOI: 10.3390/cells8050403. PMID: 31052294; PMCID: PMC6562607.
10. Hayashi Y, Ohnuma K, Furue MK. Pluripotent stem cell heterogeneity. *Adv Exp Med Biol*. 2019;1123:71-94. DOI: 10.1007/978-3-030-11096-3_6. PMID: 31016596.

Acknowledgement

The authors would like to acknowledge Clare Szybut for contributing to this work while employed at Sartorius.

North America

Sartorius Corporation
300 West Morgan Road
Ann Arbor, Michigan 48108
USA
Phone +1734 769 1600
Email: orders.US07@sartorius.com

Europe

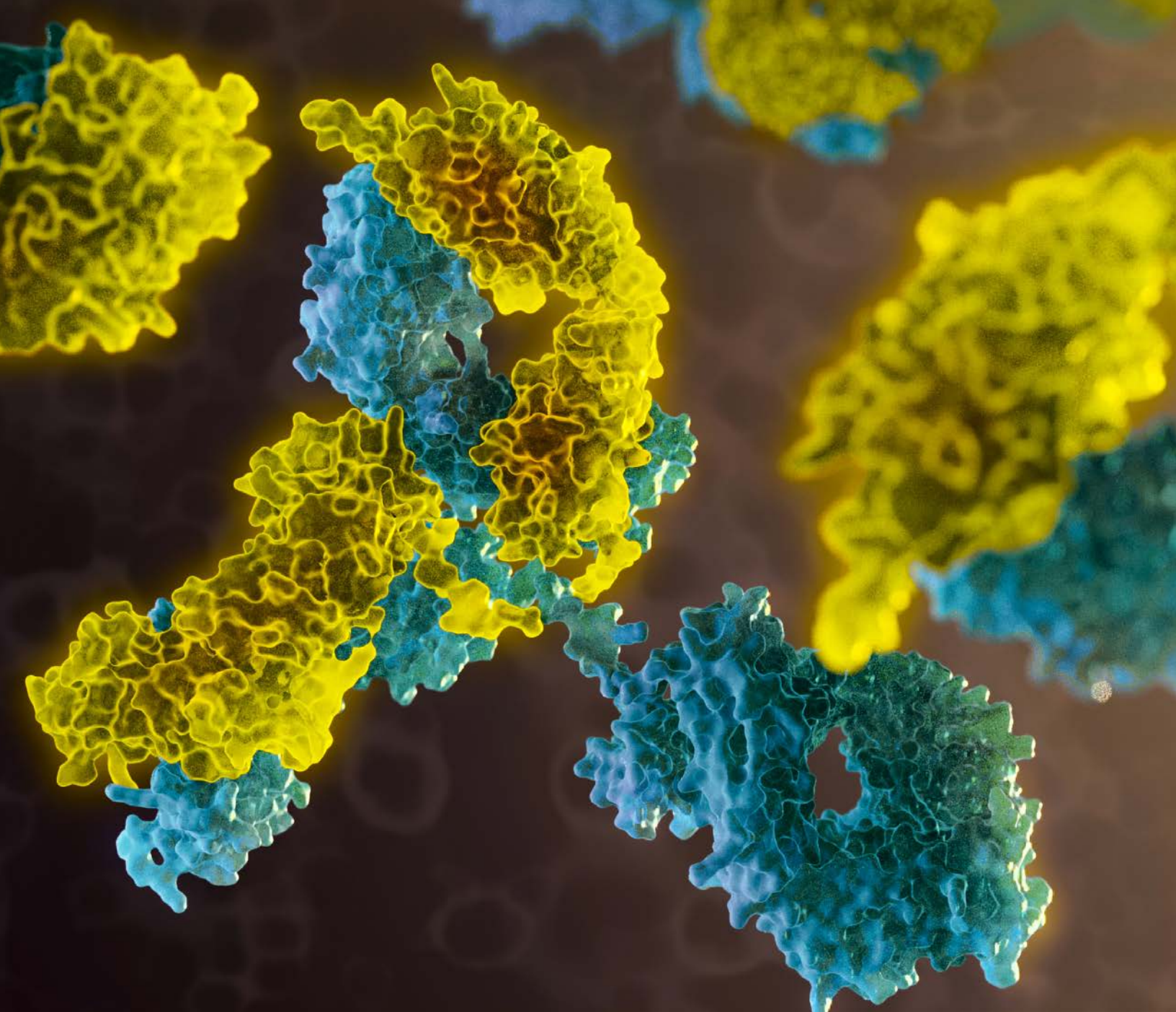
Sartorius UK Ltd.
Longmead Business Centre
Blenheim Road
Epsom
Surrey, KT19 9QQ
United Kingdom
Phone +44 1763 227400
Email: euorders.UK03@sartorius.com

Asia Pacific

Sartorius Japan K.K.
4th Floor, Daiwa Shinagawa North Bldg.
1-8-11, Kita-Shinagawa 1-chome
Shinagawa-Ku
Tokyo 140-0001
Japan
Phone +81 3 6478 5202
Email: orders.US07@sartorius.com

 **Find out more:** www.sartorius.com/iQue

 **For questions, email:** AskAScientist@sartorius.com



Simplify Antibody Discovery with iQue® Advanced Flow Cytometry

Antibody Screening

- Antibody Binding
- Antibody Quantification
- Antibody Isotyping

Functional Characterization

- Antibody Internalization
- Antibody Dependent Cell Cytotoxicity
- Antibody Dependent Cell Phagocytosis

Bioprocessing

- IgG Quantitation
- Cell Health
- Cell Proliferation

www.sartorius.com/iQue-products

© 2023 Essen BioScience. All rights reserved. IntelliCyt® and iQue® are registered trademarks and the property of Essen Bioscience. Essen Bioscience is a Sartorius Company. Specifications subject to change without notice.

Simplifying Progress

SARTORIUS